Surface chemistry of Burrup Rock art at the Yara monitoring sites October 2020

Report for Yara Pilbara Nitrates by
CBG Solutions

Prepared by Dr Ian D MacLeod
Heritage Conservation Solutions

Draft report
Version 1.6

18 December 2020

Figure 1: View of the TAN plant from site

Contents

Executive Summary

- Measurements in October 2020 were conducted on gabbro sites (7, 22 & 23) and granophyre sites (4, 5, 6 & 21) with the sites determined through the CSIRO monitoring program. Continued monitoring of the culturally significant Climbing Man site and of the adjacent split rock was also assessed.
- Replicate rock washing experiments were conducted at each site which provided evidence of the reliability of previous single measurements.
- The surface pH and chloride and the redox voltages were measured at all sites and the Pourbaix plots (voltage vs. pH) confirmed the previously determined new decay mechanisms are dominated by manganese solution chemistry
- The only site with measurable iron at the reference rocks was Yara East (site 23) and this was just above the detection limit.
- There is a strong correlation of increased colour difference between the engravings and the host rock with both the minimum and the mean pH recorded in 2020.
- Analysis of the longitudinal colour differences on each rock measurement location between 2017 and 2020 has shown that year to year differences is not much larger than 1.5 just noticeable fades (ΔE value of 2.0) but there appears to be a cumulative increasing difference over time with the values at the same pH.
- The colour differences diminish with increasing acidification of points on each site.
- Thirty-two sets of measurements of colour show that 65% show statistically reliable colour difference between background and engraved areas. The reliability of the colour measurements was checked by repeated (blind) measurements on the four spots on site 5 at Burrup road.
- All the sites had measurable boron concentrations in the rock washings that showed mobilisation of the boron containing mineral chlorite from the weathered crusts of both the granophyre and gabbro rocks. Other than surface mineralisation, the ratio of chloride to boron indicated that much of the boron comes from sea salts, where it is the secondary buffer system in seawater.
- Cyclone Damien and the associated rainfall generally washed most of the surfaces of the rocks, resulting in moderate residual chloride levels of 34 ± 11 ppm. Site 22 (Yara North West) had extremely low chloride and must have had a localised rain event in the weeks before the measurements.
- The mean nitrate concentration in wash solutions in 2020 was 0.17 ± 0.10 ppm which is lower than 0.7 ± 0.6 in 2019, 2018 and 2017. All these values are significantly less than 6.3 ppm in 2003 and 4.5 ppm in 2004.
- There is a clear link between the minimum pH and the amount of sulphate on the rock surfaces, which indicates some of the sulphate comes from anthropogenic sources.
- All sites show pH profiles which are uniform across the rock surfaces, but which increase in acidity as the measurement points move down the rock surface. This is due to accumulation of moisture and micronutrients.
- There is a need to continue surface measurements and washing of rocks to ensure that the sites are stable.
- There is a compelling need to conduct microbiome assessment of the microflora through DNA analysis to determine the nature of the colonising organisms.
- Data from the ASD spectrophotometer readings were not obtainable due to instrumental malfunctioning on the first site. CSIRO have shown that their new instruments provide comparative data with the older machines and so future work should also include the ASD colour reference work. It is proposed the Dr Ian Lau of CSIRO conduct the chromameter and ASD data at the time of the in-situ corrosion and washing data are collected.

Background

To comply with the regulations concerning retention of its operating licence, EPBC 2008/4546, Yara Pilbara Nitrates engaged CGB Solutions to develop appropriate methodologies to conduct colour monitoring measurements on the six sites surrounding the ammonia and ammonium nitrate plants in the Burrup. The lead consultant (Warren Fish) conducted meetings with the management team from Yara to develop the timetable and to engage with key community members of the Murujuga Aboriginal Corporation for permission to come to country in October 2020 to repeat the colour measurements done in previous years by the CSIRO team. A training refamiliarization session was undertaken by MacLeod by Dr Ian Lau, of CSIRO Kensington, to ensure that the spectral and colour measurements would be compliant and would provide relevant data for the assessment of the condition of the rock engravings. MacLeod retired from the Western Australian Museum in 2016 and is now the Principal of Heritage Conservation Solutions and has published peer-reviewed papers on the conservation of Aboriginal rock art and has 40-years' experience in materials conservation (Appendix I).

During the first phase (2003-2004) of research into the condition of the rock surfaces in the Burrup, several engraved rocks in the "Museum Compound" were examined regarding their acidity (as measured with a surface pH electrode), the water-soluble minerals on the rock surfaces and the microbiological activity. Samples of the rock surface were swabbed with sterile culture material and placed into prepared phials. The biological material was stored at zero degrees before being taken to laboratories in Perth (Department of Agriculture) for characterisation. Other reference measurements were conducted on Gidley and Dolphin Islands in the Dampier Archipelago to act as reference points away from industrial activities associated with the Woodside gas plant and iron ore shipping out of Dampier ports.

Analysis of the solution chemistry collected between 2003 and 2004 provided strong indications of the causal link between the amount of nitrate on the rocks and the level of microbiological activity. This in turn indicated that the acidic metabolites from the organisms were significantly contributing to the overall acidification of the rock surfaces and mobilisation of key minerals containing both iron and manganese, as well as copper and nickel. In the light of this background information, it was decided to conduct solution sampling on the rock surfaces on the six CSIRO approved sites within the 2 km radius of the Pilbara Nitrates plant. The rock irrigation data was done in conjunction with surface measurements of the pH and chloride ion activity. The wash solutions were analysed for sulphate, sulphite, nitrate, and nitrite ions, as well as for oxalate, which was found on three of the 16 reference rocks. The electrical conductivity of the wash solutions was also measured as a guide to the overall nature of the soluble minerals and salts that were mobilised during the five minutes of sample collection.

Field work was conducted on the six monitoring stations around the Yara plant in October 2020 and an additional site 4, which is close to the service road near the Woodside old flare tower. This report includes commentary on the interpretation of the colour measurements from the Konica Minolta Chromameter. The sites are part of the CSIRO colour and mineralogy monitoring of the Burrup that has been undergoing continuous evaluation for the past 14 years. In addition to conducting the required ASD spectrophotometer readings, used to determine the mineralogy of the rock surfaces and that of the associated engravings, and the chromameter measurements, a series of pH, chloride and redox potential readings were taken directly on the rocks themselves or at sites adjacent to the CSIRO monitoring points. Owing to electronic communication issues between the laptop and the ASD spectrometer at the first measurements on site 5, it was not possible to get this data in 2020. Data from the flat surface pH, chloride electrodes and redox potentials was combined with analyses from distilled water irrigation of the rocks. These analyses included all metal ions and chloride, nitrate, nitrite, oxalate, and sulphate anions. The refrigerated samples were stored off site until they were

transported by air to the Bentley based laboratories of the ChemCentre for independent NATA accredited chemical analyses.

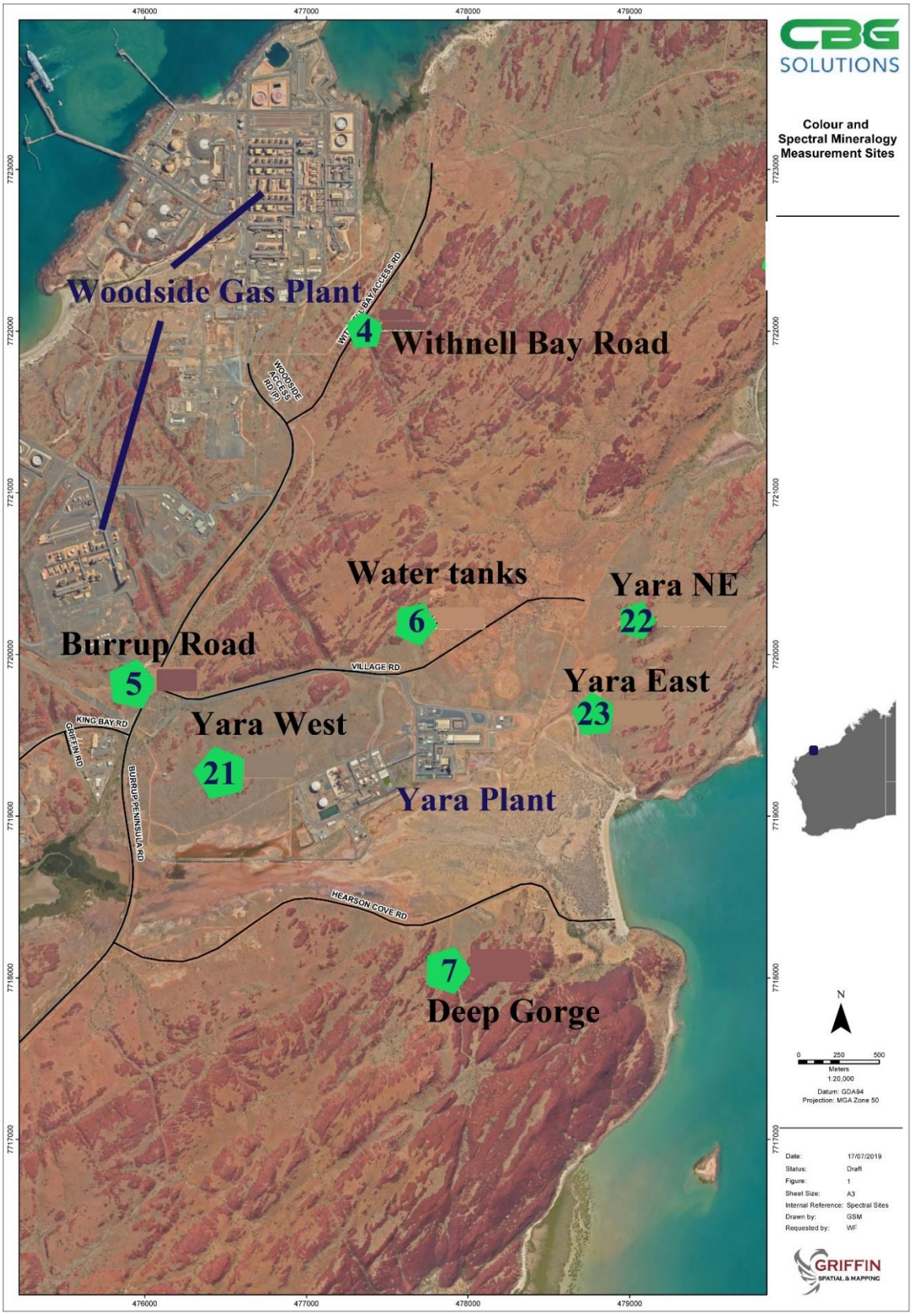

Figure 2: View of the Yara monitoring points in the Burrup peninsular

This report examines in detail the solution chemistry and provides a synthesis on the historical data relating to two sets of solution and surface pH measurements conducted in 16-17 years before the present work was conducted. The referenced sites of interest to Yara included granophyre at the Burrup Road (5), the Water Tanks (6) and Yara West (21) sites, while gabbro rocks were found on sites at Deep Gorge (7), Yara North East (22) and Yara East (23). All these sites lie within a 2 km radius of the present operational sites of the ammonia plant and the Technical Ammonium Nitrate (TAN) site. The additional site that was chemically assessed was number 4, adjacent to the Woodside plant about two hundred metres from the flare tower (see Figure 2).

Measurement of the rock surface pH and chloride concentration

The pH and chloride ion measurements taken on rocks adjacent to the CSIRO reference engraved sites in cases where concern was held regarding potential impact of the pH, chloride, and redox measurements. Other than for sites 6, 7 all measurements were done directly on the CSIRO rocks. The pH data was recorded using a flat surface pH electrode which had been calibrated each morning using standard pH buffers at pH 4 and pH 7 before the field measurements commenced. The pH meter was temperature compensated using a thermocouple connected to the TPS Aqua pH meter (pH/ORP/^{o}C) and the glass electrode was a VWR model no W7567287. Readings of the surface pH were standardised by recording the values after an elapsed interval of one minute. If the surface was more responsive and the pH reading stabilised in 40 seconds, then that value was recorded and keeping the probe in position did not alter the steady value that had been noted. Owing to the porous nature of the rock substrate prolonged equilibration times can result in pH values that are not reflective of the local microenvironment. A small amount of water is needed to keep the bulb wet and the solution in contact with the internal reference electrode. The electrical circuit of the pH electrode is completed through connecting the internal Ag/AgCl reference electrode through two fine wicks which are situated at 180^{o} to each other on either side of the glass membrane and held in place by the soft plastic ring fitting inside the 12-mm external diameter solid epoxy body. The chloride ion activity was measured using a TPS WP-90 ion-pH-mV-^{o}C meter coupled with an Orion Thermo 1609-186881 chloride ion specific electrode. The rocks were wetted with two drops (0.08 ml) of a 0.05 molar sodium nitrate solution to provide an electrolyte to stabilise the liquid junction between the sensing head and the rock surface. Stable readings of the chloride activity were obtained within a minute. The electrode was calibrated daily with a 1,000 and a 100-ppm chloride reference solution before any field measurements were made.

Analysis of sea borne salts on the rocks

The amounts of surface chloride detected on the rock surfaces provide direct evidence of the impact of the marine environment and indicate that salt weathering of rocks, with extensive dehydration and rehydration cycles apparently playing a significant role in the local environment. The wash solutions from the rock surfaces showed up a range of ions commonly associated with sea water, namely Na^{+}, K^{+}, Mg^{2+}, Ca^{2+}, Cl^{-} and SO_4^{2-}. Analysis of the way in which the concentrations varied across the Burrup was consistent with known weather patterns of prevailing winds and proximity to the sea. When the wash concentrations of sulphate are plotted as a function of the chloride, most of the data follow a linear relation that reflects the common ratios of the anions that are found in seawater. Data from the most recent irrigation data obtained in October 2020 is shown in Table 1. Significant differences from the normal ratios found in seawater are found on the rock surfaces in the Burrup, which is due to the interaction of electrolytes with the surface minerals found on the rocks.

The microenvironment of the rocks was assessed through a combination of surface chloride (Orion Thermo combination Cl electrode) and surface pH (WVR flat electrode) measurements on the rock surfaces. The first round of measurements was made using a 0.05 M $NaNO_3$ solution in distilled water electrolyte was used for chloride measurements and the pH was recorded after equilibration with two to three drops (0.04-0.06 ml) of distilled water on the rock surface. The Chemistry Centre of WA

determined the soluble nitrate, nitrite, sulphate, chloride, oxalate concentrations on the rock surfaces by ion chromatography from the distilled water washings which covered a 200 cm^2 area. Metal ions in the wash solutions were determined by inductively coupled plasma–mass spectrometric (ICP–MS) methods. This study is based on an initial survey in June 2003 (winter) of relocated engraved rocks which was then extended in August 2003 (spring) to include several sites located at a distance from known emission sources was concluded in February 2004 (summer) with repeated measurements on the Burrup. Data obtained for the 2017-2020 measurements for cations measurements were made on 200 ml samples and anions in 100 ml sample bottles collected over an area of approximately 500 cm^2. The main difference in the data collection method was that this year two adjacent rocks were washed with ultra-pure water in order to test the reproducibility of the measurements. Generally, the results of the general test of electrical conductivity of the wash solutions, gave agreement within the range of ± 5% of the values, which is remarkably close agreement (Appendix III). Where the deviations on specific anions and cations were noted, the differences were understood in terms of the local microenvironment of the rock e.g., if it was more exposed or sheltered than the other one tested.

Table 1: Ratio of salts in sea water and in the rock washings around the Yara plant

	Rock	Cl^-/Na^+	Cl^-/SO_4^{2-}	Cl^-/Ca^{2+}	Ca^{2+}/K^+	Ca^{2+}/Ba^{2+}	Mg^{2+}/Ca^2	Na^+/K^+
Sea water		**1.8**	**7.1**	**47.0**	**1.0**	**8,000**	**3.1**	**27.0**
Site 4 a	Granophyre	31	155	78	1	211	25	3.3
Site 4 b		34	130	78	1	250	22	2.3
Site 5 a	Granophyre	27	140	54	1	250	15	1.9
Site 5 b		44	78	78	2	129	24	3.5
Site 6 a	Granophyre	21	22	17	1	260	5	1.0
Site 6 b		22	39	26	1	226	8	1.1
Site 7a	Gabbro	20	20	22	4	550	7	4.0
Site 7b		15	9	12	5	741	4	4.0
Site 21 a	Granophyre	17	19	28	2	353	9	2.7
Site 21 b		25	40	36	2	310	12	3.3
Site 22 a	Gabbro	1	2	2	1	444	0.3	3.0
Site 22 b		-	-	-	2	333	0.3	3.0
Site 23 a	Gabbro	15	16	17	4	645	5	4.4
Site 23 b		4	5	10	2	887	2	5.3
CMs a*	Granophyre	50	75	60	3	385	20	3.0
CMs b		26	62	44	1	333	14	2.4

*CMs relates to the large split rock approximately 3 metres to the left of the main Climbing Man panel.

Moving sequentially across the columns in Table 1, only the hilly exposed site 22 and the second rock at site 23 show the "normal" seawater ratio of Cl/Na of 1.8 ±0.2; there was no chloride detected in one of the two washings at site 22 and this is likely due to a localised rain event. In general, it is most likely that the cause of the lower activity of sodium ions is due to them being bound onto surface reactive iron (III) minerals through characteristic ion-exchange processes. The granophyre rock sites at site 5a, 21b and at Climbing Man split rock all reflect average sea salt levels of chloride to calcium, while the other rocks have significantly lower ratios which indicate that the acidity has been mobilising calcium bearing minerals. The data on the ratio of $^{Ca}/_{K}$ is consistent with sea salt deposition but for the gabbro rocks at sites 7a, 7b and 23a the elevated ratios is an indication of potassium being adsorbed by the clay like minerals on the weathered rock surfaces.

The much higher calcium content of the gabbro rock crust, 10.9±1.9% CaO, compared with the granophyre crust of 1.4±0.8 % CaO, is reflected in the relative amounts of calcium to barium for the mean $^{Ca}/_{Ba}$ ratio for gabbro rocks was 653 ± 170 while the granophyre rocks had a mean ratio of 271 ±

74 : these differences in ratios are experimentally significant as the difference between the means is 1.6 times the sum of the standard deviations in the ratios in the wash solutions (Ramanaidou and Fonteneau, 2017). Detailed discussions regarding the low sulphate concentrations in the washings from sites 4 and 5 give rise to the high ratios of chloride to sulphate ratios. It is interesting to note that both these sites are close to the old flare tower of the NW Gas Shelf plant (Woodside partnerships) for site 4 and to Pluto for site 5, which strongly supports that these exhaust sources are not resulting in any significant SO_x deposition on the rock surfaces. A few hundred metres up the Climbing Man gully there are also high $^{Cl}/_{SO4}$ ratios at the split rock (a) and on the rock 3 metres below it (b) close to the floor of the gully. Other causes of lower sulphate activity on the rock surfaces includes interactions with clay minerals and with formation of stable surface-active minerals such as jarosite when acidic sulphate solutions react with iron (III) hydroxy oxides. There appears to be no systematic reason for the variable ratios of sodium to potassium, which are well below the 27 value for normal seawater. This is most likely due to the solubilisation of potassium ions from clay minerals on the reactive rock surfaces across the Burrup.

Environmental monitoring by Yara at weather stations

In conjunction with its normal environmental procedures Yara has three environmental monitoring stations at Burrup Road (site 5), the Water Tanks (site 6) and at Deep Gorge (site 7) for which data on the nature of the electrolytes and the pH of rainfall is recorded (Figure 3). The water is analysed for nitrite, nitrate, chloride, and sulphate, among other species and traditional variable such as hardness.

Figure 3: Location of the environmental monitoring stations around Yara plants

Key observations from the four sets of records for each of the monitoring locations between January and October 2020 are that the alkalinity of the rainwater generally follows the sodium levels, which is normal for salt levels coming from the windborne dispersal system of the local aerosols. The regression analysis follows equation 1,

$$pH_{rain} = 6.11 + 0.0079\,[Na^{+}]_{ppm} \quad \text{.....(1)}$$

For this regression equation the R^2 was 0.924 and covered six data points. The intercept value is slightly more acidic than would be expected for CO_2 saturated distilled water.

Of greater relevance is the response of the rainwater pH to the amount of soluble nitrate and in this case some of the complexities associated with the sites becomes apparent, for there are two different responses of pH. One is deemed an "active" response where the pH systematically falls in accordance with equation 2,

$$^{active}pH_{rain} = 6.82 - 8.88\,[NO_3^-]_{ppm} \quad \text{.....(2)}$$

which has an R^2 value of 0.93 and the associated errors with the intercept are ± 0.09 and the slope is ± 1.12, which represent errors of 1.3% and 12.6% respectively. When the mean rock surface pH is plotted as a function of the soluble nitrates, the slope in 2020 was -8.7 ± 1.12, which is experimentally the same as the pH dependence of the "active" rainwater. This is the first time that it has been possible to directly correlate the rainwater microbiological activity with that observed on the rocks. The difference in the data between "active" and "passive" or sterile rainwater is illustrated in Figure 4 below.

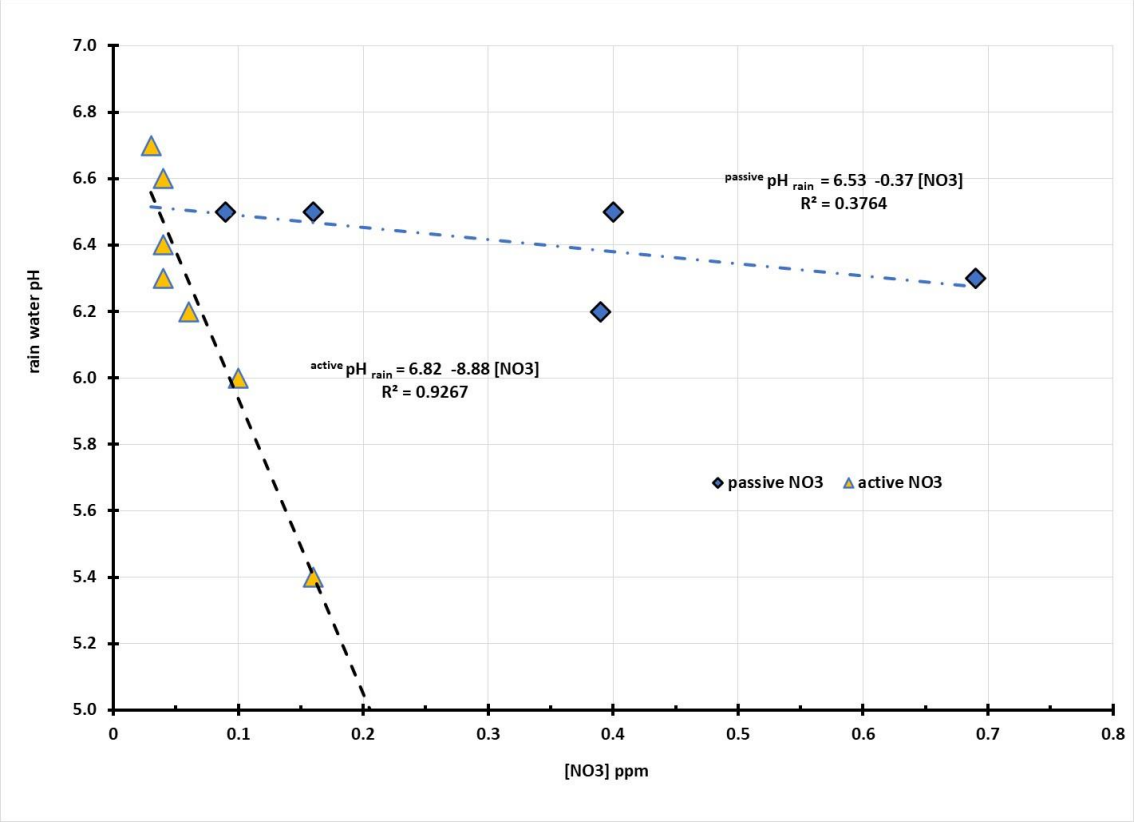

Figure 4: Plot of pH of rainwater from Yara monitoring points vs nitrate concentration

The rainwater pH value of the intercept for the nitrate response for the "passive" water samples was 6.5 which is noted as being the natural pH of CO_2 saturated distilled water. There are no systematic site differences between the rainwater collected at sites 5, 6 and site 7. The monitoring station at Deep Gorge was physically relocated from its former position at the foot of the hill on which the rock is located to a new position closer to Hearson's Cove. This took place between the 7-9 April 2020 and this does not seem to have materially affected the documentation or the biological activity reported (by inference) in the rainwater.

There was no systematic relationship between the amount of ammonia in the rainwater and the pH; the mean [NH_3] concentration was 0.10 ± 0.05 ppm with samples spread across the three sampling stations. However, when the rainwater pH was plotted as a function of the total nitrogen the regression analysis gave an R^2 value of 0.96 and the pH intercept at zero total nitrogen was 7.12 ± 0.13 and the slope of equation 3 was -4.33 ± 0.53 pH/ppm total Nitrogen,

$$^{rainwater}\ pH_{2020} = 7.12 - 4.33\ [N_{total}] \quad \text{.....(3)}$$

When the pH of the rainwater was plotted for the "passive" water samples as a function of total nitrogen there was a better fit to a linear regression than when the rainwater pH was plotted against the $[NO_3]$ concentration as the R^2 value increased from 0.38 to 0.50.

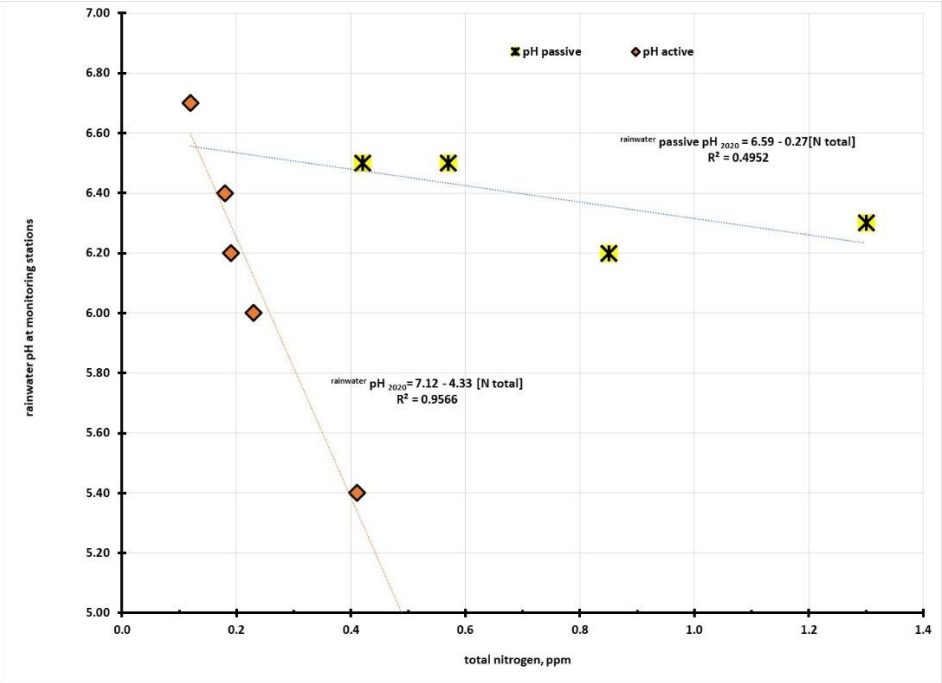

Figure 5: Plot of $^{2020}\ pH_{rainfall}$ at monitoring stations at sites 5, 6 & 7 vs. total nitrogen

The collected environmental data from the three monitoring stations, see Figure 3, also provides an insight into the nature of deposition of materials such as nitrate ions onto rock surfaces. When reviewing the nitrate content of the rainfall as a function of time it is readily apparent that in late May 2020, there was a spike in the average amount of nitrate found in the rainfall across the three monitoring stations and this may reflect opportunistic transport of the background NO_x into nitrate by reaction with the rainfall which took place on 24th/25th May 2020 (Figure 6). Data from Yara Environmental monitoring team indicated that the prevailing winds were from the North East at that time which would have brought emissions from the plant to site 5 (Burrup Road) but not to the Water Tanks site (no 6). The background NO_x emissions are around 15 mg/m^3 from the plant while the package boiler contributes between 170-90 mg/m^3. Site 6 is 1.1 km from the main plants while sites 5 and 7 are equidistant at 1.4 km. The Bureau of Meteorology records for Karratha indicated that there was 34 mm of rain that appears to have been reasonably widespread but the monitoring stations at site 5 reported 7.3 mm, site 7 some 9.8 mm and site 6 a total of 11.8 mm on the 24/25 May, so there is clearly the chance of very polarised rainfall in the region (MacLeod and Fish, 2021).

Records from the plant operators indicate that there are short-term NO_x plumes associated with the start-up of the TAN plant. This data is valuable in that it shows the direct interaction of anthropogenically sourced gases with exposed surfaces, such as rocks and monitoring stations. Future monitoring work will involve sampling of rocks and soils adjacent to the Yara monitoring stations to develop a conversion parameter that will enable emissions (mg/m^3) into solution concentrations of mg/litre so that acid loads, in terms of milliequivalents, can be calibrated across the monitoring stations.

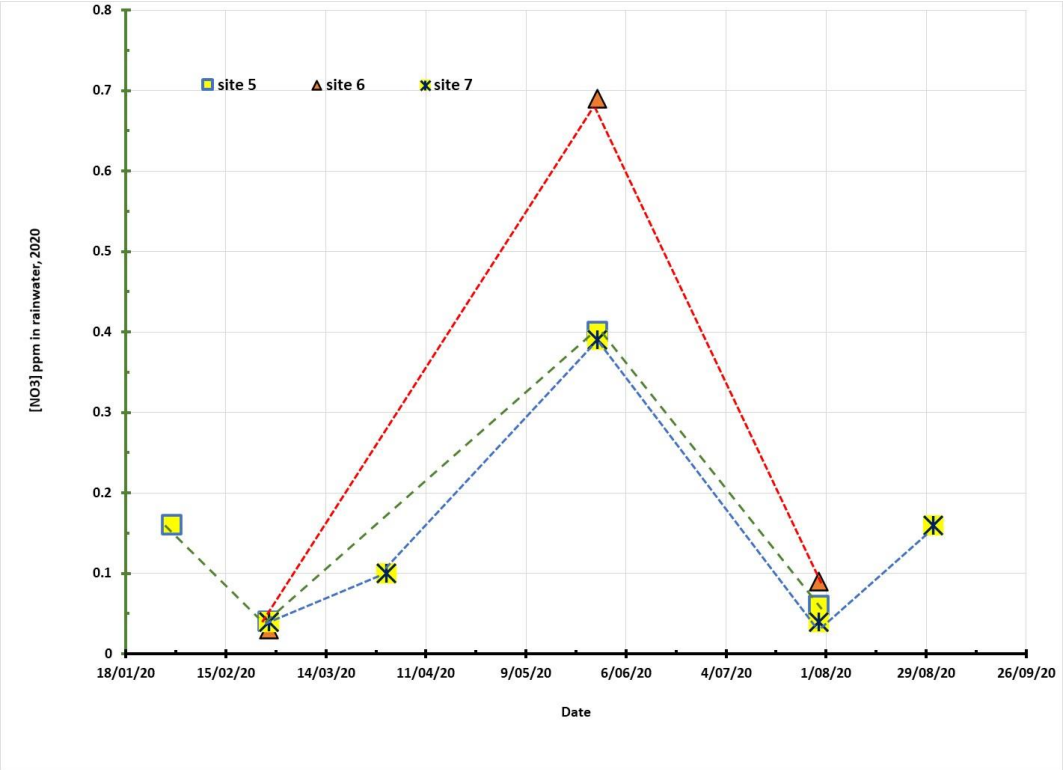

Figure 6: Distribution of nitrate across sites 5, 6 & 7 February to August 2020.

Support for the aerosols from the ocean being deposited on the Burrup rocks as being the primary sources of naturally alkaline materials comes from examination of the electrical conductivity of the filtered wash solutions. The data collected in 2020 provides strong evidence supporting this view, since there are sixteen sets of measurements across the eight sites, as shown in Figure 7.

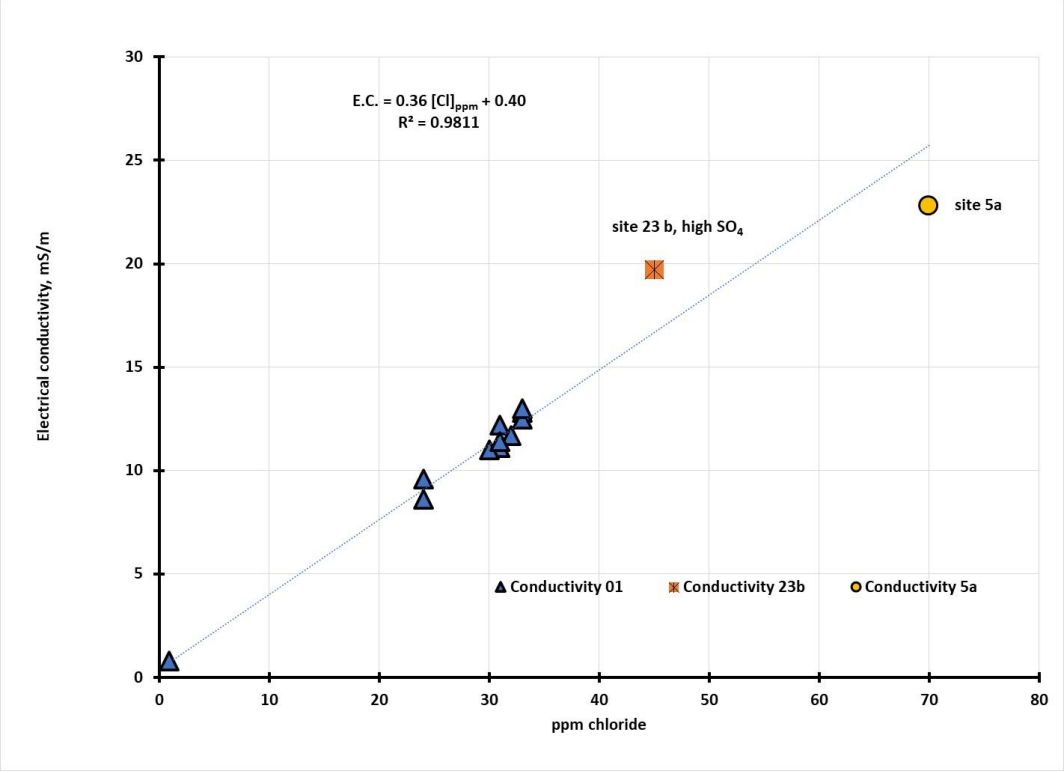

Figure 7: Plot of October 2020 electrical conductivity versus chloride in washed rocks

Since chloride is the dominant anion in seawater, it is appropriate to plot the electrical conductivity against the chloride concentration and only two of the sixteen sites deviated from a linear relationship, shown in Equation 4, and shown in Figure 7

$$\text{Electrical Conductivity} = 0.40 + 0.36\ [Cl] \quad \text{.....(4)}$$

The only significant deviation from the linear response shown in the graph and defined by Equation 4, was found on site 23b, which had higher than expected conductivity and this corresponded with higher sulphate concentration. The cause of the elevated SO_4^{2-} is not known at this stage. Site 5a at the Burrup Road location had a concentration of 5×10^{-4} ppm lead and 2.8×10^{-2} ppm zinc which may result in some formation of soluble lead complexes and hydroxy chlorides of zinc that would have resulted in diminished chloride activity and hence lower electrical conductivity than expected.

Interpretation of solution chemistry and cation mobilisation

Because the concentrations of cations in the wash solutions are low, it is more convenient to use a logarithmic value, expressed as pM, in the same format as pH represents the hydrogen ion activity. Higher pM values mean less metal ion activity since pM is equal to the log of the inverse of the metal ion concentration. When mineralisation (rock corrosion) products from the weathering of the rock crusts are dissolved this involves neutralisation of either oxides or hydroxides of metal ions. When metal hydroxides are mobilized by acid dissolution the generic dissolution reaction can be written in the form show in Equation (5),

$$M(OH)_n + n\ H^+ \text{ —> } Mn^{n+} + n\ H_2O \quad \text{.....(5)}$$

In equation 5 the *n* value is the oxidation state of the metal, typically 2 and 3 for iron and mixtures of 2, 3, 4 etc. for manganese. The concentration of the metal ions is derived from the general equilibrium constant for the dissolution of a metal hydroxide into the component elements. Thus $K_{sp} = [OH^-]^n \times [M^{n+}]$, is mathematically the same if we rewrite the expression using the reciprocal values i.e.

$$^1/K_{sp} = \{^1/_{[OH^-]^n}\} \times \{^1/_{[M^{n+}].}\} \quad \text{.....(6)}$$

Since the logarithm of $\{^1/_x\}$ is pX, then equation 6 can be expressed by the formula

$$pK_{sp} = n\ p[OH] + pM_{OH} \quad \text{.....(7)}$$

The formula, $p[OH] = pK_w - pH$, can be substituted into equation 7 then rearranged to give equation no 8, remembering that the self-ionisation constant of water, pK_w has a value of 14.

$$pM_{\text{ hydroxides}} = pK_{sp} + n(pH\text{-}14) \quad \text{..... (8)}$$

Thus, for plots of the pM values for metal ions the intercept at zero pH is equal to (pK_{sp} -14 *n*). For metal oxides of the general formula M_xO_y dissolving to give metal ions and water, the concentration of the metal is given by Equation 9,

$$pM_{oxides} = {}^1/x\ \{pK_{sp}\} + 2\{y/x\}\ pH \quad \text{.....(9)}$$

When the pM values are plotted as a function of pH it is theoretically possible to determine if the dissolution process involves a hydroxide, which has a slope of *n* for the pM vs. pH plot. If the product dissolving is a mixed valency oxide, the slope of the pM vs. pH plot is $2^y/_x$, if the soluble ion is an un-complexed free metal ion.

Mobilisation of calcium and barium

Calcium solubility from 2003-2020

The most significant difference in the behaviour observed at the beginning of the monitoring program is that for the February 2004 data there was a change of mechanism of solubilisation of calcium as the slope of the p [Ca] vs pH plots changed from one (Equation 10) to two in 2004 (see Table 2). The most likely mechanism is that for a 1:1 reaction it is the dissolution of calcium carbonate to form a soluble bicarbonate complex,

$$CaCO_3 + H^+ \rightarrow Ca(HCO_3)^+ \quad \text{.....(10)}$$

This is the reaction that dominates the solution processes for the 2003 and the results from 2017-2020. Owing to the changed microenvironmental conditions the mechanism changed to a 1:2 reaction

for February 2004 in which the calcium carbonate would have dissolved fully as the disassociated bicarbonate, as shown in Equation 11.,

$$CaCO_3 + 2\ H^+ \rightarrow Ca^{2+} + H_2CO_3 \quad \text{.....(11)}$$

The most likely reason for the change in mechanism is due to the increasing acidity of the local environment, as the mean pH changed by - 0.7 or an increase in acidity by a factor of five, as seen in Table 2 below. For calcium minerals, the slope in 2017, 2018, 2019 and again in 2020 is for dissolution as the bicarbonate. So, apart from an excursion during the acidic period in February 2004, the original slope or pH dependence of calcium solubility as originally observed in August 2003. The mean slope moved upwards to 1.5 (a mixture of reactions involving equations 10 and 11 on a 1:1 basis) in August 2019 when the acidity moved back towards the February 2004 values. With the impact of cyclone Damien in February 2020, the mean pH increased by 0.6 i.e., the acidity decreased by a factor of five times and the stoichiometry of the mobilisation of calcium minerals moved back to equation 10 or loss via formation of the soluble calcium bicarbonate.

Table 2: Solution properties of calcium and barium washings on the Burrup rocks

Date	mean pH	mean p[Ca]	mean p[Ba]	slope p[Ca]/pH	slope p[Ba]/pH
August '03	5.0 ± 0.5	3.6 ±0.4	6.6 ± 0.2	1.0 ± 0.1	0.4±0.2
February '04	4.3 ± 0.5	4.1 ± 0.6	7.2 ± 0.4	2.0 ± 0.2	2.0
November '17	5.7 ± 0.5	2.0 ± 0.6	5.2 ± 0.3	1.3 ± 0.3	0.5±0.1
Sept. '18	5.5 ± 0.8	3.3 ± 0.2	7.9 ± 3.2	1.3 ± 0.5	0.2 ± 0.1
August '19	4.6 ± 0.3	4.4 ± 0.6	7.5 ± 6.3	1.5 ± 0.2	2.4 ± 0.7
October '20	5.2 ± 0.5	4.5 ± 4.1	7.7 ± 4.7	1.2 ± 0.2	1.1 ± 0.2

The data presented in Table 2 is shown graphically in Figure 8 where there is a clear correlation between the increasing acidity of the sites and the number of protons involved in the mobilisation of calcium ions.

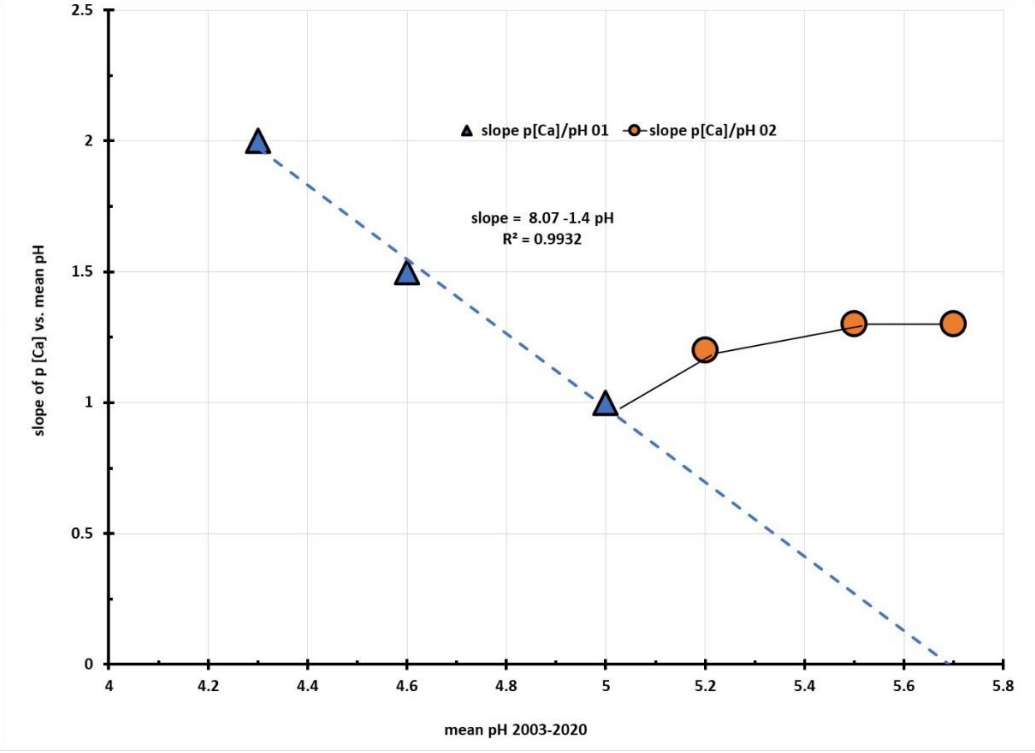

Figure 8: Plot of the seasonal variation in slope of p[Ca^{2+}] vs. pH 2003-2020

The impact of the release of ammonia, which acts as a pH buffer on the rocks, and of cyclonic rainfall is shown by the three points from August 2003, February 2004 and August 2019 form the regression line shown in Figure 8 and equation 11,

$$\text{Slope p [Ca]/pH}_{\text{seasonal}} = 8.07 - 1.4\ \text{pH} \quad \text{.....(11)}$$

The measurements from 2017, 2018 and 2020 lie as the orange circles off the regression line as these reflect the impact of cyclonic rainfall resetting the acidity clock on the rocks. It is now readily apparent that the solubility of calcium on the rock surfaces is directly affected by the mean acidity of the environment.

The chemical analysis done by CSIRO on the mineralogy of the rock crusts' weathered zones did not show up any significant amounts of barium, so it is considered likely that the presence of varying amounts of this heavy alkaline earth metal came from the sea. The chemistry of the barium minerals was considered a likely candidate to see if there was any systematic change in the rock chemistry from the time of the original measurements made in 2003 and the present round of data collected in 2020. Plots of the p[Ba^{2+}] versus pH did not follow any monotonic trend but for the more acidic years in 2004 and 2019, the slopes had a 2:1 stoichiometry which is consistent with acid dissolution of barium oxide, Equation 12, viz.,

$$BaO + 2\ H^+ \rightarrow Ba^{2+} + H_2O \quad \text{.....(12)}$$

A similar stoichiometry would be obtained for the acid dissolution of barium carbonate. With the more alkaline mean pH values observed in November 2017 (5.7 ±0.5) and ten months later in September 2018 (5.5 ± 0.8) the slope is 1.5, which means that there is a mixture of barium dissolving as a possible bicarbonate and a free barium ion. The mean ionic product of barium and sulphate for the 2020 wash solutions was 1.5 x 10^{-13} and barytes or $BaSO_4$ has a pK_s of 9.6, which gives an ionic product of 2.5 x 10^{-10} which is more than 1,650 times the mean ionic product and so no barium will be lost as barium sulphate.

Mobilisation of metal cations from the rock surfaces

Boron

The sixteen rock washings provided an opportunity to see how mobile various transition and p-block metals responded in the post cyclonic rain environment. The most soluble species was boron, with a mean pM of 5.90, which in common corrosion use could be said to be "corroding" from the rock surface since its mean concentration was 1.3x 10^{-6}M. Plots of the pM vs. pH data from October 2020 had a slope of +⅓, which on first glance appears to be anomalous. However, the equilibrium between H_3BO_3 and $HB_4O_7^-$ is governed by equation 13,

$$4\ H_3BO_3 \rightarrow HB_4O_7^- + H^+ + 5\ H_2O \quad \text{.....(13)}$$

For this equilibrium, the relationship between boron solubility and pH is

$$p[B] = -2.28 + ⅓\ pH \quad \text{.....(14)}$$

This data in summarised in Table 3, along with the transition metal ions. In determining the origin of the boron on the rocks it is instructive to look at the ratio of chloride to boron in the wash solutions, since the borate buffer system is the second most important to the carbonate system, which controls the pH of normal seawater. Chloride ions are dominant anion at 18,980 ppm in normal sea water and the boron level is only 4.6 ppm, giving a ratio of $^{Cl}/_{B}$ of 4,126 and for the 2020 Burrup rocks the mean ratio was 2,454 ± 434. There was no statistically valid difference between the ratios observed on the granophyre compared with the gabbro rocks. The cause of the 40% reduction in the chloride to boron ratio indicates that both the gabbro and the granophyre rocks are providing additional sources of boron through their own mineralogy. The detailed examination by CSIRO of the parent and weathered rock surfaces of the gabbro and granophyre rocks in the Burrup has provided an exhaustive list of the minerals that are present in the mineral crusts on the gabbro and granophyre rocks (Ramanaidou et.al. 2017). The main boron containing mineral in the Burrup rocks is chlorite, which is a complex sheet silicate mineral $(Mg,Al,Fe,Li,Mn,Ni)_{4\text{-}6}(Si,Al,B,Fe)_4O_{10}(OH.O)_8$. For more details regarding the complex solution chemistry of boron, the reader should peruse the Pourbaix Atlas (Pourbaix 158-167).

Mobilisation of transition metal cations

Analysis of the wash solutions collected in October 2020 showed that only site 23, Yara East, had any measurable iron in the washings from the two assessment rocks. The concentrations were just above the detection limit at 0.006 ppm on rock *a,* and 0.012 ppm at rock *b*. These values represent 1.1 and 2.1 x 10^{-7}M respectively and in summary the major impact of cyclone Damien on the Burrup rock art monitoring points is that the heavy rain stopped iron being lost to the environment. The concentration of zinc increased from a pM of 7.15 in 2019 to 6.84 in October 2020 and the species being dissolved (mobilised) seems to be different, owing to the fall in the pM vs. pH slope from +1.7 to +0.5. There are no common zinc minerals that give rise to this pH response, so it is likely that the zinc from the rock surfaces is bound up with other oxides and hydroxide species, which are being mobilised during the same acidification processes. For the first time since monitoring began for Yara in 2017 there was no chromium detected in the 16 wash solutions. Additionally, only sites 4b and 23b gave any vanadium in solution and the average level was quite small at 2.9 x 10^{-9}M and is very insignificant. Site 5a gave the only measurable amount of cadmium at 0.0003 ppm or 2.7 x 10^{-9}M, which is almost vanishingly small. Similarly, there was 0.0001 ppm (1.7 x 10^{-9}M) cobalt at site 6a and 23b and these metal ions are naturally found in the volcanic rocks that characterise the Burrup.

Table 3: Summary of solubility dependence of metals at monitoring points

Element	Mean pM	Standard deviation	pM vs. pH slope
Boron	5.90	0.16	4.07 + 0.33 pH
Copper	7.91	0.34	3.03 + 1.0 pH
Lead	8.99	0.29	7.04 + 0.43 pH
Zinc	6.84	0.31	4.00 + 0.50 pH

In terms of metal dissolution reactions, it is common to interpret an equilibrium metal ion concentration of 10^{-6} M or pM^{n+} of 6.0 as being essentially as "no corrosion" and so the only metal ion that just falls into that category is boron at a mean pM_B of 5.9 ± 0.2 (Pourbaix 1974). While there is discernible mobilisation of the metal ions, given the high sensitivity of the analytical methods used at the Chemistry Centre of WA, it cannot be said that there is active mineral dissolution at the sites that were examined. For copper, the mean pM Cu of 7.9 ± 0.3 comes with a 1:1 pM to pH slope, which is consistent with the dissolution of tenorite (CuO) from the mineral surfaces. It is noted that the mean solubility of zinc is higher than for copper than for lead and this is in line with the normal solubility trends for metal ions in the natural environment.

Interpretation of the pH effects on iron and manganese mobilisation in the rock patina

Previously published work by MacLeod (2005) and MacLeod et. al. (2017, 2018) has shown that at the pH values recorded in 2003 and 2004 (Appendix IV) there was measurable mobilisation of iron and manganese containing minerals. Analysis of the wash solutions from the early data sets has shown up significant concentrations of aluminium, iron, manganese, nickel, copper and some zinc and lead from the parent rock crusts. Because the mineralogy of the highly weathered gabbro and granophyre is characterized by a series of mixed amorphous iron—manganese oxides, in the form of desert varnish, iron(III) oxy-hydroxides and weathered minerals such as smectite, kaolinite, illite and mica (Clark 2004) it is not unexpected to find mobilization of metallic cations under the acidic conditions. It is helpful when undertaking a review of metal ion solubility to understand that the dissolution of the key elements in the rock patina is controlled by the pH or the acidity of the microenvironment.

The more acidic surfaces in the 2003 spring and the February 2004 summer measurements were amenable to this form of analysis and plots for iron showed that for both seasons the p[Fe] vs. pH plots have an average slope of +1.98 ± 0.06 pH which confirms the following mechanism:

$$FeOOH + 2H^+ \rightarrow Fe(OH)_2^+ + H_2O \quad \text{.....(15)}$$

The Pourbaix diagram for iron in the range of pH observed on the rock surfaces shows that the $Fe(OH)_2^+$ ion is the dominant form of soluble iron(III) under oxidizing conditions (Pourbaix 1974). The historic pH data for 2003-2004 is shown in Appendix IV. Similar plots indicate that copper is mobilized by dissolution reactions involving two protons per metal ion as is the case for nickel.

Using washing solution data for the mobilisation of aluminium allows similar plots for the solubility of aluminium with surface pH to be determined. For the Burrup rocks the aluminium mobilisation graphs had an average slope of 1.4±0.2 pH, which is consistent with the dissolution of kaolinite ($Al_2Si_2O_5(OH)_4$) to give the $Al(OH)_2^+$ ion and $AlSi_20_5^{+,}$ as shown in Equation 16,

$$Al_2Si_2O_5(OH)_4 + 3H^+ \rightarrow Al(OH)^{2+} + AlSi_2O_5^+ + 3\ H_2O \quad \text{.....(16)}$$

Kaolinite has been identified as one of the aluminium containing minerals on the Burrup rocks along with feldspar, chlorite, mica, smectite and some gibbsite (Clark 2004) and it was a major mineral identified in the CSIRO Accelerated Weathering experiments (CSIRO 2016). It is not unexpected for aluminium ions to have been mobilized under the very mild sample collection regime that was used. In October 2020 there was only one site, the Yara East site 23b, that showed aluminium in the solution washings at only 4.1 x 10^{-7} M which is close to the detection limit of 1.9x10^{-7} M. In the post cyclonic environment this data supports the supposition that mobilisation of alumino-silicates (clays) is not a rock art management issue. This information provides strong support for the lack of reactivity of the binding clay minerals in the post cyclone Damien environment.

Table 4: Mean pH and solubility of iron and manganese minerals from rock irrigation

Period	Mean pH	Mean p Fe	mean p Mn	Slope p Fe/pH	slope p Mn/pH
August 2003	4.97 ± 0.48	6.01 ± 2.60	7.17 ± 0.45	2.0 ± 0.1	0.9 ± 0.4
February 2004	4.78 ± 0.27	6.34 ± 0.44	7.31 ± 0.35	2.0 ± 0.1	2.1 ± 0.1
November '17	5.69 ± 0.51	6.80 ± 0.15	5.03 ± 0.35	0.3	1.1 ± 0.1
September '18	5.52 ± 0.84	Nil soluble	6.79 ± 0.35	Not applicable	1.2 ± 0.9
August '19	4.62 ± 0.26	6.18 ± 0.40	6.91 ± 0.48	0.40	2.3 ± 0.4
October '20	5.21 ± 0.51	6.8 ± 3.2	7.02 ± 4.2	Not applicable	1.1 ± 0.1

The lower standard deviation of the Feb 2004 and the Nov 2017 data on iron solubility provides evidence that the solubility of the iron minerals decreases with increasing pH, despite the apparent change of mechanism. Plots of the mean p[Fe] versus annual mean pH over the whole period of measurements from 2003 to 2020 shows that the slope is 1:1 until the solubility plateaus at a mean pH of 5.6, which was recorded in November 2017. In October 2020, only site 23 reported any soluble iron and even these values were close to the detection limit. The fourteen other samples returned zero soluble iron (see Table 4). As has been previously noted, manganese compounds are more soluble at neutral pH than their iron analogues are reflected in the 2017 data from the Burrup rock art washings when the mean solubility had increased to 9.3 x 10^{-6}M and the corresponding level of iron was 1.6 x 10^{-7}M or nearly sixty times less. The reasons for this lie in the ability of acidic metabolites to complex the cations found in the weathered crusts. The mean p Mn values show an average of 50 times lower solubility in 2018 than in 2017, pMn 6.8 for 2018 compared with 5.0 in November 2017, as seen in Table 4. The mean solubility of manganese has continued to decrease in 2019 and in 2020. With the decreasing manganese solubility, the iron levels are more dramatically affected by the changing pH, which is why there was only one site that had measurable amounts of iron in the wash solutions in October 2020. This observation is supported by data from Krauskopf (1957) who found that Fe compounds are less soluble than corresponding Mn compounds under naturally occurring Eh-pH conditions.

The concentration of manganese in the rock irrigation measurements done in October 2020 had a maximum of 2.0x10^{-7} M or a pMn of 6.70 at the Yara East (site 23) and when the data was plotted as

a function of surface pH, the regression analysis confirms that the likely dissolution reaction is shown in equation 15 for sites 4, 5 and 22 viz.,

$$MnO + H^{+} \rightarrow Mn(OH)^{+} \quad \text{..... (15)}$$

There was a high degree of fit of the pM and pH data, with an R^2 of 0.96, and so the pM vs. pH slope was 1.09 ± 0.12. For this equation (15) the intercept pH was 2.09 ±0.60 which simply attests to the insolubility of the MnO species in that it would need a 10^{-2} M solution of nitric acid to get a I M solution of manganese. For all the other measurement sites, the plots of pMn vs. pH gave slopes of 0.53 ± 0.10 for the Climbing Man split rock (sample 2), with sites 6 (water tanks) and site 7 (Deep Gorge) with an intercept at a pH value of 4.01 ± 0.57. The other sites at 5, 21 and 23 (Burrup Road, Yara west and Yara East respectively) had the same slope at 0.61 ± 0.12, which is statistically indistinguishable from the other three sites, with an intercept value of 3.99 ± 0.60 pH. In these cases, the dissolution of manganese from the rock surfaces follows the same pattern and mechanism but the stoichiometry is clearly something that does not relate to a separate mineral species containing oxides and hydroxides of manganese but is indicative of the dissolution of the rock varnish, with non-stoichiometric surfaces containing significant amounts of manganese.

Electrochemical characterisation of dissolution mechanism

Although in-situ measurement of pH and chloride ion activity has been part of the monitoring program since first measurements were done in June 2003, it was only after field experience on early bronze age sites in central Anatolia (Turkey) that the same methodology was applied to the rock surfaces as part of the Yara monitoring program in 2018 (MacLeod 2018). The measurement of the redox (reduction oxidation) potential is managed by placing a platinum wire electrode through a moistened sponge rubber to contact the rock surface and the reference electrode (an Ag/AgCl 1 M KCl reference) which is laid close to the point where the platinum electrode is placed, and this completes the electrical circuit.

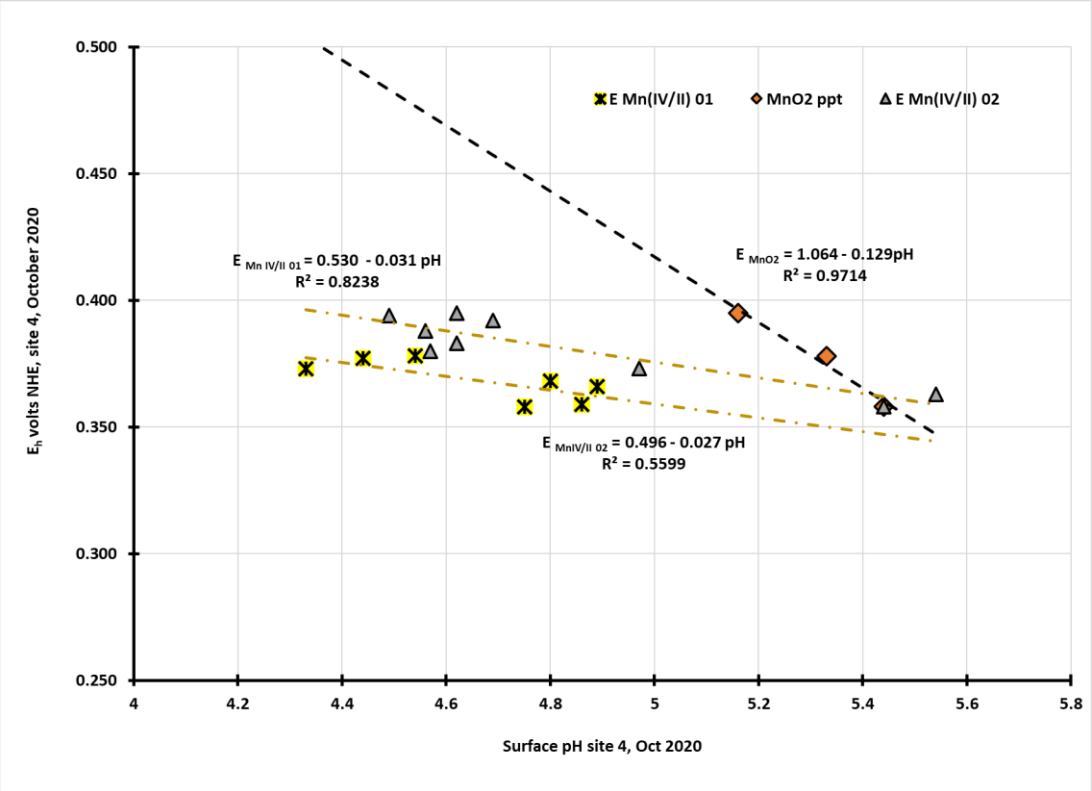

Figure 9: Pourbaix diagram for site 4, October 2020 showing two manganese reactions

The redox data is collated and then the combination of the redox potential (corrected to the normal hydrogen electrode via the calibration of the silver chloride reference voltage which was + 0.210 volts

vs. NHE) and surface pH is used to plot Pourbaix diagrams for each of the rock art monitoring sites. Inspection of the slopes in the Pourbaix diagram in Figure 9 shows that there are two mechanisms controlling the precipitation of solid phases and dissolution at site 4, at the head of the Climbing Man gully close to the Withnell Bay road. The reaction scheme shown in equation 16 is for the formation of insoluble MnO_2, in which four protons are released and two electrons are consumed,

$$Mn^{2+} + 2\ H_2O \rightarrow MnO_2 + 4\ H^+ + 2e^- \quad \text{..... (16)}$$

For this reaction, the slope of 129 ± 10 mV/pH is consistent with the formation of insoluble manganese dioxide as the outcome of an oxidative hydrolysis and precipitation reaction, since M^{4+} ions are only soluble in strong acid solutions since they readily undergo hydrolysis reactions at moderate pH values. The standard redox voltage, obtained by the regression analysis, at zero pH is the intercept value in the equation shown in Figure 9 and the value of 1.064 volts is consistent with the mechanism given in Equation 16. Details of the regression analyses for this and all the other 2020 sites are given in Appendix II and are summarised below in Table 5.

Table 5: Redox equations deduced from the October 2020 Pourbaix diagrams

Sites	slope, mV/pH	Intercept	Standard E^0
$Mn^{2+} + 2\ H_2O \rightarrow MnO_2 + 4H^+ + 2e^-$			**1.104**
4	-0.129	1.064	
$Fe^{2+} \rightarrow Fe^{3+} + e^-$			**0.771**
23	-0.064	0.665	
21	-0.062	0.669	
7	-0.059	0.732	
4	-0.064	0.673	
CM split	-0.055	0.708	
mean	**-0.057 ± 0.004**	**0.718 ± 0.029**	
$2\ Fe(OH)^+ + H_2O \rightarrow Fe(OH)^{2+} + Fe(OH)_2^+ + H^+ + 2e^-$			**0.490?**
23	-0.031	0.457	
5 i	-0.027	0.479	
4 i	-0.030	0.508	
mean	**-0.029 ± 0.002**	**0.481 ± 0.026**	
$Mn(OH)^+ + H_2O \rightarrow Mn(OH)_2^{2+} + H^+ + 2e^-$			**0.564**
22 i	-0.029	0.549	
22 ii	-0.033	0.557	
21 i	-0.033	0.568	
21 ii	-0.034	0.565	
7 i	-0.029	0.544	
7 ii	-0.030	0.542	
6 i	-0.028	0.541	
6 ii	-0.030	0.541	
5 i	-0.039	0.565	
4 ii	-0.033	0.542	
CM split	-0.038	0.595	
mean	**-0.028 ± 0.003**	**0.576 ± 0.017**	

The second type E_h/pH response shown in Figure 9 for site 4 shows the same slope of -29± 2 mV associated with an oxidative hydrolysis reaction that releases two electrons per proton, according to

equations 17 and 18. Although the slope of the Pourbaix plots is helpful in determining the ratio of protons to electrons, there are alternative relationships that both give the same slope, as shown in Equations 17 and 18

$$2\ Fe(OH)^{+} + H_2O \rightarrow Fe(OH)^{2+} + Fe(OH)_2^{+} + H^{+} + 2e^{-} \quad \text{..... (17)}$$

$$Mn(OH)^{+} + H_2O \rightarrow Mn(OH)_2^{2+} + H^{+} + 2e^{-}\ ^{-} \quad \text{..... (18)}$$

Inspection of the range of extrapolated voltages at zero pH, obtained from the regression analyses, indicates that the upper equation with the 0.530 volts relates to equation 18 and that the lower line with an intercept value of 0.496 volts vs. NHE is an indication that the iron equilibrium, expressed by Equation 17, describes the surface of the rock as measured at those points. The power of having the redox and pH measurements done on the rocks has thus been deftly described, for it demonstrates that there are competing equilibria across the rock surface, which in this case is approximately 2.4 square metres.

The changed pH on the rocks following reasonable drenching, at least on some of the surfaces, explains why there was no example of the formation of Mn_3O_4 , as shown in Equation 19, as there would have been insufficient free Mn^{2+} ions available for precipitative oxidation.

$$3\ Mn^{2+} + 4\ H_2O \rightarrow Mn_3O_4 + 8\ H^{+} + 2\ e^{-} \quad \text{..... (19)}$$

The theoretical slope for equation 16 is -0.118 pH per volt and so site 4 was the only one of the seven monitored sites that had this response. The Pourbaix data has provided unequivocal information about the competing reactions that are taking place on the surfaces of the rocks. The observation that there are electrochemically active sections of the rocks on sites 4, 7, 21 and 23 which show oxidation of free Fe^{2+} ions demonstrate the sensitivity of the electrochemical methods, since there was only soluble iron detected on rock 23. The only stable ionic species in the pH range of 4.0-5.5 is the Mn^{2+} ion. Redox processes that are commonly facilitated by fungi that reduce Mn(IV) species to Mn^{2+} ions (Gadd 2004). There is a direct increase in the manganese ions in the wash solution with increasing acidity of the rock surfaces. The solution chemistry of manganese is extraordinarily complex, with solid phases of Mn^{2+} being MnO and $Mn(OH)_2$, for Mn^{3+} there is Mn_2O_3 and for the mixed valence of Mn_3O_4, which is a mixture, like its iron analogue magnetite, of one Mn^{2+} and two Mn^{3+} ions. In addition, there are equilibria involving the precipitation of MnO_2 as in equation 16.

Part of the reason why there is a mixture of electrochemical reactions on the individual rocks can be gleaned from inspection of the pH data in the Appendixes or by looking at the annotated in Figure 10. Nigel Tonkin recorded the pH, chloride, and voltage data on all the sites, while MacLeod conducted the measurements. Statistical analysis of the pH data gives a mean value of 5.75 ± 0.43 with a maximum of 6.86 and a minimum of 4.94, indicating some local bacterial activity. Inspection of the data in Table 5 illustrates the complexity of the dissolution of manganese species from the solid phase is more complex because the only stable ionic species in the pH range of 4.0-5.5 is the Mn^{2+} ion.

Cyclone Damien had an impact on the rock surface at site 7 and the chloride profile across the rock surface shows increasing chloride activity on the right-hand side of the rock, which is closest to the ocean, the source of the sea salts.

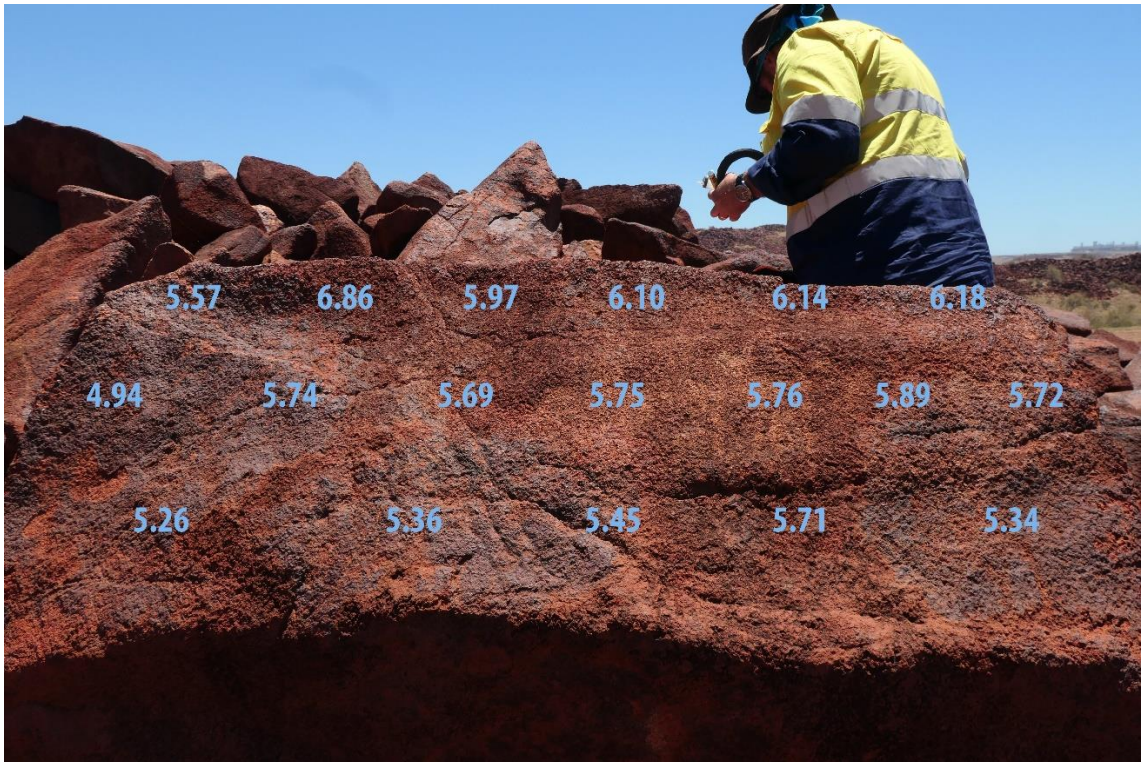

Figure 10: Deep Gorge site 7 with pH data recorded onto the image, October 2020

The extreme left of the rock was low in chloride, with values less than or equal to 5 ppm for the first 30 cm from the top to the bottom of the rock (Figure 11).

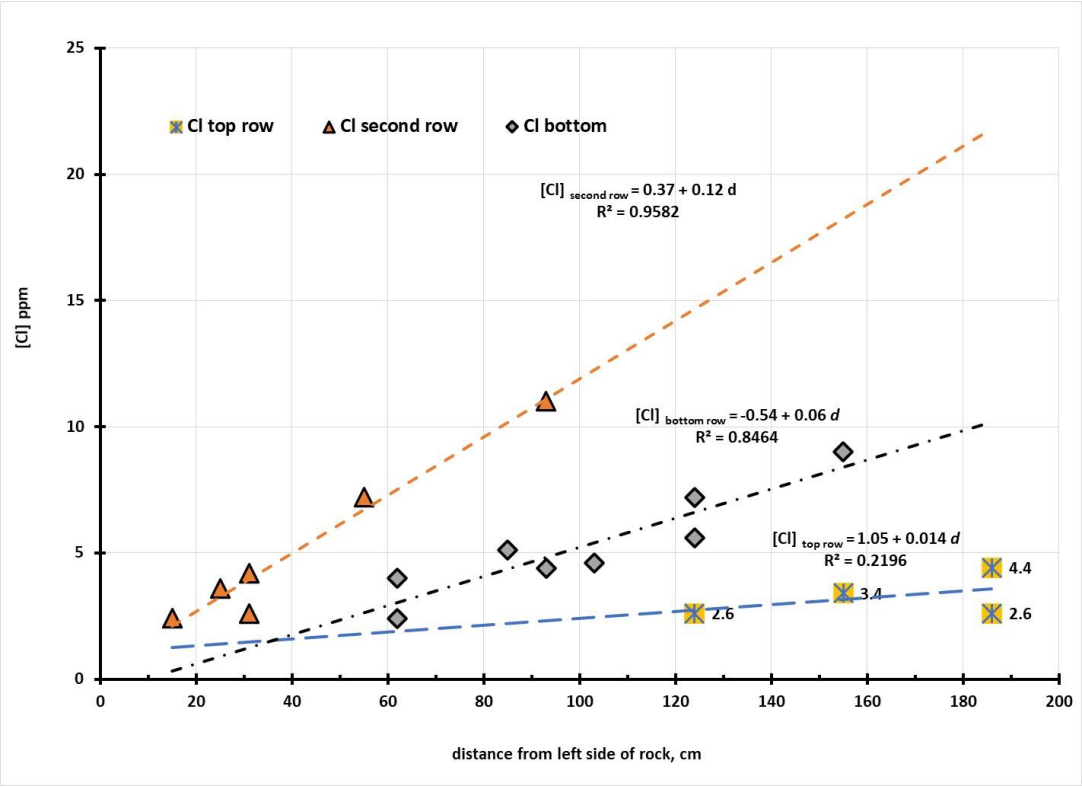

Figure 11: Plot of chloride distribution at Deep Gorge site 7, October 2020

There was a high degree of correlation, as measured by the R^2 for the second row of measurements, that showed a linear increase in chloride activity of 0.12 ppm/cm up to a maximum of 11 ppm. This relationship is given by equation 20,

$$[Cl]_{\text{second row}} = 0.37 + 0.12\,d \quad \text{..... (20)}$$

For this regression equation no 20, the value of *d* is the distance in cm from the left side of the rock. Although the total amount of chloride deposited in the eight months since the cyclone is not high, the gradient across the rock does show clear evidence of the increasing alkalinity due to deposition of sea salts. It is likely that the top layer of measurements is low in chloride ions because of night-time dew having mobilised the chlorides and moved them down to the middle of the rock, where evaporative concentration "held" them in place. The [Cl] distance slope of the second line of measurements is twice that of the bottom and 8½ times that of the top.

It is instructive to review the full range of pH data on this site, which dates to the first measurements in August 2003 and this information is shown graphically in Figure 12. A cyclonic rain event between August 2003 and February 2004 saw the pH increase from 4.6 to 5.0, thus a reduction in acidity by being washed with fresh water. The series of cyclonic rain events see Table 6, in between the years leading to 2017 saw the pH increase to 5.6, which is the natural pH of iron and manganese minerals hydrolysing in distilled water to produce a mildly acidic microenvironment. Solubilisation of Mn and Fe compounds in rock varnish can lead to removal of important compounds required to bind clay minerals to form the hard, outer layer of the varnish and to bind it to rock inner surfaces. A predominant Mn compound in rock varnish is birnessite, which has hexagonal structured sheets with binding clay minerals $\{(Na_{0.3}Ca_{0.1}K_{0.1})(Mn^{4+},Mn^{3+})_2O_4{\cdot}1.5H_2O\}$. Lefkowitz et al. (2013) demonstrated that birnessite sheets were disrupted when pH was < 7.0. Under the mildly acidic conditions observed in the Burrup, the varnish would become thinner and softer with removal of these manganese compounds.

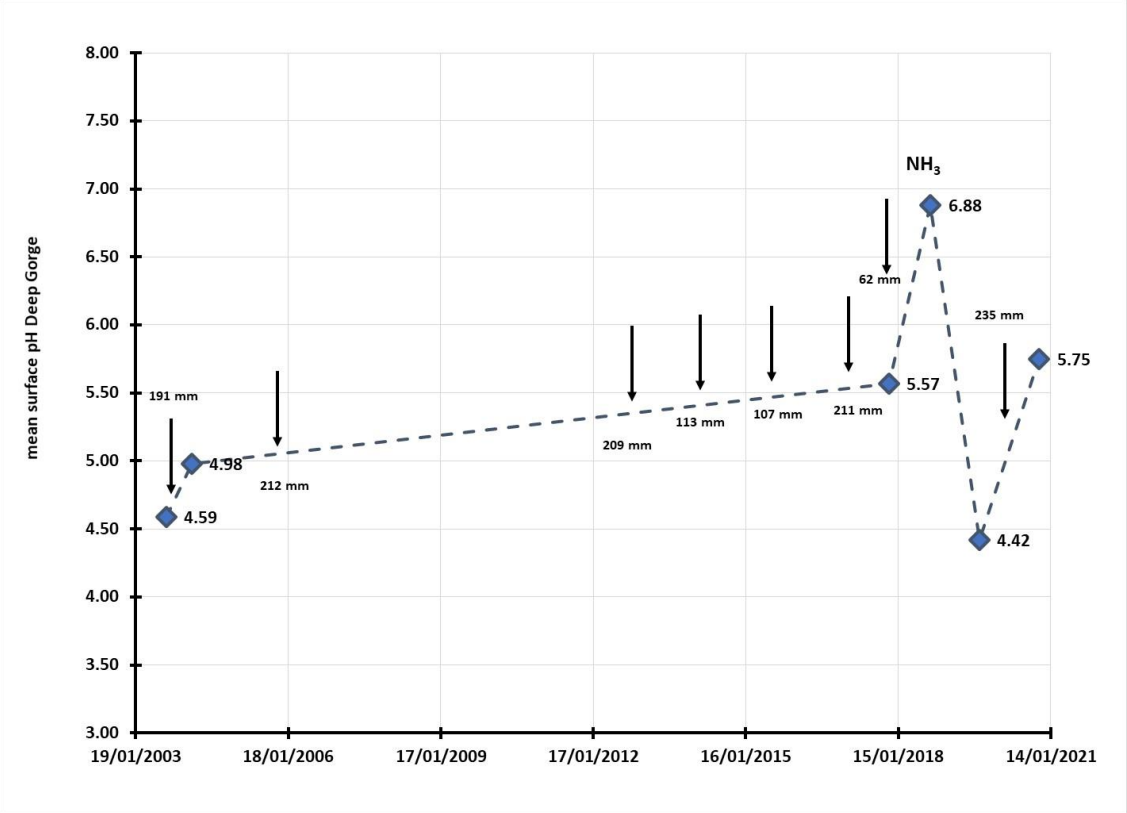

Figure 12: Mean pH at Deep Gorge between 2003 and 2020

The Yara plant producing ammonia had an accidental loss of ammonia before the 2018 pH measurements were done which may have contributed to a pH alkaline spike when the mean value at this site increased to 6.9. However, a local increase in nitrate concentration on the rock surface saw the pH fall to 4.4 in 2019 and this acidic surface was deeply washed by cyclone Damien rainfall, as noted through the chloride profiles above, to bring the pH back to 5.8, within the range of the natural pH of the Burrup rocks. This "swings and roundabouts" data profile shows that the rock are sensitive indicators of change in the microenvironment and this in turn acts as a warning sign of overall changes in the chemistry of the sites.

Table 6: Major cyclonic rainfall (mm) events in the Burrup 2003-2020

Date of rain event	Fall in mm
02 March 2004	190.8
10 January 2006	212.4
25 June 2013	209.4
31 December 2013	112.8
06 May 2014	107.4
09 February 2017	210.6
06 June 2018	62.4
8 February. 2020	73.6
9 February 2020	161.6

During the statistical analysis of the historic data on surface pH across the Burrup undertaken by Fox (Fox 2020) it was noted that there seems to be a trend toward increasing acidity when moving down the rock face and that the values tend to be isobaric moving laterally. The data shown in Figure 13 was plotted as a function of the vertical profile in cm from the foot of the rock. The pH profile is evident, and it is likely due to the availability of water and micronutrients accumulating down the rock face from the leading edge. At the foot of the rock, it is more acidic as the micronutrients have accumulated with the flow-down effect of the water percolation.

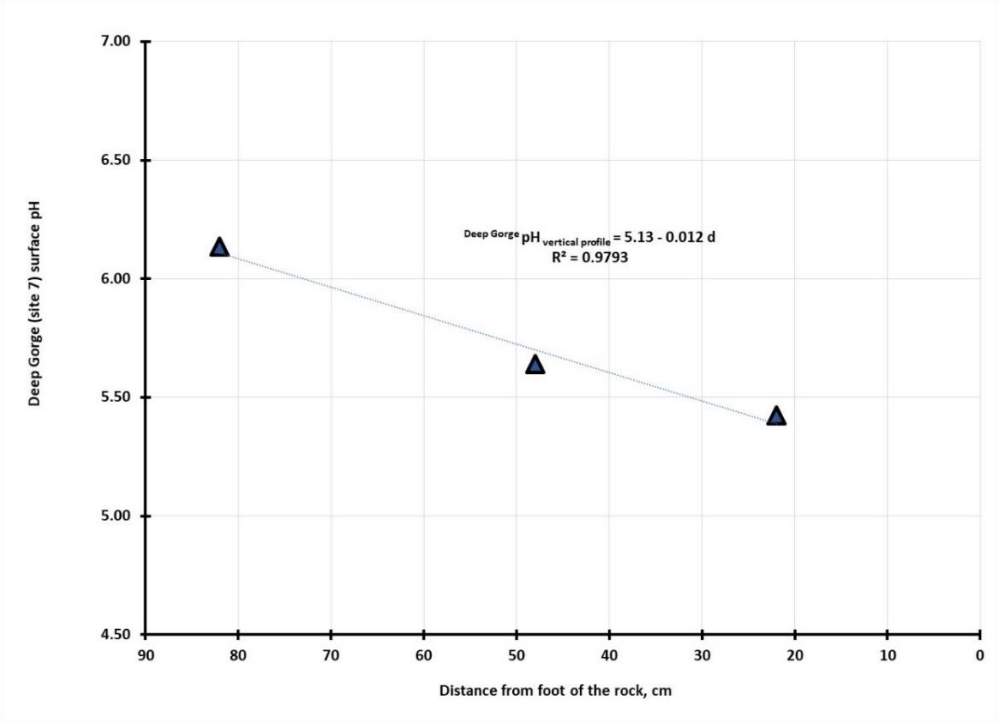

Figure 13: Acidity profile at the Deep Gorge site 7 rock as a function of distance.

Plots of the acid profiles down the rock faces across all the sites varied, without systematic differences between granophyre and gabbro rocks, in terms of the intercept or pH values at the upper most parts of the rock surfaces. This is only natural since the mean pH of each site is dependent on the amount of chloride and the amount of both nitrate and to a lesser extent, the amount of sulphate, present in the local environment. However, the graphs of the pH/cm slope as a function of the pH at the top of the rocks all have the same slope of-34.5± 0.5 pH/cm distance down from the top of the rock.

Anions in wash solutions

Oxalates:

Analyses from the five field trips showed that only two reference rocks in the collection of the Western Australian Museum had measurable amounts of oxalate ions, $C_2O_4^{2-}$, which were 1.8 mg/l from Enderby Island (B7477) and 0.7 mg/l from Happy Valley (B2494) in the Burrup. These rocks were collected at a time before there was any industrial activity on the Burrup. The washing samples analysed for oxalate were from June and August 2003, February 2004, November 2017, September 2018, August 2019, and October 2020. Other than the current year, there were no oxalates found in the wash solutions. The only sites to return oxalates in the wash solutions were site 23, which had a mean pH of 4.6 ± 0.4 and this indicates that there were active microflora or lichens etc. that were biologically active. The other location was one of the rocks by the Climbing Man, but which was located close to the gully floor. Oxalates are major biodeterioration of pigments in the Kimberley region where the monsoonal climate has characteristic wet and dry periods. By comparison, the arid climate of the Burrup is less amenable to a wide range of bacteria and plants which produce oxalates as their metabolites. The mean level of oxalate at the two locations in 2020 was 0.13 ± 0.03 ppm which indicates that oxalate does not appear to have a significant present role in biodeterioration of the rock art in the current Burrup microenvironment.

Chlorides:

The amounts of surface chloride detected on the rock surfaces provide direct evidence of the impact of the marine environment and indicates that salt weathering of rocks, with extensive dehydration and rehydration cycles, play a significant role in the local environment. The wash solutions from the rock surfaces showed up a range of ions commonly associated with sea water, namely Na^+, K^+, Mg^{2+}, Ca^{2+}, Ba^{2+}, B^{3+}, SO_4^{2-} and Cl^-. Analysis of the way in which the concentrations varied across the Burrup was possible as the February 2004 data included several remote sites such as Gidley and Dolphin Islands in the Dampier Archipelago (MacLeod 2005). The deposition of sea salt on the rock surfaces means that the carbonate and bicarbonate ions will tend to act as buffers and minimize any changes in the surface acidity resulting from a combination of microbiological and chemical reactions on the surfaces.

The initial monitoring conducted in 2003 and 2004 involved direct measurement of the surface pH and the surface chloride ion concentrations. In addition, the washing of the rock surfaces in August 2003 and February 2004 provided data on the solution concentrations of chloride ions. All the data was then assessed through linear regression analyses and the results are summarised in Table 7, which showed that the pH increased with increasing chloride ion activity. This buffering reaction is demonstrated by the relation between the pH and chloride concentration on the rocks as shown in Equation 21,

$$pH_{mean} = a + b\,[Cl^-] \quad \text{.....(21)}$$

The 2003-2004 linear regression analyses showed that there was a common slope of the pH vs [Cl] plots but they had different intercepts, as shown in Table 7. The intercept values relate to their primary geology of the underlying rocks and the impact of factors such as the amount of nitrate on the rock surfaces, which is discussed in the following section of this report. When the mean surface pH from

2020 is plotted against the mean surface chloride values it was found that for the granophyre rocks, the post cyclone Damien response was given by Equation 22, and in Figure 14.

$$^{granophyre}pH_{mean} = 4.49 + 0.029\,[Cl]_{surface} \quad \text{.....(22)}$$

This regression had an R^2 of 1.0, which provides the highest degree of confidence. By way of contrast, it can be seen in Figure 14 that the mixed gabbro sites (7, 22 and 23) and granophyre sites (CM_{split}, site 21) there is increasing acidification with increased chloride ion activity, as shown by Equation 23

$$^{mixed}pH_{mean} = 6.09 - 0.020\,[Cl]_{surface} \quad \text{.....(23)}$$

The response of the pH to the chloride concentration is shown in Figure 16, where it appears that the relationship given by Equation 23 is driven by chloride obligate bacteria and Equation 22 is the normal buffering reaction of sea salts on the surface pH. The data points that give rise to Equation 22 are all granophyre rocks at site 4, site 5 and site 6. Additionally, work needs to be conducted to increase the number of gabbro rocks being monitored as they seem to be displaying a different form of biological activity. The much more porous surfaces of the weathered gabbro provide a more secure space for the microflora in which to live. Previously it has been noted that some rocks, such as at Deep Gorge (site 7) had clearly been impacted by driving rain and that its build-up of chloride from sea salts was demonstrably coming from the direction of the prevailing winds coming from the ocean. Elucidation of the acidification and alkalinisation mechanism would be assisted if metagenomic analysis of the rock surfaces in the field conditions be conducted to establish the nature of the different groups of organisms that are controlling the pH and to see if there are measurable biological differences in the colonisation of the two rock types.

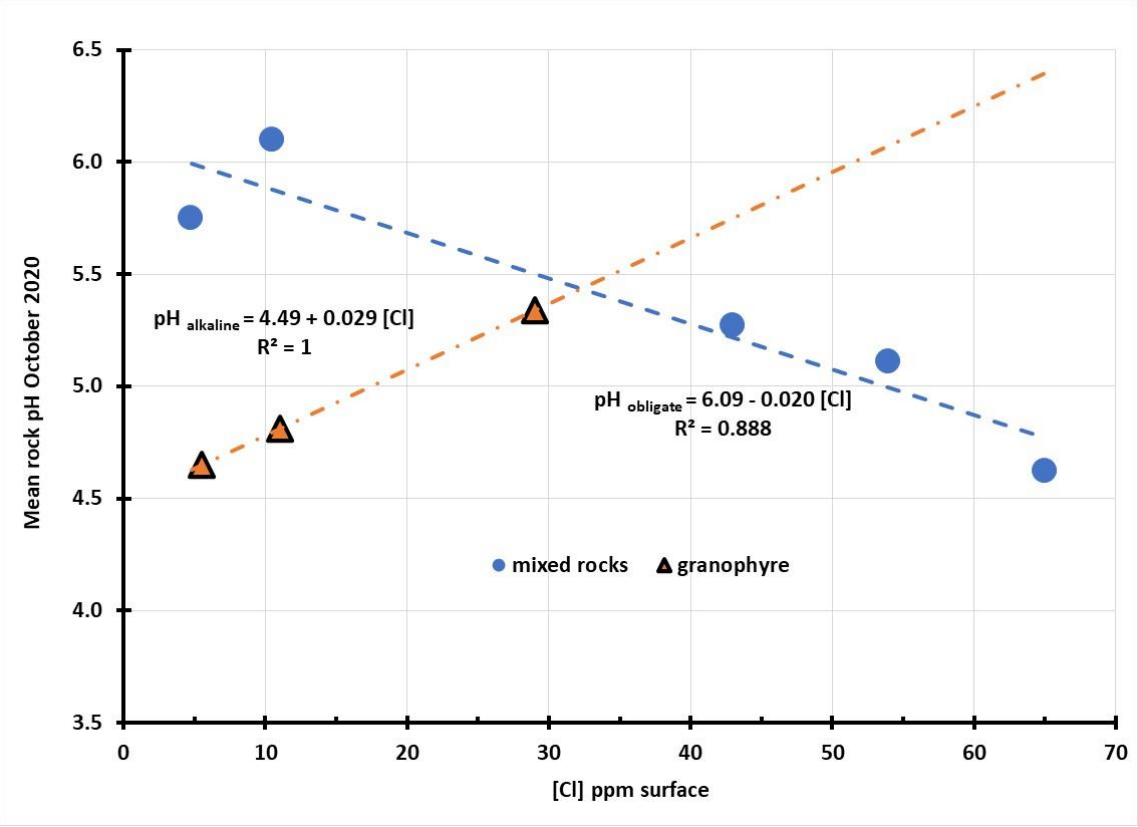

Figure 14: Plot of $[Cl]_{surface}$ on the rocks vs. the mean surface pH, 2020 readings

The data in Table 7 covers all the sets of measurements of rocks in the Burrup and in the Dampier, Archipelago shows that the build-up of sea salt deposits on the rocks does have a measurable impact on the way in which the rocks respond to changes in the chemical environment. From the data

presented in Table 7 there is a systematic decrease in the slopes of the pH vs. [Cl] graphs between 2002 and 2020, as shown in Figure 15 and equation 24 viz.,

$$\text{slope } \{^{pH}/_{Cl}\} = 0.0702 - 0.012\ pH_{\ zero} \quad \text{.....(24)}$$

This relationship confirms that all the $pH_{\ zero}$, obtained from extrapolation of the pH vs. Cl plots to the zero-chloride concentration (intercept pH value), and chloride data are intricately linked. In the absence of other factors, the ability of the rocks to minimise the response to the development of an acidic microenvironment is largely controlled by the amount of salt deposition.

Table 7: Analysis of the relationship between chloride and mean pH

Date	mean Cl ppm	Intercept, *a*	Slope, *b*	R^2
June 2003 (winter)	38 ± 40	3.4 ± 0.6	0.030 ±0.004	0.98
August 2003 (spring)	34 ± 31	3.4 ± 0.8	0.033 ± 0.003	0.98
February 2004 (summer)	21 ± 15	4.1 ± 0.6	0.023 ± 0.001	0.98
November 2017				
Site 5: Burrup Road West	32 ± 28	5.0 ± 0.9	0.008 ± 0.001	0.95
Site 6: Water tanks	191 ± 97	5.4	0.001	0.96
Site 7: Deep Gorge	22 ± 12	5.0	0.026	0.77
Site 21 Yara west	125 ± 44	5.8	0.006	0.64
Site 22: Yara north east	373 ± 24	5.3	0.009	0.70
Site 23: Yara east	13 ± 17	5.5	0.021	0.77
September 2018				
Site 4 Withnell Bay Road	2.2 ± 2.1	3.0*	2.7	0.93
Site 5: Burrup Road West	4.1 ± 3.4	4.5	0.22	0.45
Site 6: Water tanks	2.3 ± 3.2	6.1*	0.13	0.01
Site 7: Deep Gorge	19 ± 8	6.0*	0.03	0.99
Site 21 Yara west	20 ± 13	5.0	0.12	0.94
Site 22: Yara north east	10 ± 11	5.5	0.03	0.34
Site 23: Yara east	30 ± 17	3.9	0.02	0.96
August 2019				
Site 4a Withnell Bay Road	4.9 ± 2.0	4.75	0.092	0.96
Climbing Man site, split	14.4 ± 0.2	4.27	0.020	0.93
Site 5: Burrup Road West	6.3 ± 2.5	4.51	0.026	0.98
Site 6: Water tanks	9.7 ± 6.3	4.41	0.029	0.94
Site 7: Deep Gorge	8.6 ± 3.8	2.57	0.110	0.99
Site 21 Yara west	95 ± 70	4.87	0.004	0.91
Site 22: Yara north east	30 ± 5	4.18	0.015	0.98
Site 23: Yara east	30 ± 10	2.46	0.015	0.97
October 2020				
Site 4a Withnell Bay Road	11.0 ± 5.6	3.88	0.073	0.94
Climbing Man site, split	10.5 ± 8.8	5.86	0.018	0.95
Site 5: Burrup Road West	5.5 ± 4.2	3.76	0.065	0.99
Site 6: Water tanks	29 ± 17	4.39	0.015	0.98
Site 7: Deep Gorge	4.8 ± 2.4	4.75	0.112	0.88
Site 21 Yara west	43 ± 31	4.67	0.013	0.98
Site 22: Yara north east	54 ± 73	4.60	0.010	0.93
Site 23: Yara east	65 ± 20	3.44	0.018	0.94

* Sites were excluded from calculations owing to systematic errors in the intercept values

Inspection of the data in Table 7 shows that the solution washing concentration of chloride is like the surface readings at sites 4, 5 and 6. On some sites the washing concentration was lower than the surface values at sites 4, 6 and 7. When these anomalous data sets were removed from the mean calculations of the $pH/Cl_{surface}$ slopes and the mean pH, the 2018 data was found to follow the same general slope given by Equation 24 and shown in Figure 15.

Further studies to determine the precise nature of the interactions are needed and it should be noted that the solution washings were taken on rocks adjacent to the chloride and pH testing sites, other than in site 7 which had sufficient flat areas on which to place the collection device and to irrigate the areas that had been measured for pH and for chloride. By improving the methodology in 2020 and taking washings from two adjacent rocks, within 2 metres of the test rocks, an improvement in the degree of confidence of the results was made. Many of the Yara /CSIRO reference rocks have near vertical surfaces and this makes it impractical to recover samples of enough volume to allow for reliable chemical analysis of the surface wash solutions.

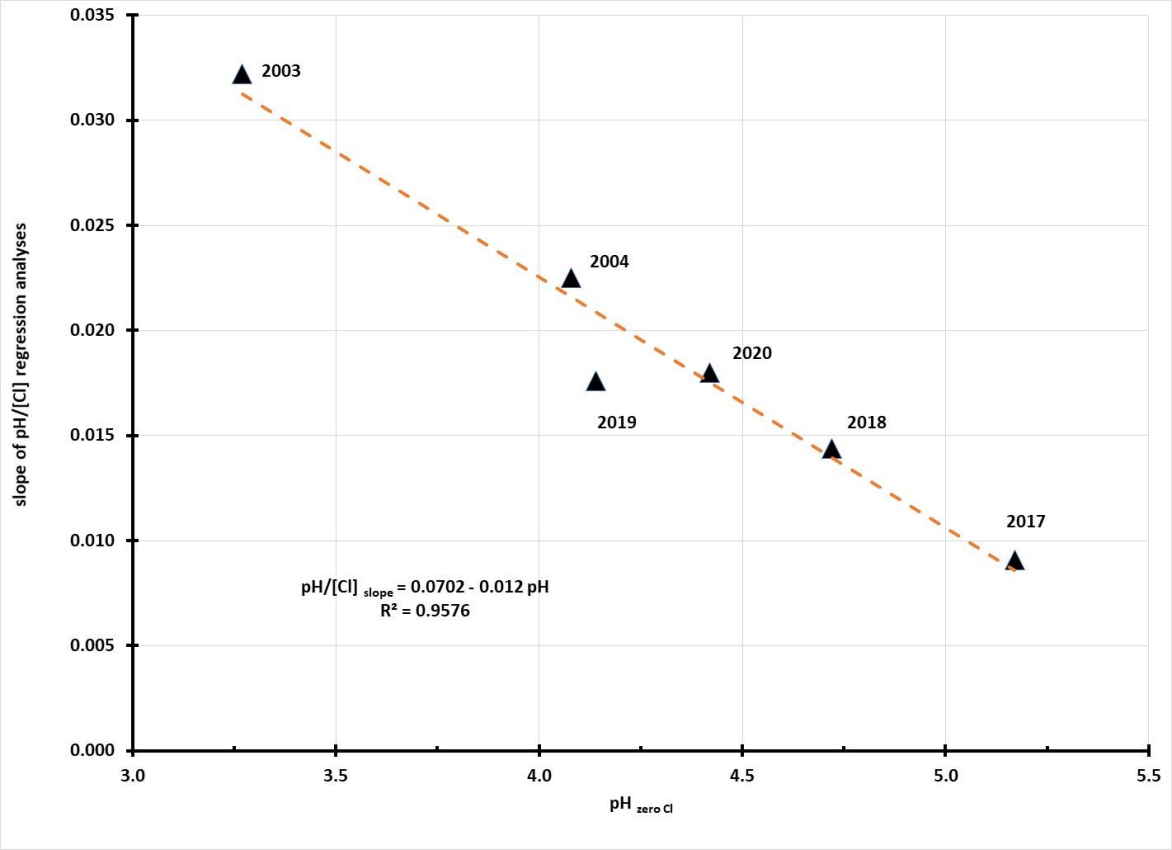

Figure 15: Plot of the slope of the pH/Cl graphs vs pH intercept at zero ppm chloride

It is interesting that the slope of the graph has not been materially affected by cyclone Damien, for the 2020 data points for the mean slope and pH_{zero} plots lie in between the values observed in 2019 and 2018.

Nitrates:

Previous studies in 2003 and 2004 had focused on the acidity and the concentration of nitrate ions, since there was strong data supporting the inference that nitrate ions were stimulating the overall microbiological activity on the rocks. Since bacterial and fungal metabolites are often acidic it was decided to check to see if there was a correlation with the number of bacteria and the nitrate levels. Data published in 2005 by MacLeod demonstrated that the logarithm of the number of bacteria was

causally related to the decreasing pH, thus the amount of nitrate ions, from both natural and human sources, was likely to be a key determinant in the overall rates of weathering of the rock surfaces in the Burrup. Owing to the contrasting nature of the engraved and background areas there was concern about the long-term impact of such accelerated ageing on the rock surfaces. Surface pH values as low as 3.5 were recorded on rocks at site 4, which was 250 metres closer to the road in the same gully as the Climbing Man panels. When the initial surface pH readings were done on the engraved goanna site 4, it was assumed that by being adjacent to the Woodside operational flare tower servicing trains 1-4, that it would be due to a high nitrate concentration. As part of the February 2004 data collection, samples of rock pH, chloride and nitrate ions were collected on rock engraving sites at Gidley and Dolphin Islands in the Dampier Archipelago, in the belief that these remote sites would be low in nitrates, owing to their distance from apparent point sources on the coastal lands associated with industrial developments.

A summary of the relevant data is shown below in Table 8, which lists the mean nitrate for 2003, 2004, 2017 through to 2020 as well as the range of the maximum to the minimum values that were recorded. The major cyclonic rainfall in February 2020, when 235 mm were recorded over two-days, appears to have had a major impact on washing the accumulated nitrate ions from the rock surfaces. Inspection of the data in Table 8 shows a four-fold reduction in the amount of nitrate, as measured on sites in a total of sixteen (16) rock locations at the eight monitoring areas.

Table 8: Nitrate concentration ranges across Burrup, ppm

Date	Maximum	Minimum	Mean ppm
August 2003	19, Withnell Bay	1.5, at Burrup SW 1–2	6.3 ± 5.1
February 2004	9.2, rock 938	1.3, Deep Gorge	4.5 ± 3.7
November 2017	1.8, site 21	0.10, site 5	0.6 ± 0.7
September 2018	1.4, site 7	0.19, site 22	0.7 ± 0.4
August 2019	2.1, site 7	0.15, Climbing Man split	0.7 ± 0.7
October 2020	0.46, site 7b	0.06, site 22 b	0.17 ± 0.10

Although the nitrate concentration was essentially the same in August 2003 and February 2004, the amount of $[NO_3]_{ppm}$, as seen in Table 8, diminished by over 40%. This is roughly in line with the 30% reduction in the mean nitrate concentration between the two sets of measurements. The data in Table 9 shows that common intercept pH values, at zero nitrate, at 5.69 for the 2003 and 2004 analyses. The common intercept value shows that the same chemical mechanism is controlling the response of the rocks in those two seasons of measurements. It should be noted that with the R^2 value of 0.97 the 2003 intercept value of 5.33 value is within experimental line fitting error the same as the 5.44 from rocks in the museum compound that was noted in February 2004. Of concern were the lower $pH_{intercept}$ values of 4.95 and 4.66 for sites that included rocks in the museum compound as well as those at the Climbing Man, Deep Gorges and Withnell Bay sites.

In the 17-years since the February 2003 data was collected, there were eight cyclonic rain events, as listed in Table 3, which deposited between 63-212 mm of rain in the region in a 48-hour period. These periods of inundation of the rock surfaces are likely to be the underlying reason for the big drop in the nitrate ion concentration found in the rock washings in November 2017 and again in October 2020. There was a 62.4 mm rainfall event on 6th June 2018 which would have caused significant washing of the rocks in the test areas. The five-fold fall in nitrate concentration would have been expected to reduce the impact of the biological activity due to the nitrate concentration, but other factors appear to have weighed heavily in bringing about a change in acidification. It has been noted that the mean chloride ion concentration on the Yara sites is approximately 30 times saltier in November 2017 than the rocks that were sampled in February 2003.

Table 9: Dependence of pH on the nitrate concentration found in wash solutions

Date	pH $_{zero\ NO3}$	Slope pH/[NO3]	R^2
August 2003	5.69, Climbing man, Deep Gorge & Compound 5.33, Burrup SW, King Bay & Compound	-0.14 -0.14	0.92 0.97
February 2004	5.69, Withnell & Compound 5.44, Compound 4.95, Withnell & Compound 4.66, Deep Gorge & Climbing Man	-0.08 -0.08 -0.07 -0.08	0.91 0.99 0.66 0.78
November 2017	6.18, Sites 5,6,7, 21, 22 & 23	+0.94 log [NO_3]	0.99
September 2018	3.14 all sites other than 22	non-linear	0.86
August 2019	4.41_{min}, sites 5, 21 & 22 3.76_{min}, sites Climbing Man, 7 & 23 $4.60_{\ median}$, sites CM, 6, 7, 22 & 23 $5.56_{\ median,}$ sites 4a, 5 & 21	+0.39 -0.22 -0.04 ± 0.02 -1.13 ± 0.59	0.97 0.87 0.43 0.79
October 2020	6.68_{mean}, sites 4, 5, 6, 21 and CM split 5.82_{mean}, sites 4, 21 & 23 $5.67_{minimum}$, granophyre & 23 $4.96_{minimum}$, sites 5 & 22	-8.7 -7.2 -5.7 -4.7	0.93 0.81 0.96 n.a.

When the regression analyses for the mean pH of the monitoring sites in 2020 were made, the error in the intercept for the granophyre sites was ±0.18 and for the other sites the error was ± 0.30. These values demonstrate that they are statistically different, which is consistent with the rougher and more complex surface of the gabbro rocks holding onto moisture for longer periods and, presumably able to retain nitrate nutrients, and so provide a better microenvironment for the microflora, which is why the intercept value of mean pH was more acidic than for the smoother granophyre rocks. However, it is noted that the data scatter for the nitrate concentration values across these groups is not statistically significant. The nitrate dependence (slope) of the rocks were experimentally the same, with the pure granophyre rocks being -8.7 ± 1.1 and the mixture of gabbro and some granophyre surfaces was -7.2 ±2.5. The mean pH at zero nitrate and the slope of the mean pH vs. nitrate plots are seen in the first two lines of the 2020 data in Table 9.The same slope means that it is the same mechanism that is controlling the pH. The data shown in the last line of Table 8 is illustrated in Figure 17, which shows the data from the use of the minimum pH collected in 2020.

There is one outlier in Figure 16, site 7b, for which there does not appear to be an appropriate mean pH for this highest level of nitrate, nor does it fit in with the minimum pH plot in Figure 17. The cause of this is that the reference rock at site 7b has an almost horizontal aspect, for ease of water collection, which does not provide the relevant input for the pH measurements which were done on a 35 degree-sloping rock. Comparative analysis of the washing solution data in Appendix III shows that the second rock on site 7 had higher sulphate and higher copper concentrations, which make this rock not truly representative of the environment of the CSIRO reference rock at Deep Gorge. The location of the rock was recorded, and it will be avoided in future work to see if more concordant data can be obtained. The R^2 value of 0.96 gives an intercept error of only 2.4% or ± 0.14 in the value of the pH (5.67) at zero ppm nitrate and this is characteristic of the natural rock pH in fresh distilled water after several minutes' equilibration with the Burrup patination that is typical of the area. The regression analysis has an 11% error in the slope for the correlation between minimum pH and nitrate viz. -5.94 ± 0.67 pH/ppm nitrate. The intercept value for the granophyre rock collection is therefore different to the value of 4.96 for the two areas (site 5b and site 22 Yara North East) for which it is likely that microclimate issues such as the wind-borne materials or subtly different microflora are responsible

for the higher acidity on the reference rocks from which the washings were obtained. The most readily discernible difference between site 5a and site 5b is that the latter has half the chloride concentration of the former at 31 ppm compared with 70 ppm.

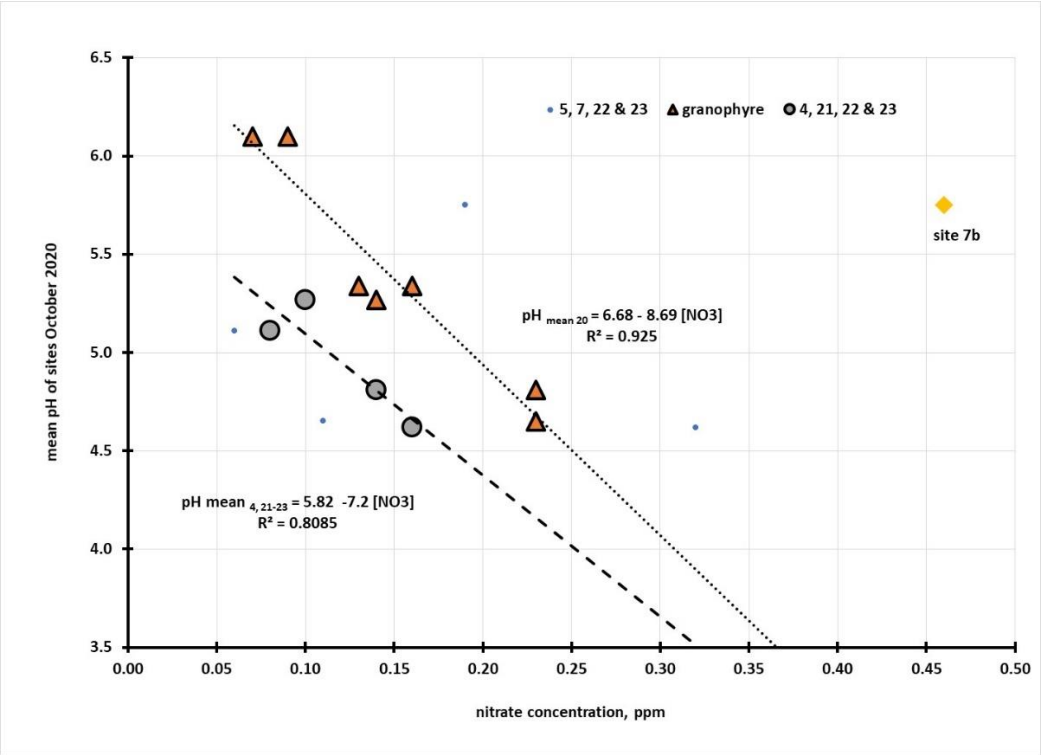

Figure 16: Plot of mean pH in 2020 against the nitrate surface concentration

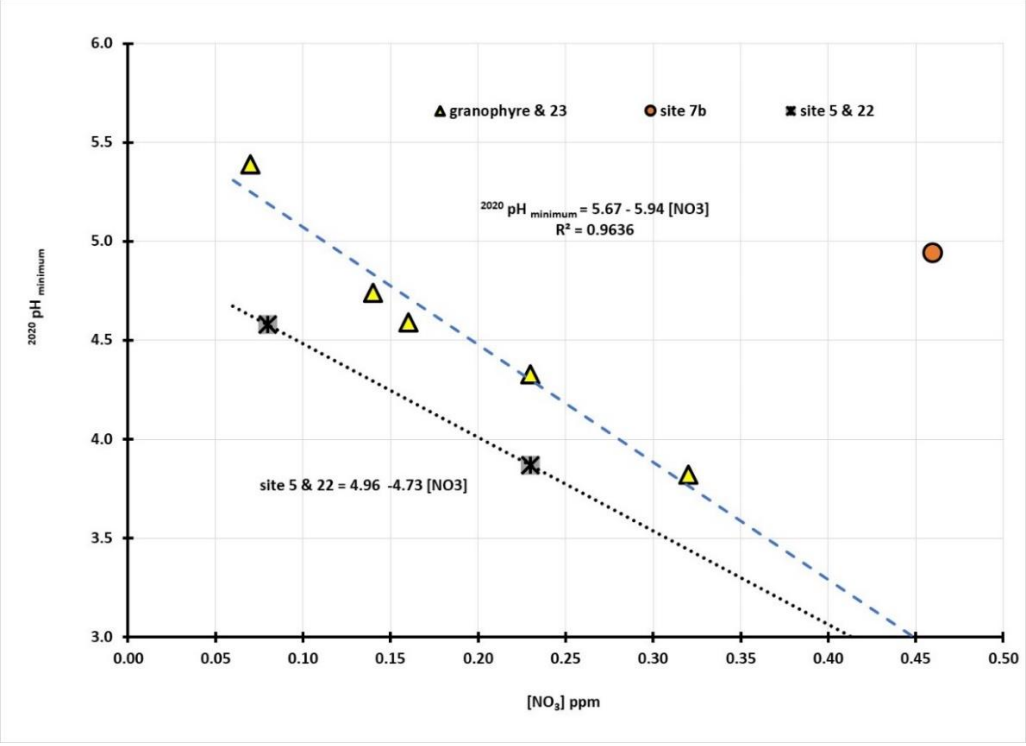

Figure 17: Plot of minimum pH as a function of nitrate concentration on rock surface

The presence of the buffering sea salts on the rock surface become more apparent when it is seen that site 22b had NO DETECTABLE chloride on the washed surfaces, hence the greater surface acidity. With only two low chloride reference points the apparent slope of this relationship cannot be compared with the average value of the five other sites.

Sulphate:

The amount of sulphate in the washings also varied from one year to the next, as shown in Table 10, which reports the data from the August 2003 and February 2004 rinses, along with the most recent data on the Yara sites from November 2017 and from September 2018.

Table 10: Range of sulphate ions in the wash solutions on Burrup and Yara sites

Date	Maximum	Minimum	Mean $[SO_4^{2-}]$ ± SD ppm
August 2003	66.7, Rock 938	1.2, Burrup SW2	9.8 ± 14.2
February 2004	26.1, Rock 938	0.8, Deep Gorge	4.9 ± 5.5
November 2017	9.8, site 23	1.5, site 22	5.2 ± 3.0
September 2018	2.2, site 6	0.3, site 22	1.2 ± 0.7
August 2019	19.1, site 21	0.4, site 4a, site 22	4.5 ± 6.4
October 2020	9.3, site 23b	0.2, site 4a	1.5 ± 2.2

The impact of the cyclone Damien on 8th and 9th of February in 2020 was variable for some sites, such as Deep Gorge (site 7) showed a general diminution of the amount of chloride salts, as directly measured across the rock surface, and other rocks such as the Water Tanks (site 6) showed higher chloride concentrations due to sheltering from the by tall neighbouring rocks. The more exposed section of the rock had significantly lower chloride concentrations.

It is apparent that there is a two-fold drop in the mean sulphate concentration in the wash solutions between August 2003 and February 2004. The data shows that there has been essentially no change in the amount of sulphate present in the 2017 compared with the 2004 readings. The highest values reported were found on rock 938 in the "museum compound" which lay inland from the Climbing Man gully and was located behind the hills from the Woodside gas production facility. Unfortunately, there is no corresponding wash solution data from the relocated rock 938 in the June 2017 report. In August 2003, the pH was 4.8 ± 0.4 and in February 2004 it was 4.9 ± 0.6 which makes them statistically the same i.e., there was no correlation between the wash solution sulphate concentration and the underlying acidity. It is not possible to state if the mean sulphate levels recorded in 2019 are fully reflective of the current environment for the data measurements in 2018 and 2020 followed cyclonic rainfall events.

Although recent statistical analyses (Fox 2020) had indicated that there might be some association of pH with sulphate in the wash solution, there was insufficient data to obtain a valued opinion, for his analysis was done prior to the October 2020 measurements. The decision to conduct duplicate rock sampling at each site has proved its worth in October 2020, since the data seen in Figure 18 shows that there is, at least for sites, 6, 7, 21 and 23 and the Climbing Man split rock, there is a strong correlation between decreasing pH and increasing sulphate, as shown in Equation 25 below.

$$^{minimum}\,pH_{SO4} = 5.82 - 0.82\,[SO_4^{2-}] \quad \text{.....(25)}$$

There is a reasonable data scatter, which is why the R^2 was 0.89, with the associated errors in the intercept value at zero sulphate, which has an error of ± 0.20 (3.5%), and the slope has a larger error of ± 0.15 or some 18 percent. The plot of the mean pH against sulphate has the same slope -0.82 ± 0.11 per ppm sulphate, but the intercept value is naturally more alkaline 6.54 ± 0.15 (2.3%) and the R^2 is higher at 0.93. The much higher R^2 value indicates that the most likely cause of the acidification is due to deposition reactions producing acid on the surface of the rock, rather than the minimum pH

value which tends to be associated with the activities of microbial organisms. The impact of the cyclone and the activity of the microflora is noted by the much greater sensitivity of the pH to [SO_4] in 2020, for in 2019 the intercept pH_{mean} values were lower at 4.7 and the slopes were also much less at -0.080 ± 0.002 pH/ppm [SO_4]. It is likely that the 2019 data was dominated by the impact of there having been no cyclonic rain events to "reset" the acidification "clock".

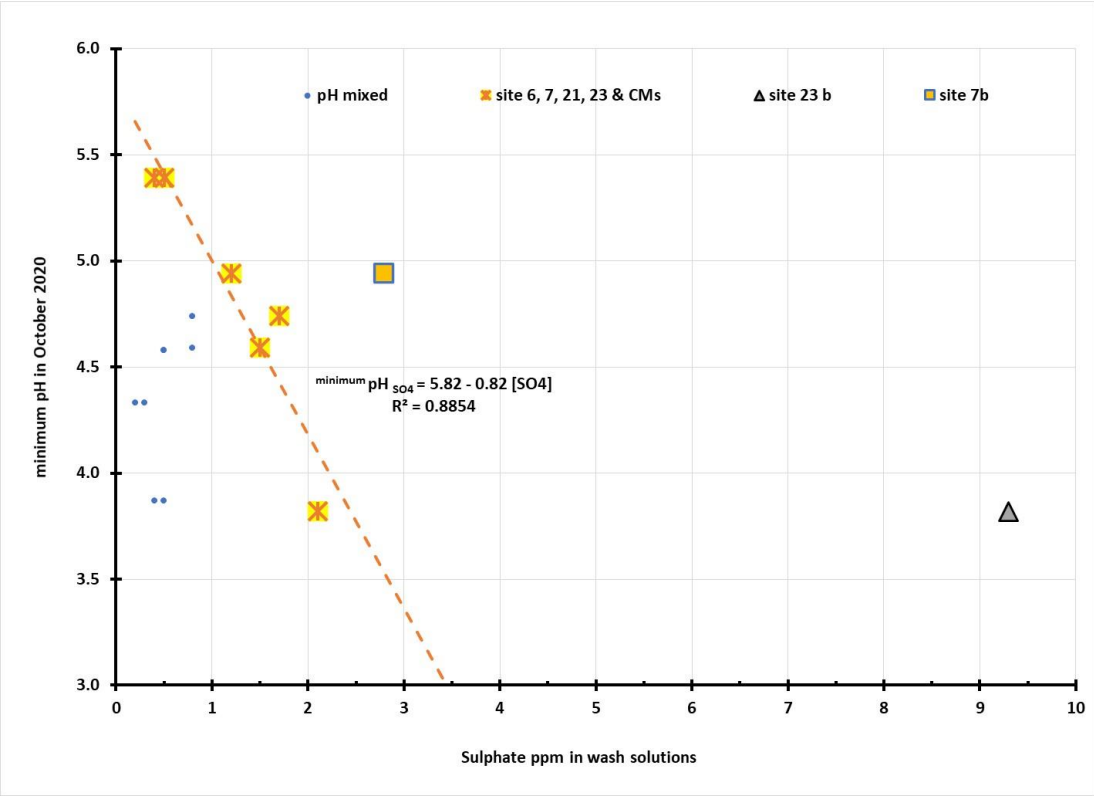

Figure 18: Plot of minimum pH versus sulphate concentration October 2020

The corresponding slope for the way in which the minimum pH responds to nitrate ions is 5.94 per ppm [NO_3^-] and the associated intercept pH value was 5.67, which is close to the sulphate pH minimum value of 5.82, but the difference is 1.4 times more acidic in the case of nitrate compared with sulphate. The nitrate-pH correlation is seven times more sensitive than with the sulphate ion values. It has been previously noted that the pH of the rock surfaces is significantly affected by the chloride levels, coming from the sea salts, so it is instructive to see how the $^{Cl}/_{SO4}$ ratios vary across the Burrup in the different periods of measurement. The normal ratio of chloride to sulphate ions in seawater is 7.1 so values that are lower than this indicate that this is due to either additional sources of chloride ions or that sulphate ions have been in some way sequestered on the rock surfaces.

Even a cursory inspection of the data in Table 11 shows that cyclone Damien has had a major impact on the amount of sulphate on the rock surfaces. For sites 4, 5, 21 and the Climbing Man split rock the amount of sulphate was ≤0.5 ppm. Since the detection limit for ion chromatography for the sulphate ion is 0.1 ppm the errors in the ratio are significantly amplified at low sulphate levels. The mean amount of chloride across the sites, other than for site 22 on top of the ridge, was 34.2 ±11.4 ppm in the post cyclone environment, which shows that the normal deposition of sea salts from the wind-borne aerosols is the dominant mechanism.

One of the most significant points to note from this current data is that for the sites in the Climbing Man gully, namely the split rock and the engraved site no 4, the amount of chloride in the wash was steady at 30.8 ± 0.5 ppm and the most likely cause of the depressed level of available sulphate is the

presence of reactive iron minerals on the surfaces which can lead to the conversion of hematite to the iron hydroxy sulphate jarosite, $KFe(SO_4)_2(OH)_6$.

Table 11: Ratios of chloride to sulphate ions in the wash solutions from Burrup rocks.

Date	**$Cl^-:SO_4^{2-}$ mean**	**$Cl^-:SO_4^{2-}$ high**	**$Cl^-:SO_4^{2-}$ low**
August 2003	5.7 ± 5.4	11.8 ± 6.6, CM* & rock 162,	3.1 ± 1.2, covering 14 sites
February 2004	21 ± 15	9.9 ± 5.1, 14 sites including CM, Rock 3	4.3 ± 1.2, covering 27 sites with Gidley & Dolphin Islands
November 2017	1.1 ± 0.3	2.2, site 22	0.7, site 7,
September 2018	2.8 ± 1.8	6.0,site 22 Yara NE	0.7, site 4
August 2019	3.0 ± 1.3	4.7 ± 0.5; 21, 22 & CM	2.1 ± 0.5; 4, 4a, 5, 6, 7, 23
October 2020	52 ± 49	**64 ± 48**; 4, 5, 6,7a, 21,23a & CM	**5.0 ± 3.4**; 7b, 22a & 23b

- CM relates to the split rock to the left of the main panel at Climbing Man

During the inspection in 2019 and 2020 of the Climbing Man site it was noted that there were "streams" of iron containing minerals flowing down from the rocks above the panels, which is indicative of active mobilisation of iron species. The other cause of lowered sulphate concentration can be due to the presence of microfossils in the rock surfaces, since the calcareous minerals react with acidic sulphate solutions to form the insoluble salt gypsum, $CaSO_4.2H_2O$. This type of reaction has previously been reported in 2003 and 2004 when reviewing data from washings obtained over a large cross-section of sites in the Burrup. The 2020 ratios of chloride to sulphate on both sites in the Climbing Man gully are in stark contrast to the value for site 4 in 2018, which indicated that a significant source of SO_x was impacting on the site or that a localised rain event had washed away most of the chloride on the rock surface.

Comparison of pH between 2017 - 2020

A summary of the differences between the two seasons of measurements is found in Table 12 and in Figure 19 below. For site 22 (gabbro), 6 and 5 (granophyre) the differences between the two sets of measurements are within experimental error i.e., there is no statistically significant difference in the acidity of the three sites. For site 23 (gabbro) and site 21 (granophyre) there was a similar increase of 0.64 ± 0.03 which is statistically the same as the mean and standard deviation when the value of site 4 is included.

The impact of cyclone Damien varied according to the specific site location. Site 5 by the Pluto exhaust stack showed a decrease in pH of -0.14, which is in line with all the previous measurements from 2017 through to 2019. For all the other sites they became more alkaline or were constant, within the normal range of ± 0. 5 pH, which is the commonly observed range of pH values that can be typically recorded on Burrup rock art sites. For the granophyre site 4 at the head of the Climbing Man gully the mean pH was decreased by 0.71 (see Table 12).

The Climbing Man site increased the pH by 0.05 which was essentially no change. For Site 21 on top of the hill above the Yara plant (Yara West) the pH increased by 0.11. The near vertical position of the rock at site23 also had a marginal increase in alkalinity of 0.15. The exposed nature of site 22 on top of the ridge showed a greater increase in pH by 0.49 and site 6 had a readily discernible increase of 0.67. The exposed nature of site 7 saw the mean pH increase by 1.33 and the greatest change was at the Climbing Man split rock where the pH increased by 1.48. The split rock is about 1.8 metres to the left of the main climbing man panel and is roughly 35° from horizontal compared with the vertical main panel at the site to its right.

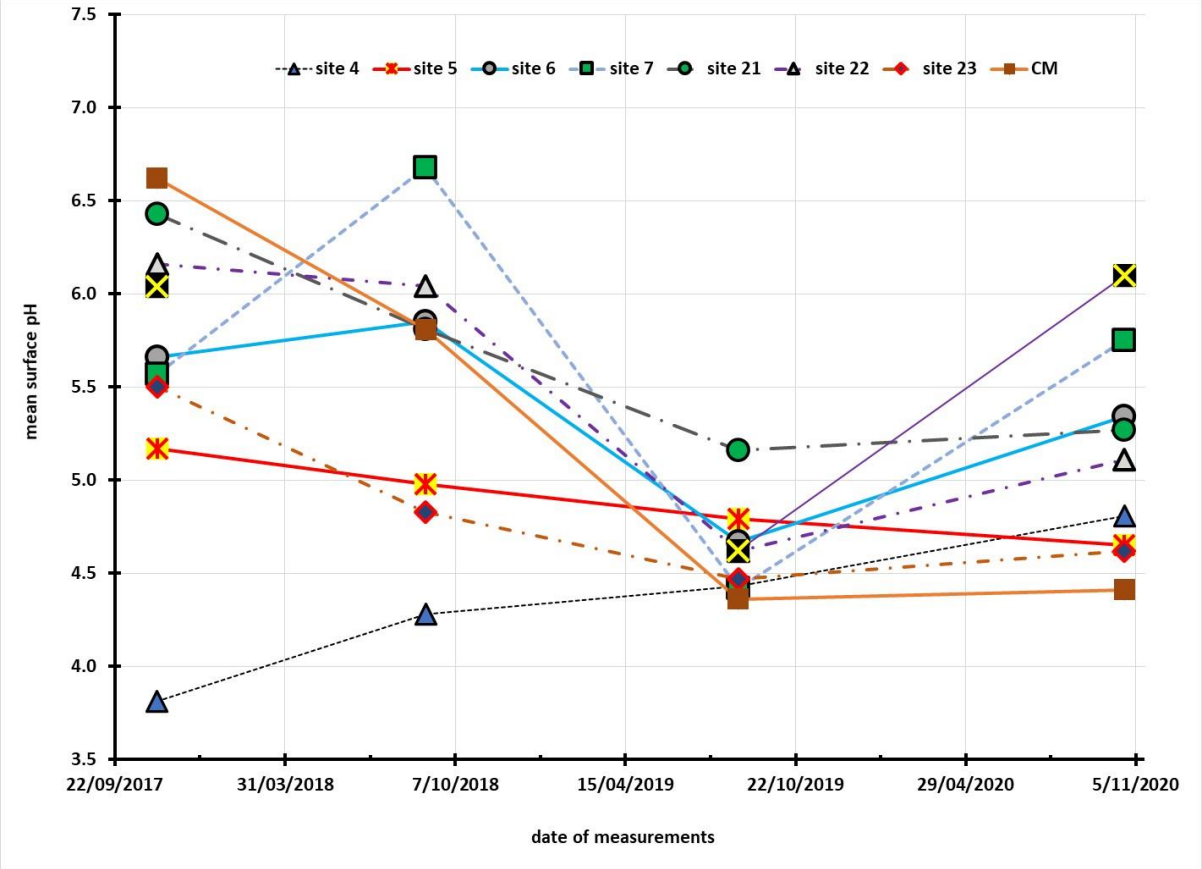

Figure 19: Comparative plots of mean surface pH across the Yara sites

Table 12: Changes in mean surface pH between 2017 and 2020

Location	2020	2019	2018	2017	pH increase, post cyclone Damien
site 23	4.62	4.47	4.83	5.50	0.15
site 22	5.11	4.62	6.04	6.16	0.49
site 21	5.27	5.16	5.81	6.43	0.11
site 7	5.75	4.42	6.68	5.57	0.33
site 6	5.34	4.67	6.03	5.66	0.67
site 5	4.65	4.79	4.98	5.17	- 0.14
site 4	4.81	5.52	4.28	3.81	-0.71
Climbing Man	4.41	4.36	5.81	6.04	0.05

When the standard deviations of the site pH measurements are considered there is only one site, site 7 at Deep Gorge, which is statistically significantly different, and this site had become more alkaline. The significance of the differences is assessed by dividing the difference in pH by the sum of the standard deviations of the two sets of data. If the quotient is less than 1 it is not significant and if above 1 then it is and at 1.4 the differences are significant in the mean pH at Deep Gorge.

Summary of the surface pH, chloride & redox at Yara sites

It should be noted that in the 2017 measurements on the Yara test sites only the surface pH and chloride ion activities were recorded. The utilisation of redox data on the Burrup rocks was not developed until July 2017 and was not adopted until after peer review had confirmed it was a viable

indicator of chemical activity on the rock surfaces (MacLeod 2019). For this section of the report, the statistical analysis of the distribution of pH, chloride, and redox potentials for each of the sites is discussed in turn.

Summary observations on site 23

Table 13a: Statistical analysis of pH values on site 23 from 2017-2020

	2020 pH	2019 pH	2018 pH	2017 pH
Mean	4.62	4.47	4.83	5.50
Standard Error	0.13	0.08	0.18	0.20
Median	4.68	4.60	4.63	5.65
Mode	4.76	4.62	4.63	#N/A
Standard Deviation	0.44	0.28	0.64	0.62
Range	1.52	0.9	2.15	1.97
Minimum	3.82	3.8	4.16	4.42
Maximum	5.34	4.7	6.31	6.39
Count	12	12	13	10

There was concern noted that there was an acidification trend for this reference rock, with a steady decrease in the pH value from 2017 through 2018 and down to 2019. There appears to be a moderate amount of nitrate in the surface washing of the rock which could supply extra micronutrients for the microflora living on the rock. Although the standard deviation of the pH values in 2019 and 2020 show that the small increase in pH between the mean values, due to the cyclonic rains in February 2020, it is more telling to see that the rains kept the minimum pH at the same level and that the rain impact was more noticeable in the five-fold decrease in acidity after the big rain.

Table 13b: Statistical analysis of redox potential and chloride levels site 23: 2017-2020

	2020 E vs NHE	2019 E vs. NHE	2018 E vs NHE	2020 Cl ppm	2019 Cl ppm	2018 Cl ppm	2017 Cl ppm
Mean	0.323	0.397	0.484	65.3	30.4	29.6	18.5
Standard Error	0.005	0.006	0.004	6.0	2.8	4.6	5.5
Median	0.322	0.395	0.482	70.5	30.0	25.0	11.5
Mode	0.311	0.395	0.287	70.0	32.0	#N/A	6
Standard Deviation	0.018	0.019	0.016	20.7	9.7	17.2	17.4
Range	0.070	0.064	0.068	71	40	53.7	50.5
Minimum	0.294	0.361	0.238	15	16	11.5	4.5
Maximum	0.364	0.425	0.306	86	56	65.2	55
Count	12	13	14	12	14	14	10

The winds coming up from Hearson's Cove explain the relatively rapid build of chloride concentration after the cyclone, but the minimum value is relatively constant, apart from the low value observed in the initial measurements in 2017. Clearly, there are salty patches on the rock surface owing to the complex topography of the near vertical surface of the engraved panel. There seems to be a steady fall in the E_h values which is consistent with lower solubilities of electrochemically active iron species, which may also be expressed in terms of a changed energy source for bacteria which can utilise the latent power in changing oxidation states with iron and manganese minerals. It is noted however, that this reference site had the only measurable amount of iron present in the wash solutions on the adjacent rock, some 1.5 metres away but which were essentially horizontal in aspect rather than being vertical.

Summary observations on site 22

This site lies high on top of a hill on a ridge running towards the coast and the small, engraved rock looks to the east and lies at about 75° to the vertical, so it is well drained. The cyclone Damien shifted the mean pH by 0.49, which is a three-fold reduction in acidity. However, it was noted that there was essentially no change in the minimum pH, which indicates that the biological activity that had been observed in 2019 was still present and active. During the 2019 on site measurements the wind was gusting strongly, with estimates of speeds up to 70 km per hour, which tended to knock the assessment team off their feet. The location is to the North East of the Pilbara nitrates plant and the mean pH for 2019 was significantly lower than it was in the two previous years. This chloride concentration on the site in 2019 is essentially the same as it was in 2017 so the change in acidity (a decrease in pH of 1.54 between 2017 and 2019 cannot be due to changes in acidity due to chloride obligate bacteria). The most likely factor bearing on this pH change is the nitrate concentration. The mean redox potential of sites 23 and 22 is remarkably similar which is not surprising since they are both gabbro rocks. On site 22 the E_h is about 100 mV less than in 2018 and this is consistent with there being less soluble iron minerals on the rock surface.

Table 14a: Statistical analysis of pH values on site 22 from 2017-2020

	2020 pH	2019 pH	2018 pH	2017 pH
Mean	5.11	4.62	6.04	6.16
Standard Error	0.10	0.03	0.17	0.15
Median	5.15	4.61	5.82	6.42
Mode	n.a.	4.55	n.a.	6.42
Standard Deviation	0.41	0.10	0.57	0.48
Range	1.35	0.37	2.01	1.3
Minimum	4.58	4.48	5.3	5.3
Maximum	5.93	4.85	7.3	6.6
Count	16	14	12	12

What stands out with the post cyclone chloride readings on site 22 in 2020 is the range of chloride ion activity, which gives a mean value of 54 ppm with an error in the mean being much greater at ± 73 ppm. During the surface chloride measurements there were glistening patches of halite (sodium chloride crystals) where moisture runs had resulted in localised concentration of the salt. The chloride distribution pattern was complex, as the upper row of 4 measurements had a mean of 61 ± 88 ppm as there was a high chloride spot of 194 ppm 20 cm across from the left side of the rock.

Table 14b: Statistical analysis of redox potential and chloride levels site 22: 2017-2020

	2020 E vs NHE	2019 E vs. NHE	2018 E vs NHE	2020 Cl ppm	2019 Cl ppm	2018 Cl ppm	2017 Cl ppm
Mean	0.392	0.382	0.492	54.2	30.3	10.2	33.3
Standard Error	0.004	0.005	0.004	18.3	1.4	3.4	7.7
Median	0.390	0.387	0.495	16.8	30.0	8.5	26.3
Mode	0.408	0.388	0.491	16.0	33.0	n.a.	n.a.
Standard Deviation	0.014	0.018	0.012	73.1	4.9	11.2	24.3
Range	0.048	0.059	0.044	236	18.0	40	82.5
Minimum	0.365	0.348	0.458	4.2	21	1.4	14.5
Maximum	0.413	0.407	0.502	240	39	41	97
Count	16	14	12	16	14	12	16

The mean chloride of the second row was 15 ± 11 ppm and the third row was the same at 13 ± 14 ppm. On the bottom right-hand corner, the chloride concentration was 240 ppm, and the mean was 128 ± 84 parts per million. Roughly one third of the pH measurements had a particularly good correlation of increasing pH with increasing chloride (due to buffer capacity increasing) which followed a starting point of pH 4.6 and increased by 0.01 per ppm chloride (R^2 was 0.93).

Inspection of the data in Table 13 b shows that between 2018 and the sequential years, the E_h had fallen but of great interest was the way in which the redox potential was affected by the chloride ion activity on the site. For 70% of the pairs of data points, there was an increase of 0.3 mV per ppm of chloride and for the balance of the points they had the same increase of E_h with chloride but had a more anodic starting voltage of 0.398 volts. When the Pourbaix diagram for site 22 is reviewed it is noted that all the E_h / pH profiles had the same slope of -29 mV, which relate to the manganese controlled redox equilibria, as indicated by their mean $E_{\text{zero pH}}$ of 0.553 ± 0.002 volts vs. NHE. This explains the fall of the mean E_h from the higher value in 2018, i.e., it is due to the lack of mobilisation of iron ions on the surface.

Summary observations on site 21

Inspection of the pH data in Table 14, shows that were it not for the intervention of cyclone Damien's drenching of the site in February 2020, the trend of increasing acidity would likely have continued. The fall of 1.27 in pH from 2017 to 2019 represents an increase of acidity by a factor of 18 and so the halt of acidification represents good news for this important monitoring site. For Site 21 (Yara West) there is an apparent systematic fall in the mean pH from 2017 through 2018 to 2019, however the large standard deviation of the 2018 data means that there is no statistically significant difference between the successive years. However, there is a continuing fall (increase in acidity) in the pH for the minimum value from 5.8 in 2017, to 4.9 in 2018 to 4.6 in 2019, which follows the trend in the mean values. It is also helpful to see that the minimum pH continued to fall from 5.8, the natural pH of weathered gabbro and granophyre, to 4.6 over the three-year period. This demonstrates that the fall in $^{\text{mean}}$ pH from 2017-2019 is not an isolated issue and that the change in acidity is real. It is also seen in Table 14a that the maximum pH has fallen from 7.3 to 5.6 between 2017 and 2019.

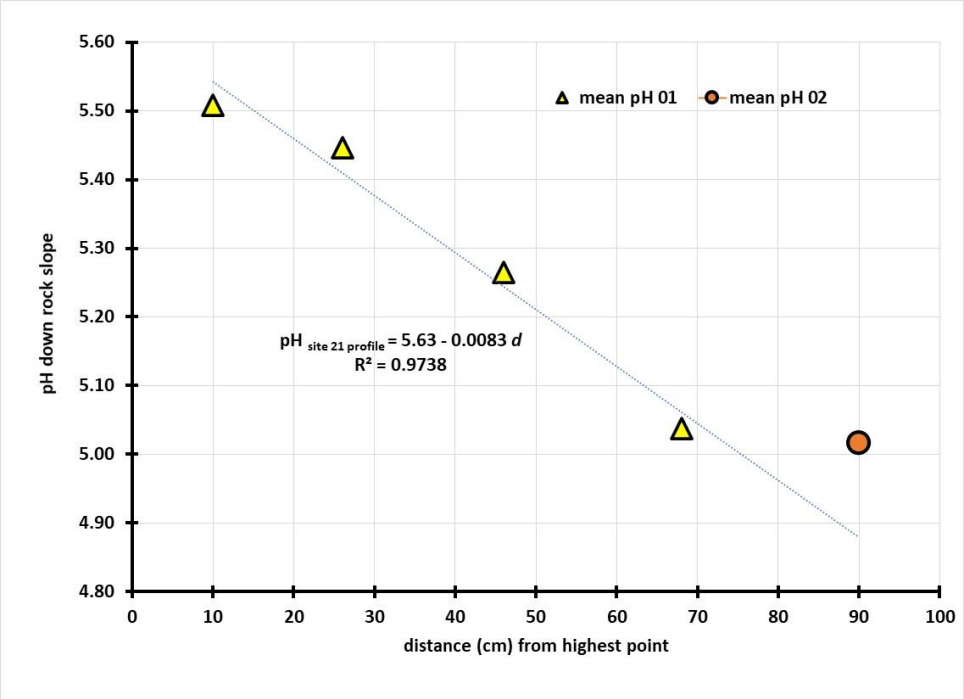

Figure 20: Plot of pH profile down the slope of rock 21 from October 2020

The pH profile shown in Figure 20 is consistent with the movement of moisture down the slope and the gradual accumulation of soluble nitrate and other anions that promote microbial activity.

The chloride readings in 2020 showed lower maximum levels than in 2019, which is hardly surprising given the intensity of cyclone Damien and the February rainfall. It was noted during the 2020 data collection that where the slope of the flat rock varied and water naturally pooled, the chloride levels could jump by as much as 200% within the space of ten centimetres. Plots of the rock surface chloride levels against the pH showed a linear increase in pH as the chloride concentration went from 20-80 ppm, with slightly different pH intercepts at zero [Cl] ppm ranging from 5.18 to 4.28. The one point that did not follow the trends was the point of the highest chloride concentration, at 160 ppm, when the pH was 4.77, which indicates that at high chloride activity there may be enough salt present to activate the chloride obligate bacteria and so increase the acidic metabolites and thus lower the pH values. The very exposed position of the flat rock on top of the hill meant that, like site 22, the research team was nearly blown over by the extremely strong winds that only abated once we had come down from the top of the hill into the plain. Lower chlorides are associated with a reduced buffering capacity to resist the acidification due to metabolic activity of the microflora and this site may have increased acidity due to the activity of chloride obligate bacteria.

Table 15a: Statistical analysis of pH values on site 21 from 2017-2020

	2020 pH	2019 pH	2018 pH	2017 pH
Mean	5.27	5.16	5.81	6.43
Standard Error	0.06	0.09	0.18	0.14
Median	5.31	5.21	5.70	6.44
Mode	5.49	5.21	n.a.	5.98
Standard Deviation	0.27	0.30	0.65	0.45
Range	1.08	0.97	2.1	1.5
Minimum	4.74	4.60	4.90	5.80
Maximum	5.82	5.6	6.9	7.3
Count	22	16	13	13

The mean E_h or redox potential for the site was much the same as it was in 2019 and the Pourbaix diagram indicated that five of the 22 measurement points lined up with the major electrochemically active materials being rich in iron. However, this is not reflected in soluble iron reporting in the wash solutions, but they are essentially different tests of surface reactivity.

Table 15b: Statistical analysis of redox potential and chloride levels site 21: 2017-2020

	2020 E vs NHE	2019 E vs. NHE	2018 E vs NHE	2020 Cl ppm	2019 Cl ppm	2018 Cl ppm	2017 Cl ppm
Mean	0.379	0.369	0.487	43	95	20	143
Standard Error	0.003	0.005	0.204	7	20	4	14
Median	0.379	0.369	0.489	33	68	21	136
Mode	0.378	n.a.	0.484	22	25	n.a.	214
Standard Deviation	0.014	0.018	0.209	31	70	13	44
Range	0.071	0.066	0.229	140	225	46	126
Minimum	0.333	0.340	0.472	20	25	1	88
Maximum	0.404	0.406	0.499	160	250	47	214
Count	22	16	13	22	16	13	13

Fourteen of the other reference points on the rock showed that the 29 mV/pH slope and the E^0 was associated with manganese equilibria and so it can be noted that the active components in the rock

surface patina are dominated by manganese ions. Plots of the E_h against chloride ion activity show that the redox equilibria respond positively to the increasing presence of chloride, at approximately 0.6 ± 0.1 mV per ppm of surface chloride ion.

Summary of observations on site 7, Deep Gorge in October 2020

The long-term interactions of the Deep Gorge site (no 7) with the microenvironment in the Burrup has been monitored, on and off, since 2003 and is summarised in Figure 21, which shows that when cyclonic rain events took place in March 2004 the pH increased from 4.59 to 4.98, which amounts to a 2½ decrease in acidity. Between the readings in February 2004 and those taken in 2017 there were five cyclonic rainfall events which dumped a total of 852 mm of rain in the area. The net measurable effect of this was to increase the pH from 4.98 to 5.57 which is nearly a four-fold reduction in acidity. Exposure to an accidental loss of ammonia from the Yara plant in the middle of the year in 2018 may have contributed to an increased pH of 6.88, but this fell to 4.42 by the time the measurements were repeated on the same rock some fourteen months later. The increase in acidity seems to be strongly linked to an increase in the amount of nitrate ions present in the local microenvironment. Following the February 2020 cyclonic rain, during which 235 mm fell in two days, the pH moved to a more alkaline value of 5.75 i.e., the rainfall seems to be "resetting" the acidity decay clock. The annual increase in pH for Deep Gorge is 0.037or just over a factor of 8½% per annum over the 2004 to 2017 interval during the cyclonic rain events.

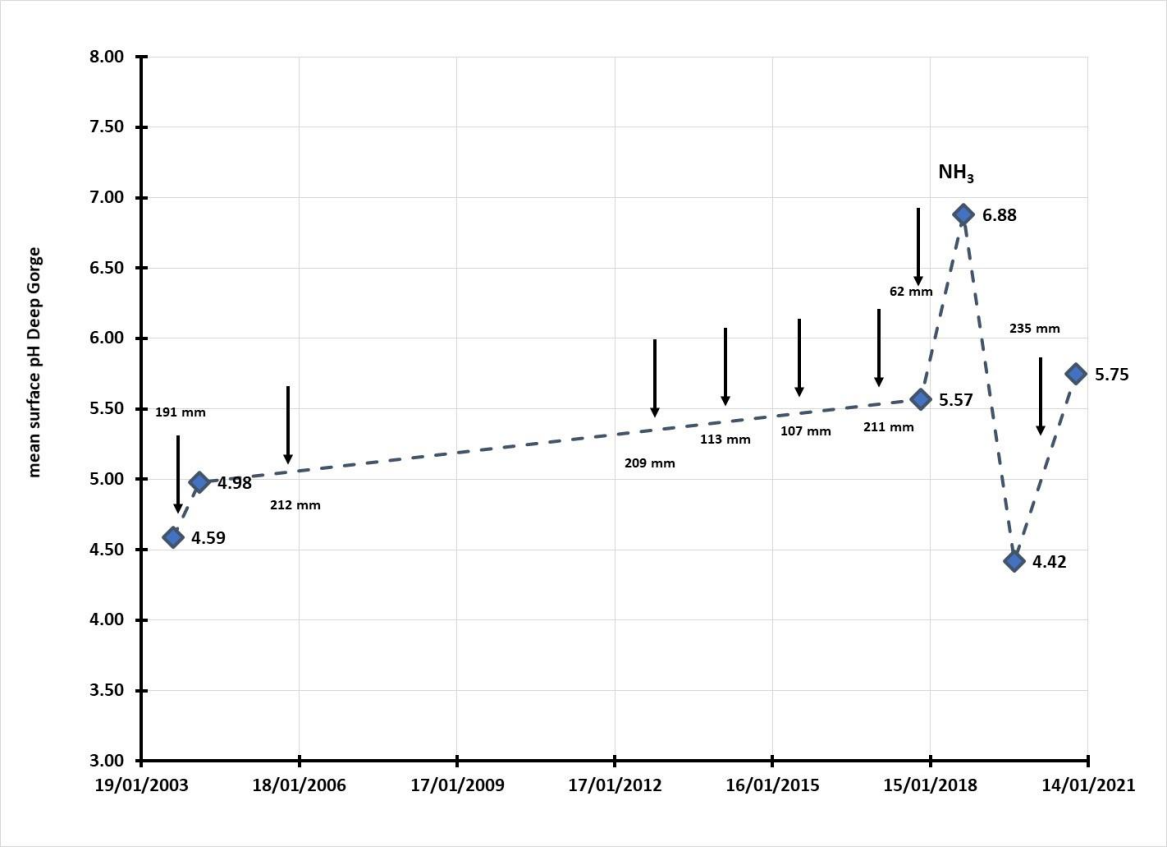

Figure 21: Mean pH at Deep Gorge site between 2003 and 2020 with cyclonic rainfall in mm noted on the chart.

Inspection of the surface chloride data underlying the summary shown in Table 18 a & b shows a steady decrease in the amount of sea salt that has accumulated, via salt spray deposition with the cyclone in February 2020 clearly removing a significant amount of acidity and salt deposits from the rock surface. Plots of the mean chloride (ppm) since monitoring for Yara began in 2017 shows a steady decrease of approximately 6 ppm per year, which leaves little buffering capacity on the rock surface

and so this makes the pH data at site 7 more sensitive to changes in the chemical microenvironment. Part of the complexities of this site are reflected in the "see saw" shape of the pH time plots, but there are indications that the pH decreases with increasing chloride, which is contrary to other sites. This is consistent with localised activity of chloride obligate bacteria which are those microorganisms which need salt for their metabolic activities.

In the anomalously alkaline year of 2018, the higher mean E_h value of 0.429 ± 0.025 at a mean pH of 6.68 ± 0.39 places the rock surface data into the stability region of the equilibrium between Mn^{2+} and Mn_3O_4, which is characterised by the Pourbaix slope being four times the Nernstian slope 59 mV per pH change. The more acidic values of 5.6 ± 0.4 in 2017 and 4.4 ± 0.4 in 2019 favour an equilibrium between the partially hydrolysed $Mn(OH)^+$ ion and its Mn(IV) partly hydrolysed ion $Mn(OH)_2^{2+}$, as shown in Equation 19. The cyclonic rain in February 2020 "neutralised" the developing acidity at site 7 and brought the pH back to 5.8 ± 0.4, which is essentially the same as when measured in 2017 – see Figure 21.

Table 16a: Statistical analysis of pH on site 7, Deep Gorge 2017-2020

	2020 pH	2019 pH	2018 pH	2017 pH
Mean	5.75	4.42	6.68	5.57
Standard Error	0.10	0.13	0.12	0.11
Median	5.73	4.52	6.67	5.53
Mode	n.a.	n.a.	7.02	5.90
Standard deviation	0.43	0.44	0.39	0.42
Range	1.92	1.67	1.14	1.49
Minimum	4.94	3.31	6.06	4.92
Maximum	6.86	4.98	7.200	6.41

It is also noted that with the change in the mean pH from 6.7 ± 0.4 to 4.4 ± 0.4 in 2019 also brought about a change in the Pourbaix diagram. In 2018 the dominant electrochemical process involved the formation of significant amounts of the manganese equivalent of magnetite, namely Mn_3O_4 while for the 2019 measurements the slope had changed to 29 mV per pH unit and that the dominant mechanism was controlled by Equation 18 viz.,

$$Mn(OH)^+ + H_2O \rightarrow Mn(OH)_2^{2+} + H^+ + 2e^- \quad \text{..... (18)}$$

The E_h and pH data from 2020 showed that equation 18 was the dominant electrochemical reaction describing the site, with 13 of the 18 sets of readings conforming to this relationship. However, there were signs of iron reactions from the surface with higher pH and E_h readings giving equation 27

$$Fe^{2+} + H_2O \rightarrow Fe(OH)^{2+} + H^+ + e^- \quad \text{..... (27)}$$

This equation had an intercept value (zero pH) of 0.732 volts which is close to the standard oxidation/reduction potential for iron (III)/(II) of 0.77 volts vs. NHE. Inspection of the Pourbaix Atlas of Electrochemical Equilibria in Aqueous Solutions (Pourbaix 1974) shows that the range of voltage and pH on site 7 is more consistent with the equilibrium given by equation 18, since the observed values are too alkaline for free Fe^{3+} ion to be stable, but the $Fe(OH)^{2+}$ is stable in this environment.

As in previous monitoring years, it was noted that there was a strong correlation between higher E_h and increased chloride concentration, as shown by equation 28, which shows that the redox potential increases by 2.2 mV per ppm of chloride,

$$^{site\ 7}E_h = 0.361 + 0.0022\ [Cl] \quad \text{.....(28)}$$

The R^2 for the five measurements was 0.97 provides a high degree of confidence in the reality of the apparent connection with increased redox activity with increased chloride across the rock surfaces.

Table 16b: Statistical analysis of chloride and Eh on site 7, Deep Gorge 2017-2020

	2020 Cl ppm	2019 Cl ppm	2018 Cl ppm	2017 Cl ppm	2020 Eh vs. NHE	2019 Eh vs. NHE	2018 Eh vs. NHE
Mean	4.8	8.6	18.6	21.5	0.379	0.368	0.429
Std. Error	0.6	1.1	2.5	3.7	0.003	0.006	0.008
Median	4.3	7.2	17.3	24.0	0.379	0.366	0.432
Mode	2.6	6.9	n.a.	30.0	0.386	0.355	0.432
Std. dev.	2.4	3.8	7.8	11.7	0.014	0.020	0.025
Range	8.6	13	28.8	27.8	0.049	0.061	0.082
Minimum	2.4	4.3	8.2	7.2	0.142	0.339	0.380
Maximum	11	17.3	37.0	35.0	0.191	0.400	0.462

The intercept voltage is essentially the same as the redox potential for the equilibrium between Mn_3O_4 and Mn_2O_3 (Pourbaix p 288) at the mean pH of the rock surface in 2020. The rock on the reverse side of the kangaroo image at site 7,that was used for colour monitoring, was systematically assessed for surface pH, chloride, and redox potential. The mean pH of 5.9 ± 0.7 was not statistically different to the 2017 value of 5.7 ± 0.2 and although there was the full suite of chloride readings taken (13 compared with 4 in 2017) the much lower chloride content is perhaps only reflected in the more acidic minimum pH reading of 4.7 in 2018 compared with 5.3 in 2017. With less sea salt to buffer the acidic metabolites it is not unexpected to have a more acidic minimum pH value. The mean redox voltage was 0.194 ± 0.020 which is the lowest voltage of all the seven sites examined and this is a reflection that this rock was heavily impacted by rain from cyclone Damien, which has effectively stripped the surface rock of readily soluble iron and manganese minerals.

The changing nature of the rock surface is shown through the examination of the way in which the pH varies, or remains constant, across and down the sloping rock surface where the surface measurements were conducted. The rock surface slopes away at an angle of roughly 60^o and on the left side the pH falls at the rate of 0.012 pH per cm increasing distance from the leading rock surface. The intercept, the pH value at the top of the rock, was 5.13, which is typical of the natural mineralogical equilibration with water through hydrolysis reactions of the metal ions (Figure 13) reproduced from previous discussions for facilitating comparative analysis.

Previous statistical analysis (Fox 2020) indicated that the lateral distribution at constant height was a constant but that the pH decreased with movement towards the bottom of the rock, where moisture and micronutrients naturally migrate. The mean pH of the first six measurement at the 5 cm distance from the upper edge of the rock was 6.14 ± 0.42, while some 28 cm lower the mean pH was 5.64 ± 0.32 (an increase of just over three times in acidity) to a final mean pH of 5.42 some 60 cm below the first line of measurements. This pH value is 66% higher acidity than the line of measurements above it.

The top row has a small chloride ion profile across the rock with the values increasing from a low of 2.6 ppm on the left side of the rock to 4.4 ppm on the right side. The greatest separation of chloride content is seen in the middle row of measurements, with the [Cl] increasing from a low value of 2.6 to 11 ppm with an R^2 for the liner regression of six points being 0.96. The chloride profile at the bottom edge of the rock sees the chloride ion activity being half as great as in the middle row, with the salt levels increasing from 2.4 to 7.2 during the 85 cm traverse of the rock. All the chloride distribution data is consistent with rain coming in from the coast and washing the rocks during the cyclone. This rain event in February 2020 was followed by deposition of salty deposits from the prevailing westerly winds but with a sharp fall off with chloride as the wind-borne salts deposit on the surface.

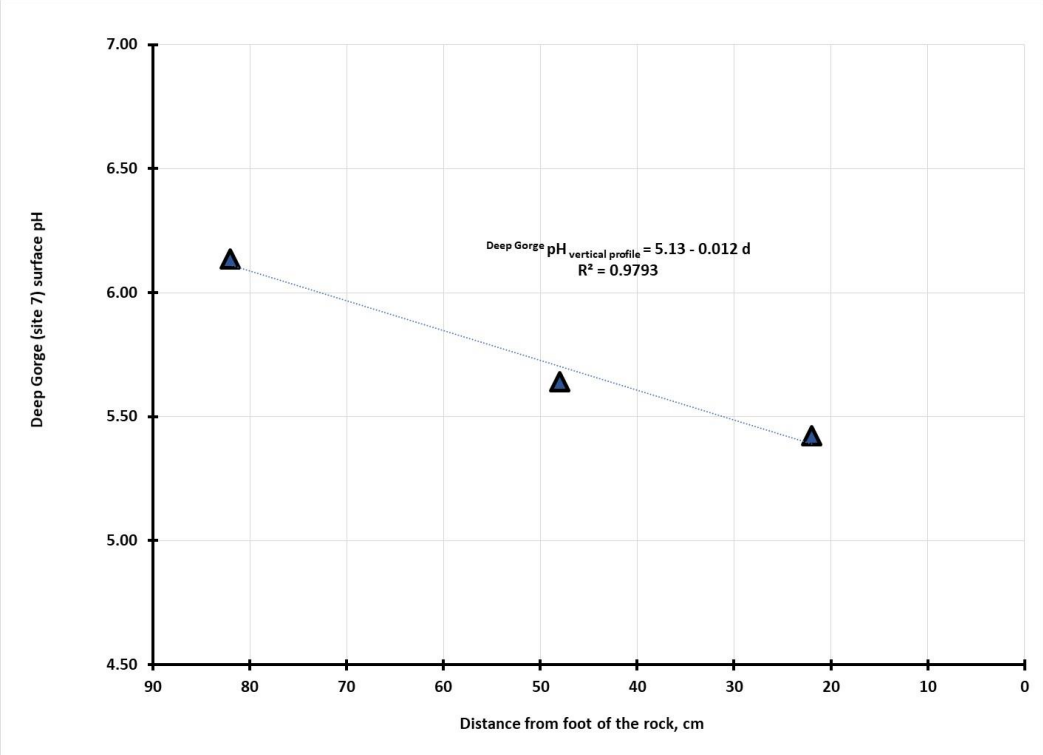

Figure 13: Plot of the pH profile down the rock face at site 7 (repeated from page 24 for convenience)

Summary of observations on site 6, Water Tanks in October 2020

The rock immediately adjacent to and approximately 50 cm forward of the engraved rock at site 6 was systematically assessed for surface pH, chloride, and redox potential in 2020, 2019 and 2018 and for both pH and chloride in 2017. The pH data collected in 2020 significantly less acidic than in 2019 because of the impact of the rain from cyclone Damien. Although cyclonic rain before the 2018 measurements had reduced the mean chloride from 191 to 2.3 ppm this dramatic fall in chloride does not account for the small increase in the mean pH in 2018 – the slight increase is acidity reflects lower surface concentration of transition metal ions such as Fe^{3+}, $Mn^{2+}$and Mn $^{3+}$ which readily undergo hydrolysis. The Pourbaix diagram for site 6 in 2020 showed up the presence of some iron (III) species, with three measurements indicating that these were electrochemically active species.

However, the site is dominated by fourteen data points that follow equation 18, namely the oxidation of $Mn(OH)^{+}$ ions to the dihydroxy manganic ion, $Mn(OH)_2^{2+}$ which remain in solution. Within experimental error the E_h values in 2020 are much the same as in 2019 and 2018. The main impact of the cyclone has been the large shift in the mean pH towards more alkaline values. The 2020 Pourbaix diagram had a slope of 29 mV per pH and so the most likely reaction is seen in Equation 16 viz.,

$$Mn(OH)^{+} + H_2O \rightarrow Mn(OH)_2^{2+} + H^{+} + 2e^{-} \quad \text{..... (16)}$$

Analysis of the E_h and chloride measurements on the large rock showed that there is a systematic increase in the redox potential on the site as the amount of surface chloride ions increases. The E_h value increases at the rate of + 1.3 mV/ppm chloride, which is consistent with the expected manner of formation of weak chloride complexes enhancing the kinetics of the relevant redox couples that are being measured on the rock surface during the testing procedures.

Table 17a: Statistical analysis of pH on site 6, Water tanks 2017-2020

	2020 pH	2019 pH	2018 pH	2017 pH
Mean	5.34	4.67	5.85	5.66
Standard Error	0.08	0.05	0.19	0.07
Median	5.41	4.64	6.11	5.76
Mode	5.46	4.59	4.70	5.85
Standard deviation	0.35	0.18	0.70	0.22
Range	1.42	0.58	1.7	0.57
Minimum	4.59	4.43	4.7	5.28
Maximum	6.01	5.01	6.4	5.85
Count	18	15	12	10

The impact of cyclone Damien in February 202 can be seen below in Figure 22, which shows the mean pH as a function of years of measurement.

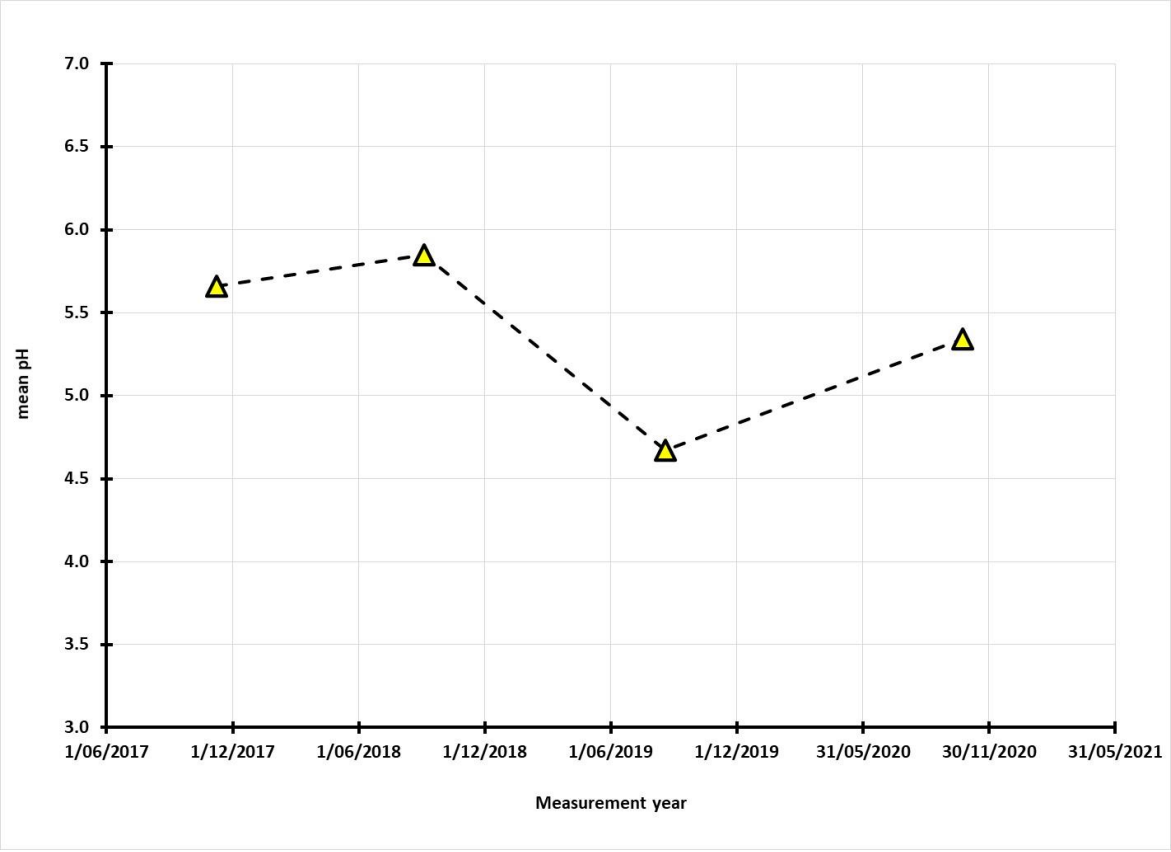

Figure 22: Plot of the mean pH at site 6 as a function of rainfall and recording date

When the pH data was plotted as a function of the chloride readings the pH gradually increased with increasing chloride concentration at the rate of 0.015 pH per ppm of chloride. This movement towards more alkaline pH with chloride concentration reflects the ocean-based origins of the chloride ions, for the deposition of wind-borne chloride brings with it a loading of alkaline salts associated with the carbonate and borate buffers present in normal seawater.

Table 17b: Statistical analysis of chloride and Eh on site 6, Water tanks 2017-2020

	2020 Cl ppm	2019 Cl ppm	2018 Cl ppm	2017 Cl ppm	2020 Eh vs. NHE	2019 Eh vs. NHE	2018 Eh vs. NHE
Mean	29	9.7	2.3	190.8	0.385	0.391	0.396
Std. Error	4	1.8	0.9	48.6	0.002	0.005	0.006
Median	23	8.5	1.2	164.5	0.386	0.390	0.403
Mode	22	n.a.	n.a.	n.a.	0.385	n.a.	0.403
Std. dev.	17	6.3	3.2	97.3	0.010	0.017	0.020
Range	60	21	11.3	218	0.045	0.050	0.068
Minimum	14	3	0.3	108	0.365	0.369	0.358
Maximum	74	24	12	326	0.41	0.419	0.426
Count	18	14	10	12	18	15	10

The trend of the pH in moving down the rock face towards more acidic values has also been observed. The rate of fall in the ^{mean} pH at site 6 was -0.08 pH/cm distance, as measured from the bottom or foot of the rock. The rain from the cyclone appears to have swept across the reference rock from the west to the eastern faces since the mean [Cl] for the eastern end of the rock was 19.8 ± 4.3 ppm compared with the more sheltered value of 71.0 ± 4.2 ppm in the so-called "rain shadow" of adjacent upright large granophyre rocks.

Summary of observations on site 5, Burrup Road

When the pH data in Table 18a is reviewed that thing that makes this site stand out is that there is a continuous trend towards more acidic values as the years progress from 2017 to 2020, as indicated by the mean pH data. Although the changes appear to be well within the normal boundaries of the variability noted in pH readings on other sites, with a typical standard deviation of ± 0.50 pH, the concern in this case is that there appears to have been no real impact of rainfall from cyclone Damien on this site, i.e., there was no upturn in the pH that moved the values towards the alkaline cycle. The simplest explanation for the pH data is that the rainfall did not hit the reference rock. In comparison with the other sites, the lower minimum pH value of 3.87, compared with 4.63 the year before in 2019 shows that there is localised microbial activity on the rock. This spot occurs towards the centre line close to the bottom of the engraved panel, where it is natural for moisture and micronutrients to accumulate.

The maximum pH values in 2020 are indistinguishable from those in 2019 and are essentially the same as in 2017 (Table 18a). It is noted that there was cyclonic rain between the 2017 and 2018 measurements and the shift to a more alkaline maximum pH in 2018 at a value of 5.58 indicates that at this time, the rock was impacted by the rain from the cyclone. It was noted that in 2020 the range of E_h was only 19 mV compared with 131 mV in 2019. In 2020 the Pourbaix diagram plots show that nearly half the voltage measurements are consistent with a 1:1 ratio of electrons to pH, which is consistent with equilibria involving oxidation of the $Fe(OH)^+$ ion, as shown in equation 27,

$$Fe(OH)^+ + H_2O \rightarrow Fe(OH)_2^+ + H^+ + e^- \quad \text{.....(27)}$$

The balance of the E_h and pH measurements correlated with oxidation of the $Mn(OH)^+$ ion, as in equation 18, in which the soluble Mn(IV) dihydroxy ion is soluble and inherently can wash off the rock.

$$Mn(OH)^+ + H_2O \rightarrow Mn(OH)_2^{+2} + H^+ + 2e^- \quad \text{.....(18)}$$

It is important to note that the subtle increase in mean acidity on site 5 means that there were no equilibria relating to the formation of Mn_3O_4, the manganese equivalent of magnetite.

Table 18a: Statistical analysis of pH values on site 5 from 2017-2020

	2020 pH	2019 pH	2018 pH	2017 pH
Mean	4.65	4.79	4.98	5.17
Standard Error	0.08	0.05	0.12	0.18
Median	4.72	4.72	5.02	5.17
Mode	n.a.	4.72	4.87	n.a.
Standard Deviation	0.30	0.17	0.43	0.60
Range	1.18	0.49	1.61	1.68
Minimum	3.87	4.63	3.97	4.36
Maximum	5.05	5.12	5.58	5.17
Count	14	16	12	14

This insoluble purple black mineral is formed when soluble Mn^{2+} ions are oxidized in equation 19 shown below.

$$3Mn^{2+} + 4\ H_2O \rightarrow Mn_3O_4 + 8\ H^+ + 2e^- \quad \text{.....(19)}$$

Thus, minerals that form in one year can at least be partially or completely dissolved between one year and the next, which explains to a large extent the apparent variability of the colour measurements on the rock surfaces.

Table 18b: Statistical analysis of redox potential and chloride levels site 5: 2017-2020

	2020 E vs NHE	2019 E vs. NHE	2018 E vs NHE	2020 Cl ppm	2019 Cl ppm	2018 Cl ppm	2017 Cl ppm
Mean	0.372	0.391	0.467	5.5	95	20	143
Standard Error	0.002	0.011	0.003	1.1	20	4	14
Median	0.373	0.394	0.466	3.9	68	21	136
Mode	0.372	0.377	0.458	n.a.	25	n.a.	214
Standard Deviation	0.006	0.038	0.011	4.2	70	13	44
Range	0.019	0.131	0.032	13.3	225	46	126
Minimum	0.362	0.318	0.453	1.5	25	1	88
Maximum	0.381	0.449	0.485	14.8	250	47	214
Count	14	16	13	14	16	13	14

The redox potential or E_h increased linearly with the chloride ion concentration at the rate of 1.1 ± 0.1 mV per ppm chloride and the values of E_h at zero chloride were typical of equilibria involving Mn(IV)/Mn(II) species. The pH response to the sea salt effect of increasing alkalinity with increasing chloride concentration had a slope of +0.08 pH/ppm chloride but at least half the measurements showed the reverse trend which indicates that chloride-obligate bacteria are present on the site 5 CSIRO specimen rock. This is consistent with the most acidic pH of 3.87 being associated with the higher chloride levels observed on the lower sections of the rock. The pH profile on the rock surface showed a general linear decrease in the pH at the rate of 0.0083 pH/cm down from the top of the surface.

Summary of observations at CSIRO Site 4, near Withnell Bay road

The CSIRO reference rock no 4 is located close to the Withnell Bay Road some 250 metres up the gully from the bisecting roadway. In the following commentary, this rock was always viewed as a "canary" rock in terms of being that much closer to the point sources of anthropogenic pollutants such as NO_x and SO_x from the main NWSP on the opposite side of the road. It is within a few hundred metres of the main flare tower for the older parts of the plant. The surface pH, chloride and E_h data was collected

in the same manner as the other sites. The rock is large, and 18 sets of measurements were taken beginning at the upper left-hand side and moving in five steps across before moving down the rock face to the left and then stepping down to keep up a zig-zag sampling patter. Owing to the diminishing size of the rock only four sampling points were taken towards the bottom or foot of the rock. The site is about 75° to the vertical. On the 22nd of October, the air temperature was 31.6 °C and the rock temperature was 43.8 °C, with and a relative humidity of 48%.

The Pourbaix diagram for site 4 in 2020 is significantly different from the six formal controlled sites in that it shows an equilibrium between Mn^{2+} ions and the solid black-brown precipitate of MnO_2 or manganese dioxide. The regression analysis is described by equation 16,

$$Mn^{2+} + 2\ H_2O \rightarrow MnO_2 + 4H^+ + 2\ e^- \quad \text{.....(16)}$$

The anticipated slope for this reaction is 2 x 59 mV/pH or 118 mV/pH and the observed slope was 129 ± 8 mV/pH which is strong evidence, with an R^2 of 0.9714, that the description is apt. The other data points followed the common manganese (II) to manganese (IV) reaction given by equation 18,

$$Mn(OH)^+ + 2\ H_2O \rightarrow Mn(OH)_2^{2+} + H^+ + 2\ e^- \quad \text{.....(18)}$$

This equation gives a Pourbaix slope of 29 mV/pH as expected for the 1:2 ratio of protons to electrons. As has been commonly noted in this October 2020 seasonal report, the pH was more acidic as the sampling points moved down the rock face and the pH fell at the rate of -0.013/cm which is like other granophyre sites in the Burrup.

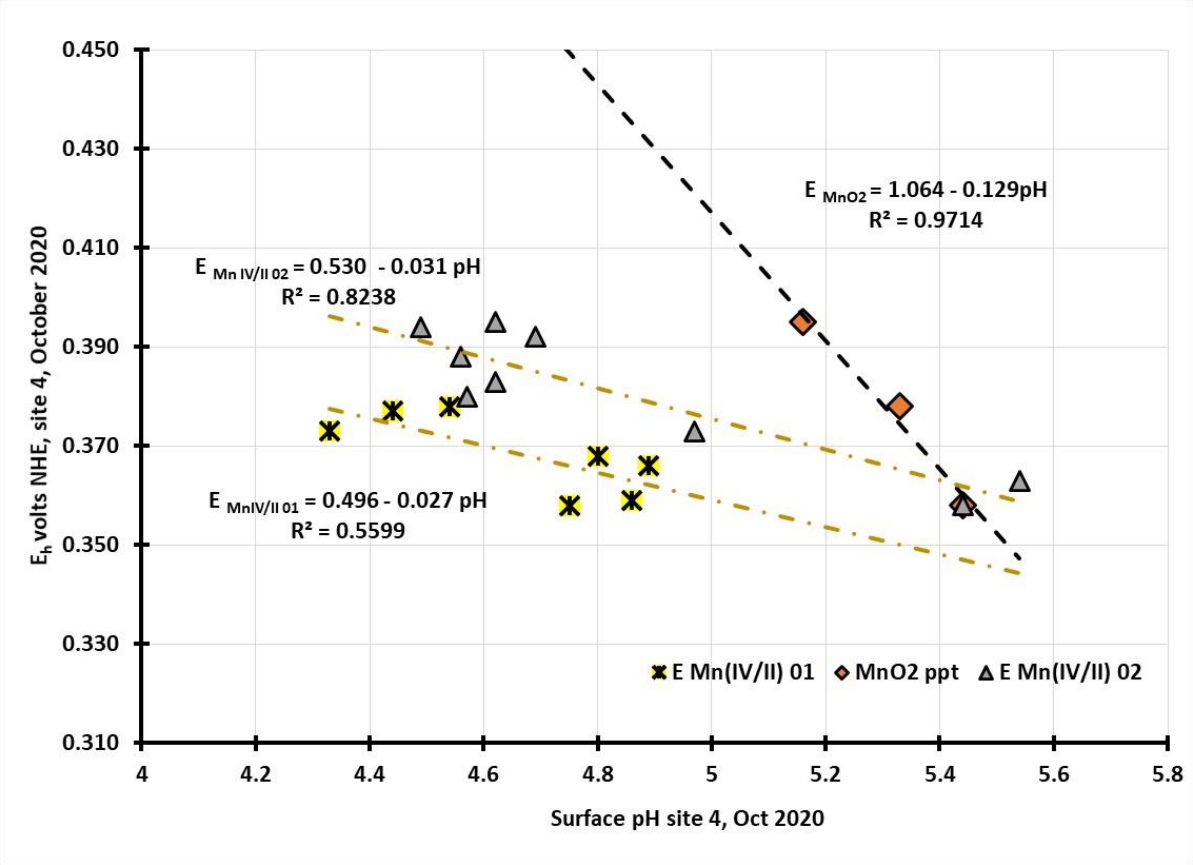

Figure 23: Pourbaix diagram for site 4, October 2020

Inspection of Figure 23 shows that two sets of measurements were showing the same -29mV/pH slope but owing to the roughness of the rock surface there was some instability in the E_h readings, so the data points are scattered and so this is reflected in the lower R^2 values for the regression analyses. For the more anodic intercept with an R^2 of 0.82 the slope was 31 ± 5 mV/pH and for the more scattered data points with the 34 mV less positive $E_{zero\ pH}$ the slope with an R^2 of 0.56 was 27 ± 11 mV/pH. The

upper regression line mainly consisted of data points on the upper and more exposed section of the rock while most of the other points related to the lower half of the large rock.

Table 19a: Statistical analysis of pH values on site 4 from 2017-2020

	2020 pH	2019 pH	2018 pH	2017 pH
Mean	4.81	4.43	5.52	3.81
Standard Error	0.08	0.10	0.24	0.17
Median	4.72	4.48	5.34	4.05
Mode	4.62	4.48	5.34	4.05
Standard Deviation	0.35	0.35	0.92	0.52
Range	1.21	1.12	2.90	1.44
Minimum	4.33	3.83	4.38	2.98
Maximum	5.54	4.95	7.28	4.42
Count	18	15	12	9

Table 19b: Statistical analysis of redox potential and chloride levels site 4: 2017-2020

	2020 E vs NHE	2019 E vs. NHE	2018 E vs NHE	2020 Cl ppm	2019 Cl ppm	2018 Cl ppm
Mean	0.377	0.392	0.485	11.0	4.4	2.2
Standard Error	0.003	0.004	0.003	1.3	0.5	0.5
Median	0.378	0.389	0.485	9.0	3.8	1.4
Mode	0.358	0.376	0.480	9.0	2.8	1.5
Standard Deviation	0.013	0.015	0.011	5.6	1.9	2.1
Range	0.037	0.037	0.046	31.2	5.9	6.6
Minimum	0.358	0.375	0.467	21.8	2.6	0.5
Maximum	0.395	0.412	0.513	6.2	8.5	7.0
Count	18	15	12	18	15	12

This site generated quite complex pH and chloride data, which is best illustrated in Figure 24, which is a plot of the surface pH against the chloride concentration. The upper sections of the rock had the most acidic intercept, which reflects the surface activity and response to the buffering effect of sea salts, as reflected in the chloride ion activity, and this area had a regression equation reflecting this (Equation 29),

$$pH_{\text{top section}} = 3.97 + 0.11\,[Cl] \quad \text{.....(29)}$$

The R^2 for this equation was relatively low at 0.80 and this is reflected in errors of ± 0.03 in the slope and ± 0.25 in the intercept value.

When the data from the lower section of the large rock is plotted against chloride activity a similar trend to that see for the top section of the rock is seen, in that the pH regularly increases with the chloride ion concentration, as shown in equation 30,

$$pH_{\text{lower section}} = 3.88 + 0.073\,[Cl] \quad \text{.....(30)}$$

This data set had a much stronger R^2 value at 0.94 so the errors in the slope of ± 0.0085 and ± 0.095 were correspondingly smaller.

The intercept value of 3.9 ± 0.1 makes it almost identical to the response to sea salt in 2019 when the intercept value was 3.5 ±0.2 pH at zero ppm surface chloride. Inspection of table 19b of the chloride levels shows that although still small, at 11.0 ppm in 2020, it is higher than in 2019 when the [Cl] was

only 4.4 ppm. Higher chloride means higher intercept values of the pH and so the behaviour of the rock surface, with those areas of decreasing acidity with increasing chloride, are internally consistent across time.

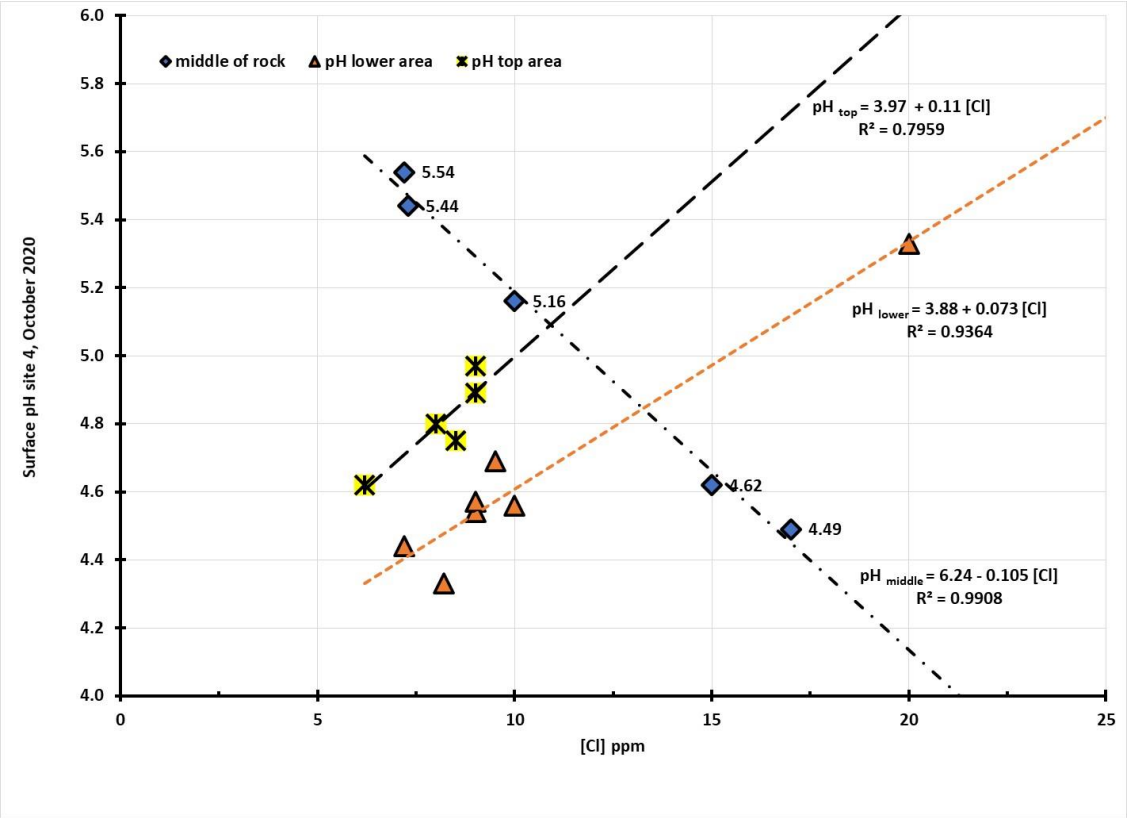

Figure 24: Plot of mixed pH response on site 4 to chloride ion activity, October 2020

For the middle sections of the rock, from the top to the bottom, there was a reverse trend, shown by the regression equation 31, where the pH was seen to become increasingly acidic with increasing chloride ion activity.

$$pH_{\text{middle of rock}} = 6.24 - 0.11\,[Cl] \quad \text{.....(31)}$$

Inspection of figure 24 shows that there is a strong regression analysis with an R^2 value of 0.99 and the intercept $pH_{\text{zero Cl}}$ was 6.24 ±0.07 and the slope was -0.11± 0.006. The corresponding equation in the 2019 site assessment had a more acidic intercept value of 5.23 and a slightly steeper slope at -0.19 pH per ppm chloride. Decreasing pH with increasing chloride is an indicator of the activity of chloride obligate bacteria (Equation 31).

The apparent sensitivity of the location of the measurement points on the rock surface was again reflected in the redox voltage measurements. Measurement points to the left and midline of the rock showed an increase in E_h with increasing chloride, with an intercept (zero chloride) voltage of 0.329 ±0.006 and a slope of 3.8 ± 0.4 mV/ppm chloride and the associated R^2 value was 0.97. Ten of the other measurement points from the mid-line to the right-hand side of the rock had an R^2 of 0.90 and an increase of E_h with chloride at the rate of 11.4 ± 1.4 mV/ppm chloride and an E_h at zero chloride of 0.277 ± 0.012 volts vs. NHE. The much lower $E_{\text{zero Cl}}$ voltage indicates that there is a difference in the mineralogy of the centre line of the rock towards the right-hand side.

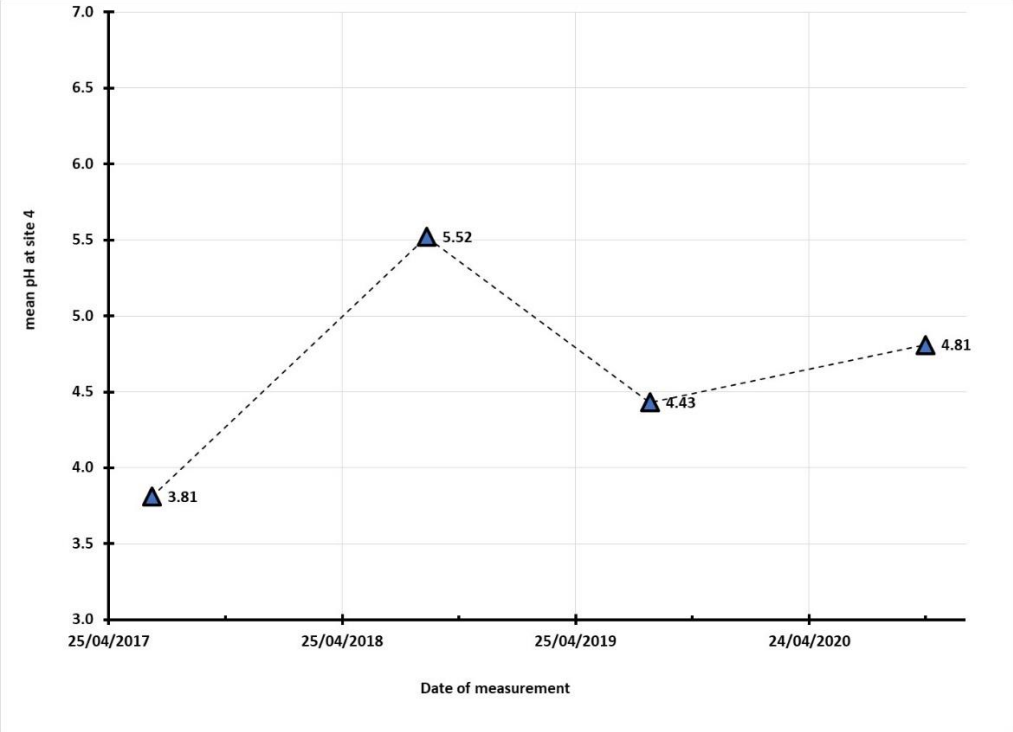

Figure 25: Plot of annual mean pH at site 4 from 2017-2020

Inspection of the annual pH data in Table 19a (above) and in Figure 25 below shows that the site has moved from being the most acidic of all sites measured between 2017 and 2020 to become one of the average pH sites. The cyclonic rainfall event on the 6th June 2018, before the measurements were taken on September 4, appears to have had a major impact on the rock surface, since the mean pH increased from 3.8 to 5.5, which represents a 50-fold reduction in acidity. Within a year the site pH had decreased to 4.4, over 12 times more acidic than in the previous year and this acidification trend was stopped through the intervention of cyclone Damien in February 2020, which resulted in the increased mean pH to 4.8. Given that the typical pH of weathered gabbro and granophyre rocks in the Burrup is around 5.6 ± 0.2, the post cyclone pH is still more acidic than would be expected in the absence of anthropogenic growth stimulants such as nitrate ions. The nitrate concentration on the sample *a* rock was 0.23 ppm and on rock *b* the level was 0.14 ppm nitrate, which is clearly enough to stimulate microbiological activity.

Environmental impact on the Climbing Man site 2003-2020

Owing to the nature of the main panel at the Climbing Man site, it is only practical to record the pH values, since other measurements require more physically demanding procedures. Thus, the surrogate rock a few metres to the left of the main panel has been used for measurements of the redox, pH and chloride data over the years. However, this unique situation is of great benefit as it allows for a direct comparison of the impact of the rock orientation on the adsorption of gaseous emissions and, indirectly, provides a measure of how rain events impact on the rock art sites. Owing to the singular cultural value of the main panel, measurements have been made on the pH of this site since 2003, apart from the hiatus period between February 2004 and July 2017. The Fox report (Fox 2020) conducted statistical analysis of the changing pH values across the Burrup. His findings, inter alia, was noted that the pH was generally consistent across the rock surface but that there was an increase in acidity as the measurements progressed down the rock surface from the top towards the bottom.

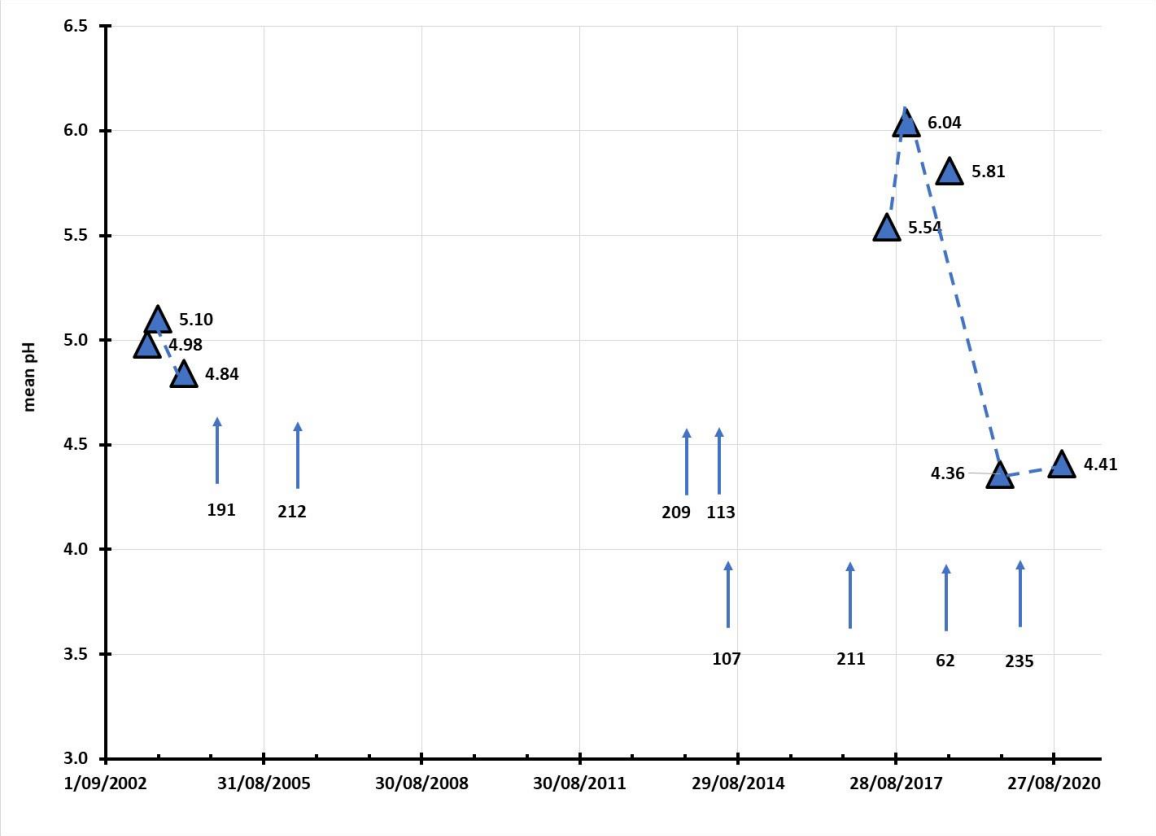

Figure 26: Mean pH at Climbing Man from June 2003 to October 2020, showing mm of cyclonic rainfall.

Previously published work (MacLeod 2012) had shown that the availability of water was a key determinant in the overall level of microbiological activity on Burrup rocks. As moisture migrates down a sloping rock face the surface pH will reflect an increased concentration of micronutrients and moisture and so the acidity will increase. On the near vertical (5°) Climbing Man panel the slope varied from 0.033-0.037 pH/cm while on the split rock (approximately 35°) the slope varied between 0.007 and 0.009 pH/cm. Clearly the impact of the migration of water and micronutrients down a steep slope is much greater than on a gentler slope. The mean pH of the Climbing Man panel is shown in Figure 26.

The impact of cyclonic rain on the Climbing Man panel shown in Figure 26 resulted in an alkaline shift between 2004 and 2017 and between the end of June and the beginning of November there must have been some localised rain event, which shifted the mean pH to 6.04. The normal process of adsorption of NO_x gases and other emissions results in acidification of the rock surfaces, which fell from 5.8 to 4.4 in eleven months. The post-cyclone Damien mean pH is well within experimental standard deviations so in effect the cyclonic rain event had no impact on this main panel, as it is in a rain shadow with protection by adjacent high rocks which offer some protection from weather coming in from the westerly direction.

Observations on the Climbing Man split rock adjacent to the main panel

Given that only pH data could be safely recorded on the main panel on the Climbing Man, the detailed electrochemical measurements were conducted on the nearby "split rock" which is within three metres left of the main frieze. Plots of the E_h and pH data from this site gave Pourbaix diagrams which indicated that there was a combination of electrochemical reactions taking place on this site. Almost half the data sets gave regression equations that indicated that the oxidative hydrolysis of Fe^{2+} ions to

produce $Fe(OH)^{2+}$ ions gave the expected Nernstian slop of -0.055 ± 0.006 volts per pH for a one electron oxidation step producing one proton, as in Equation 27,

$$Fe^{2+} + H_2O \rightarrow Fe(OH)^{2+} + H^+ + e^- \quad \text{.....(27)}$$

with an intercept value of 0.708 ± 0.005 volts vs. NHE which is in the vicinity of the E^0 for the Fe^{3+}/Fe^{2+} redox system, which is +0.77 volts vs NHE. It was noted that the washing data from two nearby rocks some three metres down the slope gave no detectable iron and had a mean concentration of 5.5 ± 2.9 ppb manganese. These data points were found towards either the left or the right-hand side of the large rock. The other data sets followed equation 19, with a Nernstian slope of -0.038 ± 0.007 volts per pH and an intercept (zero pH) voltage of 0.595 volts vs. NHE which is consistent with the Mn(IV)/Mn(II) redox couple,

$$Mn(OH)^+ + H_2O \rightarrow Mn(OH)_2^{2+} + H^+ + 2\ e^- \quad \text{.....(18)}$$

These data points were focused on the middle of the rock. If the mean pH recorded in 2003-2004 is correlated with the 26th June 2017 value there is a strong linear regression, R^2 0.96, and a daily slope of -0.0002 pH or a fall of 0.073 pH per year.

As was found for sites 4, 6, 7, 21, 22 and 23, the cyclone in February 2020, which brought a total of 235 mm of rain over two days, the surface of the "split rock" adjacent to the left of the Climbing Man panel, was significantly impacted by the rain which caused an alkaline shift of 1.5 pH or a factor of thirty times less acidic than in 2019. This alkaline shift is in marked contrast to the main panel where there was no discernible impact of the cyclone. The sheltering nature of adjacent rocks was also noticed on site 6 (water tanks) where there was a readily discernible increase in surface chloride as the rock was traversed from the exposed left-hand side towards the right hand, sheltered side, of the monitoring rock. The adjacent Climbing Man split rock had a mean chloride concentration of 7.1 ± 0.9 ppm in the middle of the rock but in a 25 cm band, the concentration was 23.4 ppm – the likely cause for this deviation is due to a combination of run-off as this area was from the bottom of the rock and was due to evaporative concentration.

Plots of the pH profiles down the large split rock adjacent to the Climbing Man had variable slopes, depending on which part of the rock was considered. For points at the foot of the rock the pH increased from 5.09 by 0.008 pH/cm movement up the rock face. For the mid-line, the intercept was 5.36 and the increase in pH was 0.009 pH/cm and for data collected from the right edges of the rock, the pH at the bottom was 5.69 and it increased by 0.007 pH/cm. Within experimental error the pH slopes down the rock are the same at a mean rate of 0.008 pH/cm; this simply confirms the common mechanism of biological control of the pH when there is an adequate supply of water and micronutrients.

The E_h values increased to more positive values as the chloride ion activity increased. Although the split rock only had time to accumulate 35 ppm chloride after the cyclone in February 2020, it was enough to elevate the E_h by 24.5 millivolts. The variable nature of the differences in pH between the split rock and the main Climbing Man panel is illustrated diagrammatically in Figure 27

The main point to note from the data displayed in Figure 27 is that at times cyclonic rain brings about significant washing of the split rock and minimum impact on the main panel at the Climbing Man site. When the delta pH is negative the main panel has been more heavily impacted than the adjacent rock and such changes are more noticeable because of the greater underlying acidity on the main panel compared with the split rock which has been more frequently subjected to the impact of rain events.

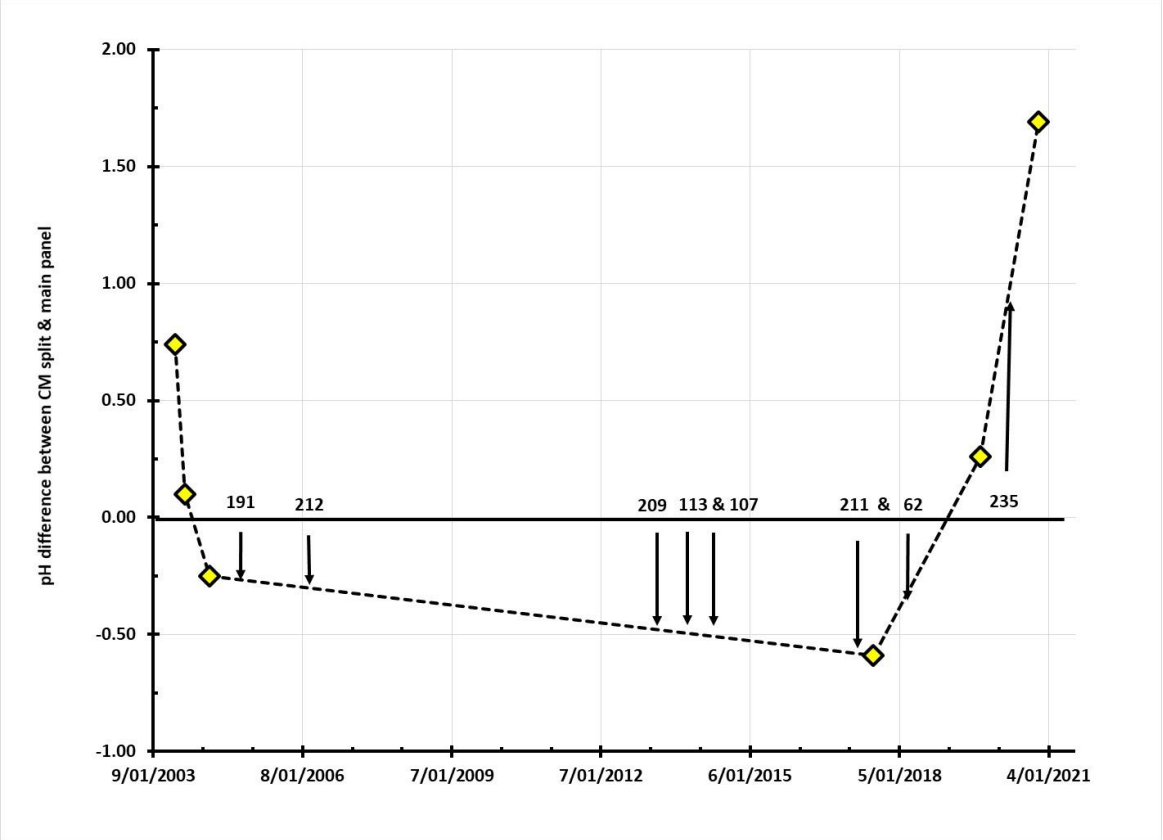

Figure 27: Plot of the δpH (Climbing Man split – main panel) vs. cyclonic rainfall

It was noted that on the CSIRO monitoring rock 4 some 250 metres up the gully, there were parts of the large rock where there was convincing evidence of the acidity increasing with the chloride ion activity. It is therefore not unexpected that the surrogate Climbing Man split rock shows similar behaviour. There was no pH response at higher chloride levels, between 25 and 35 ppm, which is probably due to buffering capacity resisting the acidification reactions. In the low range of 6-12 ppm chloride the pH increased significantly by +0.096 pH/$[Cl]_{ppm}$ and for this reaction, the intercept pH was quite alkaline at 7.18. It is likely that this alkaline pH is simply an artefact of the line fitting algorithm. In the absence of confirmatory data on the presence of chloride obligate bacteria on the Climbing Man rocks, it seems more reasonable to leave the question open for future determination.

Table 20a: Statistical analysis of pH values on the Climbing Man split rock from 2017-2020

	2020 pH	2019 pH	2018 pH	2017 pH
Mean	6.10	4.62	5.81	6.04
Standard Error	0.08	0.05	0.10	0.21
Median	6.13	4.59	5.93	6.05
Mode	6.21	n.a.	5.97	5.48
Standard Deviation	0.30	0.16	0.39	0.61
Range	1.18	0.56	1.27	1.68
Minimum	5.39	4.4	5.19	5.26
Maximum	6.57	4.96	6.46	6.94
Count	14	12	14	8

Table 20b: Statistical analysis of redox potential and chloride levels CM split: 2017-2020

	2020 E vs NHE	2020 Cl ppm	2019 Cl ppm
Mean	0.375	10.5	14.4
Standard Error	0.007	2.3	3.0
Median	0.374	7.1	12.2
Mode	0.378	n.a.	4.6
Standard Deviation	0.027	8.8	10.5
Range	0.109	31.1	35.5
Minimum	0.352	4.1	4.6
Maximum	0.461	35.2	40.1
Count	14	14	12

Colour measurements

Measurements conducted in October 2020

Colour measurements were conducted on sites 4, 5, 6, 7, 21, 22 and 23 using the Konica-Minolta Chromameter (KMC) with a set of 10 independent measurements on the background and engraved surfaces at the four designated reference points. Previous work in 2019 and 2018 had used 20 measurements but statistical analysis by Microfading Australia showed that this produced too many random errors, owing to the challenges of positioning the sensing head on areas characterised by high microtopography. The details of the colour measurements made in 2020 have been compared with those made in 2019, 2018 and in 2017. Following advice from Microfading Australia at the end of their 2019 report, the sampling protocol was changed so that before measurements each rock area was dusted with a dry paint brush to clear loose iron ore dust from the surface. Colour measurements on inhomogeneous surfaces is fraught with difficulty but by applying simple house cleaning protocols the sampling errors were minimised.

The initial analysis of the colour differences was conducted using the methodology outlined in the CSIRO September 2008 Report (CSIRO 2008) which involved using the CIE standard formula for colour difference by taking the square root of the differences between the L, a and b values recorded by the Konica Minolta Chromameter. The formula used for determining the colour difference was as noted below in Equation 32,

$$\text{delta } E_{97} = \{(L_b-L_e)^2 + (a_b-a_e)^2 + (b_b-b_e)^2\}^{½} \quad \text{.....(32)}$$

In Equation 32 the subscripts after the L, a and b values relate to the *b* for the background and *e* for the engraved surfaces. When comparing the colour data, it should be noted that the 2017 measurements were characterized by scatter due to the dust. Owing to the cyclonic rain that preceded the 2018 data collection there was much less dust on the rock surfaces. A moderate amount of surface dust was noted in 2019 and this issue was managed with a light "dusting" from a soft and very flexible natural bristle paint brush for the data collection, which had a smaller data scatter than the data points from 2019. Owing to uncertainties associated with the assessment of the colour difference readings on each of the six sites, both the original data and the calculated delta E values were reviewed by Bruce Ford of www.microfading.com. This review was necessary as there have been major revisions by colour conservators regarding the evaluation of what are statistically reliable measurement of colour differences. Using the criterion that the MCDMt (total mean colour distance from the mean)/Delta E > 0.5 the sites were assessed for colour difference between the background and the engraved areas as being compliant or not.

The primary colour difference data between the background and the engraved areas for 2020 is reported in Table 19 below. The data was collected with a measurement area of 8 mm. Owing to some operational challenges with the instrument settings the data collected for site 5 was repeated the

following day on all the four testing locations, many of which are difficult to get the head accurately positioned. Thus, for site 5 there was generally good agreement in the colour differences for spots 1-3 but the exceptionally low colour difference for spot 4 in the initial data set was replaced with a value that was roughly twice that originally observed. The low $^{5}\Delta E_{4}$ (site 5 spot 4) was due to the difficulty in properly locating the actual reference points for the background and the engraved areas. With the benefit of hindsight, the $^{4}\Delta E_{2}$ value at 0.31 was also due to challenges in correctly matching up the background and engraved reference points. For site 6, the Water Tanks, the low difference in this granophyre site is due to the poor colour contrast between the background and the engraved areas, as shown in Figure 29.

Table 21: Colour differences for 2020 on four spots on each site ΔE (background – engraving)

$pH_{minimum}$		spot 1	spot 2	spot 3	spot 4
4.33	site 4	5.09	0.37	2.82	2.46
3.87	site 5	3.91	5.22	5.80	1.85
3.87	site 5 repeat	3.49	3.85	4.50	3.49
4.59	site 6	0.63	0.95	0.47	1.47
4.94	site 7	4.05	3.55	1.67	1.53
4.74	site 21	3.89	3.56	4.11	5.74
4.58	site 22	6.20	2.81	3.79	3.34
3.82	site 23	2.11	3.40	3.66	1.35

In the commentary on the electrochemistry on each of the Yara monitoring sites it had been noted that when the pH falls by as little as 0.3 some species such as MnO_2 do not precipitate but tend to be lost as $Mn(OH)_2^{2+}$ (equation 18) and that formation of the purple black mineral Mn_3O_4 is favoured when the pH moves in the alkaline direction by the same increment. In order to see if the colour contrast between the background and engraved areas was in response to changes in the chemical environment, the ΔE data was plotted as a function of the surface pH on the rocks. It had been reported in 2019 that the colour contrast was quantifiable as a function of the difference in minimum pH between 2019 and the preceding year of 2018.

For the data collected in 2020, the colour contrast between the background and engraved areas in 11 of the 24 spots showed a set of clear responses of increasing colour contrast with decreasing minimum pH. In simple terms, this means that as the rock surfaces become more acidic the repatination processes that are the result of natural weathering are being modified, as a thin layer of precipitated mineralisation is removed. Regression analysis on the three lines, listed as equations 33-34, show that the slope of equation 33 is -3.88 ± 2.81 ΔE/pH; the large error is associated with a low R^2 value of 0.65.

$$\Delta E_{upper} = 22.1 - 3.88\ pH_{minimum} \quad \text{.....(33)}$$

The second line was described by equation 34, which had an R^2 of 0.95, which gave a much lower standard deviation of the slope which was ΔE/pH with a value of -2.92 ± 0.68,

$$\Delta E_{middle} = 19.8 - 4.06\ pH_{minimum} \quad \text{.....(34)}$$

From the errors in the slope of equations 32 and 33 they can be said to be essentially the same value and the intercept ΔE value of equation 32 was 22.1 ± 13.4 at zero pH and for equation 33 the intercept value was 19.8 ± 2.1 and so the two responses shown in figure 28 are experimentally one and the same.

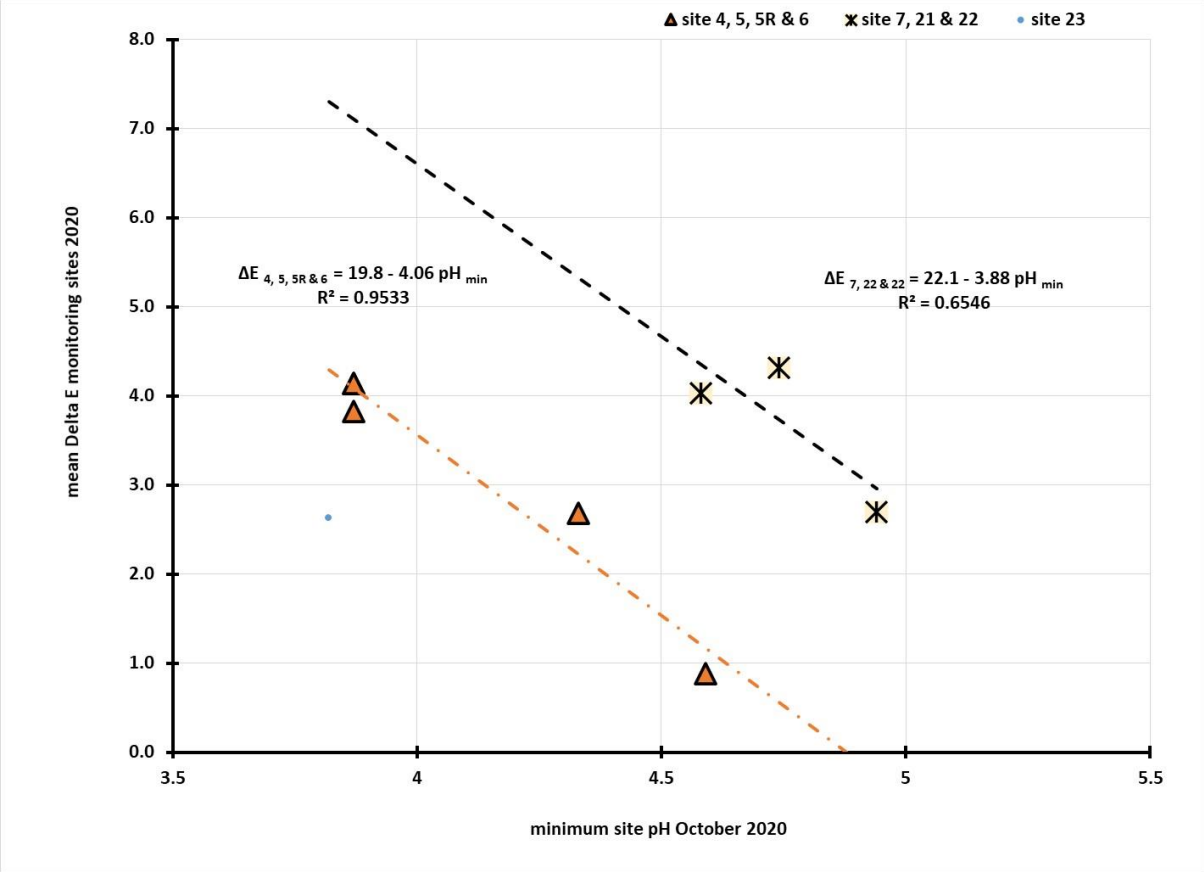

Figure 28: Plot of the contrast difference versus the changes in minimum pH

Inspection of the data plots in Figure 28 illustrates those locations where the colour contrast values are getting close to the limit of human eye in perceiving a just noticeable fade, at the value of ΔE of 2.0. The data point for site 23 lies to the left of equation 33 (for sites 4, 5 and 6) which simply means that the acidity level that brought about the change in colour contrast at the measurement points was much closer to the predicted value of 4.2 from equation 33. This pH is typical of the third column of measurements approximately 90 cm from the left-hand side of the rock, which is about 25 cm from the line of spots 1-3 on the right-hand side of the engraved rock, so the $pH_{minimum}$ was used for site 23, which was not a good choice for the model.

The value of using the chromameter for monitoring the colour difference between the background and engraved areas is clearly seen in Figure 29, which shows the background and engraved images at site 6, the Water Tanks. With a mean ΔE value of 0.88 ± 1.8, the instrument is much better at picking up changes than is the human eye. This provides a note of extreme caution to those commentators who say that "I can see the colour contrast has changed" for their perceptions are not borne out of reality on the rock surfaces.

This lack of contrast is not just due to the nature of the rock substrate, for when the colour difference at site 5 (Burrup Road) is viewed its ΔE values vary from a minimum of 3.0 to 5.0, which are readily discernible as shown in Figure 30. Both rocks illustrated in Figures 29 and 30 are made of granophyre. The most likely reason why there is little colour contrast on rock 6 (Water Tanks) is that the site is much older than the engraved image of the cormorant on site 5 (Burrup Road).

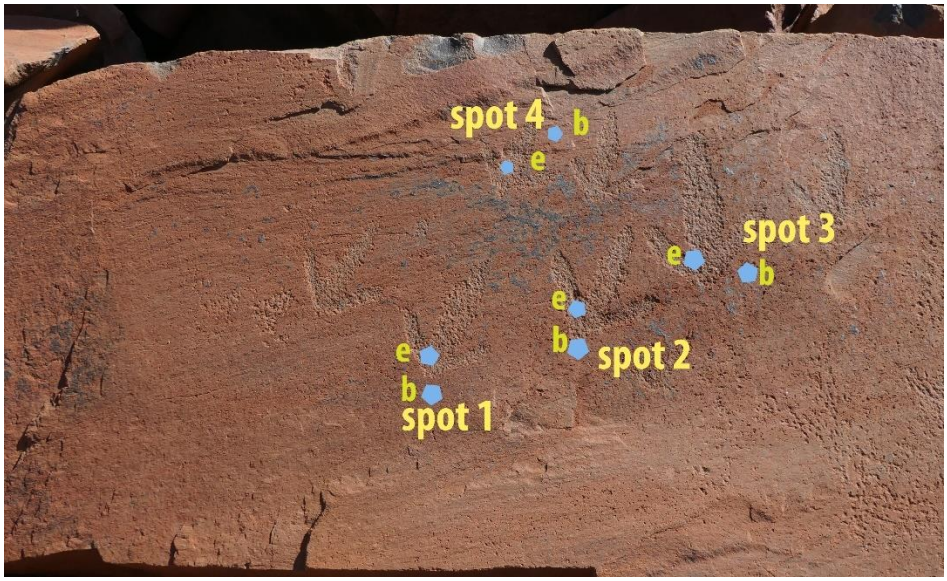

Figure 29: Reference rock no 6 (Water Tanks) with spot locations showing background and engraved areas

When the colour difference data from October 2020 was plotted as a function of the mean pH, there were two main responses of colour with acidity, as shown by equations 35 and 36, as noted below.

$$\Delta E_{upper} = 25.9 - 3.84\ pH_{mean} \quad \text{.....(35)}$$

Like the relationship shown for the $pH_{minimum}$ data in equation 32, the rocks with the greatest colour contrast were at sites 7 and 22, but naturally the slope and the intercept values are significantly different. For equation 35 the R^2 value was 0.97 so the data fitted well with a slope error of ±0.45 and an intercept error of ± 2.5, which brings it down to the standard deviation correction range of equation 36, which had an error of ± 1.5 ΔE. The lower colour difference values reported in equation 35, were dominated by the granophyre sites at site 4, 5 and 6, with the gabbro site 23 included

$$\Delta E_{middle} = 21.5 - 3.87\ pH_{mean} \quad \text{.....(36)}$$

The regression data fit (R^2) for these colour measurements was 0.94 and so the error of the slope was ± 0.30 while the error in the intercept was ± 1.5, which makes the slopes and intercepts being unable to be statistically distinguished as being separate. The third data set was like that defined by equation 36 but with a slightly different slope. The differences in the intercepts of equations 32 and 33, for minimum pH and those for equations 35 and 36, are simply an arithmetical adjustment to cope with the differences in the mean and minimum pH on each of the seven sites.

Put in the simplest of terms, a much more readily interpretable set of ΔE colour change data, as measured by the Minolta Chromameter, is obtained when the colour differences are plotted as a function of the minimum pH observed for each site.

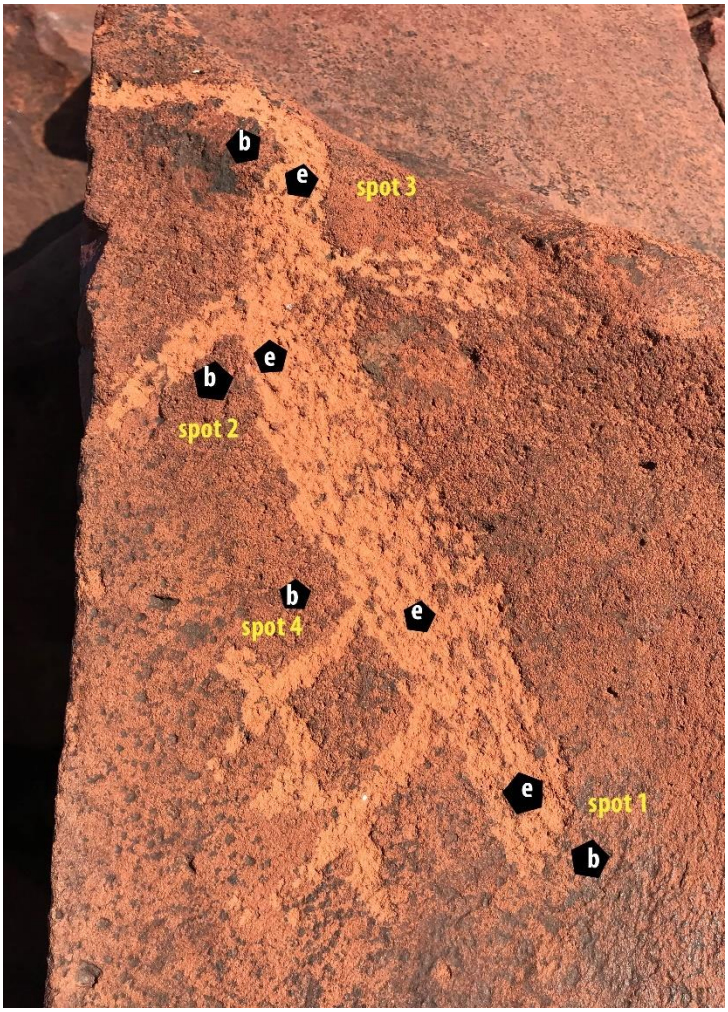

Figure 30: Site 5 showing locations of the sampling points at Burrup Road

Colour differences across the sites between the years 2017-2020.

A series of calculations by Microfading Australia (Ford 2020) were conducted in which the data was statistically analysed to see if the mean colour differences between the background and the engraving at each reference point on the monitored rocks was meaningful. If the answer was YES, then a Y value is placed in Table 20 and if not then a clear NO or N is listed against those data points. This considers the internal variability in the sets of ten (10) colour measurements taken on each reference point. The microtopography of the rocks naturally makes collection of reproducible spectra a challenge, but one that does clearly reap dividends, as shown by the previous discussion where the colour difference values of ΔE have been shown to correlate well with the minimum pH recorded on each site. When the cut off parameter of the mean colour difference divided by the ΔE value was above 0.5 or in that region, the commentary in Table 20 is noted as ~, for being possibly yes and possibly no.

When the data was reviewed it was found that a good method was to plot the change in colour contrast against the change in the mean pH between the given time intervals. Thus, when the differences between the first measurements in 2017 and those in 2018 were considered only the sites 5, 6 and 7 showed a linear response of increasing colour contrast as the sites became more alkaline. This supports the redox data that shows increasing pH brings about precipitation of fresh mineral species, which diminishes the colour contrast between the background and the engravings. For the measurements in 2019 compared with the original data in 2017 all the sites were more acidic i.e., δpH was negative and the same sites had a linear response, given by equation 37,

$$\Delta E_{2019\text{-}2017} = 3.44 + 1.3\ \delta pH_{2019\text{-}2017} \quad \text{.....(37)}$$

The intercept value at no change in pH had increased from 1.3 to 3.4 and the slope had increased from 1.0 to 1.3 times the difference in the mean pH of the sites. The other three data points showed a random distribution of colour difference with the pH differences.

Table 22: Colour differences between background and engraving and significance

site	ΔE00 2017	ΔE00 2018	ΔE00 2019	ΔE00 2020	Signif. 2017	Signif. 2018	Signif. 2019	Signif 2020
S5 spot1	5.83	5.31	4.84	4.00	Y	Y	Y	Y
S5 spot2	6.70	5.81	6.66	5.77	Y	Y	Y	Y
S5 spot3	7.61	4.81	9.86	6.38	Y	N	Y	Y
S5 spot4	4.15	6.45	5.78	2.14	Y	Y	Y	N
S6 spot1	1.51	2.04	1.91	0.72	N	~	Y	N
S6 spot2	1.02	2.15	0.88	0.71	N	N	N	N
S6 spot3	1.86	2.80	1.54	0.45	~	~	N	N
S6 spot4	3.10	2.33	1.83	1.30	Y	N	N	N
S7 spot1	6.75	2.51	3.56	4.25	Y	N	N	Y
S7 spot2	3.01	2.47	3.30	3.44	Y	N	~	Y
S7 spot3	3.84	5.67	5.14	1.53	Y	Y	~	Y
S7 spot4	4.60	5.50	4.40	1.53	Y	~	N	N
S21 spot1	5.34	7.99	4.62	4.27	Y	Y	Y	Y
S21 spot2	3.00	3.86	5.44	4.12	N	~		Y
S21 spot3	5.23	4.15	3.97	4.76	Y	Y		Y
S21 spot4	3.88	6.63	5.53	6.33	Y	Y		Y
S22 spot1	6.63	2.56	1.02	6.49	Y	N		Y
S22 spot2	2.43	1.16	2.80	3.07	Y	N		Y
S22 spot3	4.61	3.12	2.71	4.15	Y	Y		Y
S22 spot4	3.91	3.98	5.32	3.63	Y	Y		Y
S23 spot1	2.17	3.47	3.32	2.01	Y	~		N
S23 spot2	2.52	4.31	1.34	3.34	Y	Y		N
S23 spot3	6.97	3.48	1.05	3.39	Y	Y		Y
S23 spot4	2.65	3.28	4.65	1.43	~	Y		N
S4 spot 1			3.56	5.28		Y		Y
S 4 spot 2			1.91	0.30		N		N
S 4 spot 3			1.60	2.96		~		Y
S 4 spot 4			1.04	2.33		N		N

By the time of the fourth year of monitoring in 2020 the colour difference behaviour showed more systematic responses, as shown in equation 38, which are also shown diagrammatically in Figure 31 and arithmetically in equation 38,

$$^{upper}\Delta E_{2020\text{-}2017} = 16.6 + 12.15\ \delta pH_{2020\text{-}2017} \quad \text{.....(38)}$$

When the intercept value at no change in pH is plotted as a function of the number of days in between when the readings were taken, there is a moderate fit for a linear regression with an R^2 of 0.98 and a relationship given by equation 39,

$$^{intercept}\Delta E_{year\text{-}2017} = 0.0195\,d - 4.99 \quad \text{.....(39)}$$

In this equation *d* is the number of days between seasonal measurements: the error in the slope of the equation is ± 0.0015 or 8% and the larger intercept error is ± 1.05 or some 21%. Additional data would assist with the determination of the rate equation since there should be a correction factor close to zero at zero-time difference, however the fit is sufficiently good to enable predictions to be made on how much the colour contrast will change with time and pH.

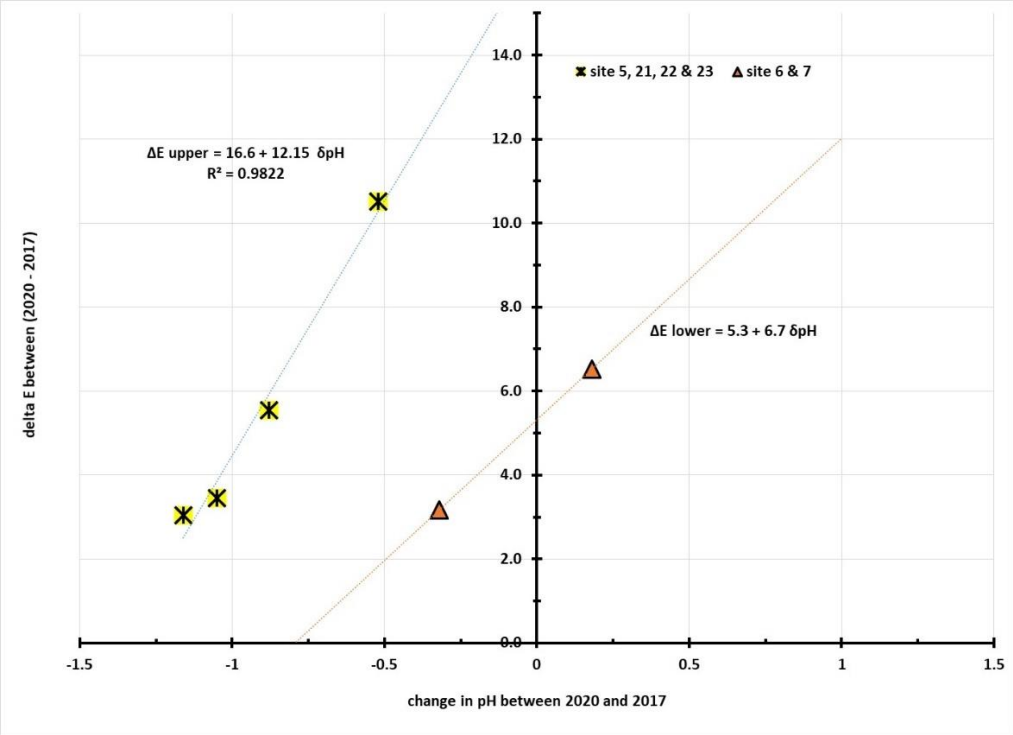

Figure 31: Plot of difference in colour (background – engraved) vs. difference in pH 2020 – 2017.

A review of the information presented in Figure 31 shows no differentiation between gabbro and granophyre rock types but there appears to be differentiation based on the angle of the rock. The upper group of sites 5, 21, 22 and 23 are all either steep sided like 5, 22 and 23 or are essentially flat like site 21. Site 7 is at about 35° from the vertical and site 6 is about 55^0 from the vertical plane. In his report Fox noted that the response of the rocks to adsorption processes seems to be responding to the cosine of the angle and in these variables, this angle on inclination seems to be a differentiating factor. Those sites which have the greatest response to increasing the colour difference have next to no net change in the annual mean pH.

When the same values of colour difference between the years is plotted as a function of the change in the minimum pH a quite different picture emerges. Using the same data base of colour change and the same methodology as with the mean pH data, it turned out that the dependence on change in pH or slope was much less and the intercepts were also much lower. There was no general trend with time and the mean colour difference was independent of time and change in the minimum pH and had a mean value of 3.8 ± 0.4.

Conclusion

The analysis of the relationship between the pH and the amount of metal ions reporting to the wash solutions enabled the mechanism controlling the release of manganese containing minerals to the wash solutions to be determined. From a combination of the Pourbaix diagrams and the regression analyses of the voltages at zero pH, the formal redox voltages of the electroactive species could be obtained. In all sites the dominant minerals were manganese related materials. There was only one site (site 23, Burrup NE) where a vanishingly small amount of iron, just above the detection limit of 0.005 ppm, was found in the wash solutions. However, the presence of electrochemically active iron minerals was picked up on five sites, as shown by the relationships between the pH and the voltage measured at the platinum electrode (see Appendix II for details). These locations included sites 4, 7, 21, 23 and the non-Yara monitoring site of the split rock at the Climbing Man. The redox data has confirmed that manganese exists in a range of oxidation states on the rock surface, from Mn (II) to Mn (IV) and these compounds are either present as soluble Mn^{2+}, $Mn(OH)^{+}$, $Mn(OH)_2^{2+}$ and the black MnO_2, which all compete in a series of equilibria, which are controlled by the prevailing acidity or alkalinity, which is ultimately the controlling factor in the rock patination. The re-examination of the data obtained from the previous studies indicates that this change of mechanism for the release of manganese ions into the wash appears to be subtly controlled by the alkalinity associated with increased salt deposits.

Analysis of the relationships between the surface pH and the ions associated with wind borne sea salts has shown that it is most likely that calcium is reporting to solution through the formation of a mixture of calcium carbonate dissolving to produce either free Ca^{2+} ions or the soluble calcium bicarbonate. Increasing chloride ion concentration is an indicator of increasing deposition of sea salts on the rock surfaces. One major effect of the increased salts is that it produces a buffering effect and appears to be inhibiting the activity of micro-organisms associated with the metabolism of nitrogen (nitrate) containing species found on the rock surfaces. The impact of eight major cyclonic downpours between February 2003 and February 2020 has significantly reduced the amount of bio-available nitrate and this has brought about an amelioration of the previous rates of mobilisation of surface minerals. The impact of cyclone Damien was variable in that some sites, such as Burrup Road (site 5) continued in its trend to increasing acidity while the main panel at Climbing Man gully was essentially unaffected i.e., the mean pH of the site was within the range of experimental values previously observed. However, measurements at the split rock, lying at approximately 35 degrees from the horizontal, and located less than three metres from the main Climbing Man panel, was drenched with cyclonic rain and the mean pH increased from 4.6 to 6.1. The generally low surface chloride concentration on the rocks is due to the generalised heavy rain that fell eight months before the present round of measurements were conducted.

For the six sites examined in and around the Yara facility there is a decreased amount of sulphate ions than cannot be explained by the increased presence of sea salts. The mean sulphate in 2017 was 5.2 ± 3.0 which decreased to a value of 1.2 ± 0.7 ppm in 2018. However, in 2019 it had increased to 4.5 ± 64 ppm before falling to 1.5 ± 2.2 ppm in 2020. One of the washing rocks at site 23 (Yara East) had the maximum of 9.3 ppm sulphate while the adjacent rock, some 2.5 metres away, reported a wash value of 2.1 ppm. There is no readily apparent explanation for the large difference observed in the sulphate concentration on this site. The Deep Gorge rocks at site 7 gave 1.2 and 2.8 ppm while all the other reference sites had an average value of 0.7 ± 0.5 ppm. Detailed modelling of the dispersion of plumes from Woodside Petroleum operations and from the shipping facilities at Dampier may provide an insight into the origins of the extra sulphate at sites 23 and site 7. Plots of the minimum pH as a function of sulphate ion concentration indicated that for sites 6, 7, 21, 23 and the Climbing Man split rock site there was a linear relationship between the sulphate ion and the minimum pH, which fell by approximately 0.82 per ppm of sulphate. In essence the sulphate ions appear to have increased the acidity from a pH of 5.8 to 3.8 as the concentration increased to 2 ppm. However, it was noted that

above this level of sulphate there is no apparent further increase in acidity. Presumably, the increased sulphate above 2ppm is associated with increased sea salt concentration which has its natural buffering capacity. This is the first direct evidence of the impact of SO_x on the surface acidity, and hence mobilisation of minerals, on the Burrup reference rocks.

The impact of soluble nitrate on the rock surface pH is much greater on a ppm basis but on a milliequivalent ratio, since sulphate can provide two moles of acid and nitrate only one, each ppm of sulphate has the potential for 0.020 milliequivalents while nitrate provides 0.016 milliequivalents. Plots of the minimum pH against the nitrate concentration showed that for all the granophyre sites and for site 23 (Yara East) there was an R^2 of 0.96 for the regression analysis between the minimum pH and the nitrate level, with the pH falling from 5.7 to 3.8 as the nitrate concentration increased from zero to 0.32 ppm. The highest nitrate level was recorded on the second washing rock at site 7, which had a value of 0.46 ppm but had a pH of 4.94, which indicates possible buffering from industrial emissions including the ammonia. Data from the monitoring station at site 7 had shown evidence of industrial emissions being the likely cause of lowered biological response to the nitrate concentration.

Colour measurements with the Minolta chromameter have proved to be instrumental in determining what the changing nature of the rock surfaces on both the background and the engraved areas as they respond to changes in rainfall and the associated pH of the microflora living on the rocks. The 2020 data generally indicated increasing colour contrast with decreasing minimum pH. In simple terms, this means that as the rock surfaces become more acidic the repatination processes are halted due to the removal of a thin layer of precipitated mineralisation. It was found that for all sites, other than Yara East (site 23), the ΔE values all decreased with increasing pH and at the same rate of 3.97 ± 0.13 ΔE per pH increase. This data covered a $pH_{minimum}$ range from 3.8 to 4.9. This observation is supportive evidence for the commentary that the changing environmental conditions which bring about changed pH alter the redox reactions occurring on the surface. These reactions change the conditions favouring either dissolution of the repatinated surfaces (increasing colour contrast) or precipitation of new minerals (decreasing colour contrast) at higher pH values. When the ΔE is plotted as a function of the mean pH, similar results are obtained to that using the minimum pH, for the slope is experimentally the same at 3.85 ± 0.03 over a pH range of 4.6 to 5.8, and the ΔE values ranged from 6.2 to 0.62, which is well below one just noticeable fade value at a ΔE of two.

Having access to four years of colour difference data it was possible to plot the colour differences between the first year of 2017 and subsequent annual revisions until the present data was collected in 2020. It was also possible to analyse the changes that took place between 2018, 2019 and 2020. The most productive investigation was that of using the colour differences mapped against the differences in the mean pH of the various seasons of site visits. The same trends in reduction of colour difference in the background readings with increasing acidity were noted. The changes in the colour contrast of the engraved and background areas in the first few years was relatively small but when the data from 2020 was compared with the initial readings in 2017 the background measurements went from a ΔE value of 26 to 3 as the acidity increased from no change to a δpH of -0.72, equivalent to an increased acidity by a factor of just over five times. Similarly, the ΔE for the difference between the background and the engraved areas saw ΔE fall from 17 at no pH change to 3 at a pH change of –1.16 or an increase of acidity by a factor of just over 14 times. This data related to sites 5, 21, 22 and 23 while sites 6 and 7 had a lower response with ΔE falling from 5 at zero change to 3 a pH difference of -0.3 or with a doubling of acidity.

The conclusion of this colour study is that the work should continue so that the dynamics of changing colour contrast can be determined. There is unequivocal evidence that the changes in colour contrast

are affected by the changes in the mean and in the minimum pH observed on the rock art sites at the reference positions.

END of REPORT

REFERENCES

Arthur, I, 2004, Report on the identification of yeasts and moulds from rocks in the Burrup, Mycology, Department of Health Laboratories, Western Australia, Unpublished report, 1-6.

Burford, E P, Fomina, M and Gadd, G M, 2003, Fungal involvement in bioweathering and biotransformation of rocks and minerals, *Mineralogical Magazine* 67 (6), 1127–1155.

Clark, R, 2004, Identification of surface minerals in weathered rocks from the Burrup peninsula, unpublished report to the Burrup Rock Art Monitoring Scientific Committee, November 2004, 1–18.

Ford, B., 2020, Report to Heritage Conservation Solutions on analysis of colour differences between engraved and background sites in the Burrup, unpublished report November 2020, pp 1-24.

Fox, D., 2020, Statistical Modelling of Rock Surface pH Data from the Burrup Peninsula, Western Australia 2003 – 2019, Unpublished report to GBH Solutions by Environmetrics Australia, September 2020 p 1-93.

Gadd, G M, 2004, 'Mycotransformation of organic and inorganic substrates', *Mycologist* 18 (2), 60–70.

Lau, D, Ramanaidou E., Furman, S., Hacket A., Caccetta M., Wells M., McDonald B., 2008, *Burrup Peninsula Aboriginal Petroglyphs: Colour Change and Spectral Mineralogy 2004–2007*, CSIRO Materials Science and Engineering, Clayton, Victoria, Australia, 1-44.

King, J, 2003, Report on the identification of bacteria, yeasts, moulds, and fungi in the Burrup, unpublished report, Department of Agriculture, Perth, Western Australia.

MacLeod, I D, 2003, A micro-environmental study of rocks on the Burrup: effects of water and nutrients on pH and microflora, unpublished report, Western Australian Museum, 1–66.

MacLeod, I.D., 2017, Report to the Murujuga Aboriginal Corporation; Impact of industrial emissions on the pH and Eh of engraved rock art on the Burrup peninsula", Unpublished report of Heritage Conservation Solutions, pp 1-17.

MacLeod, I.D, 2019, Collecting in-situ data in the field and laboratory: artefact corrosion and conservation, Japanese Institute for Anatolian Archaeology, http://www.jiaa-kaman.org/en/consymposium_2019.html, pp 1-18

Markley T., Wells M., Ramanaidou E., Lau D., and Alexander D., 2015, Burrup Peninsula Aboriginal Petroglyphs: Colour Change & Spectral Mineralogy 2004–2014, CSIRO report, EP1410003 October 2015, 1-189.

North, N A, 1982, Corrosion products on marine iron, *Studies in Conservation* 27, 75–83.

Pourbaix, M., 1974, *Atlas of electrochemical equilibria in aqueous solutions,* National Association of Corrosion Engineers, Houston, Texas USA pp 1-644.

Ramanaidou E., Walton G. and Winchester D., 2017, Extreme Weathering Experiments on the Burrup Peninsula / Murujuga Weathered gabbros and granophyres, EP172193 May 2017, 1-62.

APPENDIX I: MacLeod publications on rock art conservation

Refereed journal articles

Haydock, P. & MacLeod, I.D. (1987) “The use of micro-meteorological studies as an aid to the conservation of aboriginal rock art”. *ICOM Committee for Conservation*, Sydney, September 1987, p 1149-1153.

MacLeod, I.D. (1991) "Microclimate modelling in old museum buildings". *Historic Environment-Conservation in Context: Artefact and Place,* 8(1&2), p 37-41

Ford, B., MacLeod, I.D., and Haydock, P., (1994) "Rock art pigments from the Kimberley region of Western Australia: identification of the minerals and conversion mechanisms", *Studies in Conservation* 39, p 57-69.

MacLeod, I.D., Haydock, P., Tulloch, D. & Ford, B. (1995) "Effects of microbiological activity on the conservation of aboriginal rock art" *AICCM Bulletin* 21(1), 3-10

MacLeod, I.D., Haydock, P & Charton, E., (1996) "Avian guano and its effects on the preservation of rock paintings" *Preservation of Rock Art 1995 AURA Occasional Papers 9*, Ed. Andrew Thorn & Jacques Brunet p 60-64.

MacLeod, I.D., Haydock P. and Ford, B. (1997) “Conservation Management of West Kimberley Rock Art: Microclimate studies and Decay Mechanisms” *Kimberley Society Occasional Paper No 1. Aboriginal Rock Art of the Kimberley* Ed K.F. Kenneally, M.R. Lewis., M. Donaldson and C. Clement, Kimberley Society Inc, Perth, Western Australia. pp 65-69.

MacLeod, I.D., (2000) “Rock art conservation and management: the past, present and future options”, *Reviews in Conservation,* 1, pp 32-45.

MacLeod, I.D., and Haydock, P., (2002) “Microclimate modelling for prediction of environmental conditions within rock art shelters”, Preprints for ICOM-CC Triennial Meeting, Rio de Janeiro, Brazil September 2002, Vol II, 571-577.

MacLeod, I.D. (2005) “The effects of moisture, micronutrient supplies and microbiological activity on the surface pH of rocks in the Burrup peninsula”, Preprints for ICOM-CC Triennial Meeting, Den Haag, The Netherlands, September 2005, Vol II 386-393

Black, J., MacLeod I.D., and Smith, B., (2017), Theoretical effects of industrial emissions on colour change at rock art sites on Burrup Peninsula, *J Archaeological Science*: *Reports* 12, 457-462.

MacLeod, I.D. and W. Fish. (2021) Determining decay mechanisms on engraved rock art sites using pH, chloride ion and redox measurements with an assessment of the impact of cyclones, sea salt and nitrate ions on acidity. In *Transcending Boundaries: Integrated Approaches to Conservation. ICOM-CC 19th Triennial Conference Preprints, Beijing, 17–21 May 2021,* ed. J. Bridgland. Paris: International Council of Museums.

Unpublished Reports

MacLeod, I.D., Haydock, P. and Ford, B (1991)- "Conservation research into the preservation of rock paintings in the West Kimberley region of Western Australia", Report to the Western Australian Heritage Committee, pp 1-89

MacLeod, I.D., Haydock, P & Charton, E., (1992) "The effects of avian guano on the preservation at *Walga Rock*". Report to the Australian Institute of Aboriginal and Torres Strait Islanders Studies, Canberra, pp 1-45.

MacLeod, I.D., Haydock, P and Ford, B (1994) *Conservation research into the preservation of rock paintings in the West Kimberley Region of Western Australia: Wet Season Report*. Report to the Heritage Council of WA, March 1994, pp-143.

MacLeod, I.D. and Haydock, P., (1996) *Research into the Conservation or rock paintings in the West Kimberley: Microclimate data analysis* Report to AIATSIS, May 1996, pp 1-132

Ford, B., Officer, K. and MacLeod, I.D., (1999) *A study of lichen invasion of Nursery Swamp II, Aboriginal Rock Art Site, Namadji National Park, Australian Capital Territory, Final Report May 1999*, Australian Capital Territory National Parks Association, Canberra 1999, pp. 1-28.

MacLeod, I.D., (2003) "The microenvironment of rocks on the Burrup: analysis of the relationships between nutrient supplies, surface pH and microflora – preliminary report, Report to the Minister of Culture and the Arts, pp 1-55.

MacLeod, I.D., (2017), "Report to the Murujuga Aboriginal Corporation; Impact of industrial emissions on the pH and Eh of engraved rock art on the Burrup peninsula", pp 1-17.

MacLeod, I.D., (2018), "Conservation analysis at the Yara monitoring sites 2018"

MacLeod, I.D., (2019) "Conservation analysis at the Yara monitoring sites 2019"

APPENDIX II: Electrochemical analysis of reactions from Pourbaix diagrams 2020

Sites	slope, mV/pH	Intercept	R^2	No of points
$Mn^{2+} + 2\,H_2O \rightarrow MnO_2 + 4H^+ + 2e^-$				**E^0 1.104**
4	-0.129	1.0641	0.9714	3
$Fe^{2+} \rightarrow Fe^{3+} + e^-$				**E^0 0.771**
23	-0.064	0.665	0.961	3
21	-0.062	0.669	0.893	4
7	-0.059	0.732	0.929	5
4	-0.064	0.673	0.931	3
CM split	-0.055	0.708	0.960	6
mean	-0.057 ± 0.004	0.718 ± 0.029		
$Mn(OH)^+ + H_2O \rightarrow Mn(OH)_2^{2+} + H^+ + 2e^-$				**E^0**
$2\,Fe(OH)^+ + H_2O \rightarrow Fe(OH)_2^+ + Fe(OH)^{2+}\,H^+ + 2e^-$				**E^0**
23	-0.031	0.457	0.813	8
5 b	-0.027	0.479	1.000	2
4 a	-0.030	0.508	0.520	8
mean	**-0.029 ± 0.002**	**0.481 ± 0.026**		
22 a	-0.029	0.549	0.910	7
22 b	-0.033	0.557	0.959	6
21 a	-0.033	0.568	0.560	4
21 b	-0.034	0.565	0.807	5
7 a	-0.029	0.544	0.793	4
7 b	-0.030	0.542	0.979	6
6 a	-0.028	0.541	0.886	6
6 b	-0.030	0.541	0.887	8
5 a	-0.039	0.565	0.690	4
4 b	-0.033	0.542	0.888	8
CM split	-0.038	0.595	0.850	7
mean	**-0.028 ± 0.003**	**0.576 ± 0.017**		

APPENDIX III: Chemical analysis of the wash solutions from the CSIRO monitoring sites October 2020.

Concentrations are in mg/L other than electrical conductivity which is in mS/m

Client Id	Site 4a	Site 4b	Site 5a	Site 5b	Site 6a	Site 6b	Site 7a	Site 7b
Al								
B	0.015	0.012	0.03	0.013	0.014	0.013	0.01	0.01
Ba	0.0019	0.0016	0.0052	0.0031	0.0077	0.0053	0.002	0.0027
Ca	0.4	0.4	1.3	0.4	2	1.2	1.1	2
Cd			0.0003					
Cl	31	31	70	31	33	31	24	24
Co								
Cu	0.0013	0.0006	0.0045	0.0004	0.0011	0.0009	0.0005	0.0004
ECond	11.4	11.1	22.8	11.1	12.8	12.2	8.6	9.6
Fe								
K	0.3	0.4	1.4	0.2	1.6	1.3	0.3	0.4
Mg	9.8	8.9	19.9	9.4	10.2	10.1	7.3	7.4
Mn	0.0029	0.0026	0.0088	0.0038	0.0098	0.0072	0.0045	0.0054
NO3	0.23	0.14	0.23	0.11	0.16	0.13	0.19	0.46
Na	1	0.9	2.6	0.7	1.6	1.4	1.2	1.6
Ni								
Oxalate								
Pb			0.0002		0.0005	0.0001		
S	0.2	0.1	0.5	0.2	0.7	0.4	0.5	1.1
SO4	0.2	0.3	0.5	0.4	1.5	0.8	1.2	2.8
V		0.0002						
Zn	0.013	0.011	0.028	0.01	0.012	0.012	0.008	0.007

Appendix III continued

Client Id	Site 21a	Site 21b	Site 22a	Site 22b	Site 23a	Site 23b	Climbing a	Climbing b
Al						0.011		
B	0.013	0.01			0.016	0.029	0.01	0.01
Ba	0.0034	0.0029	0.0009	0.0009	0.0031	0.0053	0.0013	0.0021
Ca	1.2	0.9	0.4	0.3	2	4.7	0.5	0.7
Cd								
Cl	33	32	0.9	<0.5	33	45	30	31
Co						0.0001		
Cu	0.0008	0.0005	0.0005	0.0003	0.0015	0.0032	0.0003	0.0007
ECond	12.5	11.7	0.8	0.3	13	19.7	11	11.4
Fe					0.006	0.012		
K	0.7	0.4	0.4	0.2	0.5	2	0.2	0.5
Mg	10.3	10.4	0.1	0.1	10.8	10.8	9.8	9.8
Mn	0.0036	0.0035	0.0014	0.0011	0.0068	0.011	0.0034	0.0075
NO3	0.14	0.1	0.08	0.06	0.16	0.32	0.07	0.09
Na	1.9	1.3	1.2	0.6	2.2	10.5	0.6	1.2
Ni								
Oxalate					0.1	0.2		0.1
Pb						0.0002		
S	0.7	0.4	0.2	0.1	0.9	3.4	0.1	0.2
SO4	1.7	0.8	0.5	0.5	2.1	9.3	0.4	0.5
V						0.0001		
Zn	0.011	0.008	0.007	0.005	0.009	0.009	0.007	0.007

APPENDIX IV: Surface pH measurements 2003-2004 in the Burrup

	17-Jun-03	28-Aug-03	23-Feb-04
Location		pH	pH
Dampier W1		5.03	4.90
Dampier W1		4.85	4.82
Dampier W1		5.14	4.77
Dampier W1		5.13	5.18
Dampier W1		4.61	4.47
Dampier W1		4.95	4.59
Dampier W1		4.37	4.80
Dampier W1		4.10	4.88
Dampier W1		4.49	4.76
Dampier W1			4.71
Dampier W1			4.64
Dampier W1 mean		**4.74**	**4.77**
Dampier W1 st. dev.		**0.37**	**0.19**

Dampier W2		4.30	4.41
Dampier W2		4.34	4.32
Dampier W2		4.96	4.61
Dampier W2		4.80	4.63
Dampier W2		4.86	4.40
Dampier W2		4.72	4.27
Dampier W2		4.78	4.16
Dampier W2		4.94	4.78
Dampier W2		4.82	4.50
Dampier W2		4.33	4.68
Dampier W2 mean		**4.7**	**4.5**
Dampier W2 st. dev.		**0.3**	**0.2**

				27-Feb-04
Burrup SW1		4.70	4.43	4.63
Burrup SW1		4.69	5.33	4.76
Burrup SW1		4.94	4.52	4.97
Burrup SW1		4.49	4.89	4.79
Burrup SW1		4.96	4.68	4.78
Burrup SW1		4.16	4.60	4.92
Burrup SW1		4.42	4.92	3.89
Burrup SW1		4.66	4.98	4.94
Burrup SW1			5.01	4.94
Burrup SW1			4.65	5.02
Burrup SW1 mean		**4.63**	**4.80**	**4.76**
Burrup SW1 st. dev.		**0.27**	**0.27**	**0.33**

Burrup SW2		5.39	4.88	4.87
Burrup SW2		5.32	4.49	4.68
Burrup SW2		4.64	4.82	4.83
Burrup SW2		4.44	4.83	5.16
Burrup SW2		4.60	4.72	4.83
Burrup SW2		5.43	4.69	4.80
Burrup SW2		5.00	4.65	4.98
Burrup SW2		5.40	4.72	5.00
Burrup SW2		5.38	4.63	5.19
Burrup SW2			4.59	5.24
Burrup SW2 mean		**5.07**	**4.70**	**4.96**
Burrup SW2 st. dev.		**0.40**	**0.12**	**0.19**

27-Feb-04

King Bay 1		4.89	4.61	4.91
King Bay 1		4.37	5.34	4.73
King Bay 1		5.27	5.15	4.46
King Bay 1		4.98	4.69	4.79
King Bay 1		5.41	4.39	4.64
King Bay 1		5.30	4.70	4.98
King Bay 1		4.85	5.02	4.80
King Bay 1		4.94	5.00	4.87
King Bay 1		6.04	5.12	4.93
King Bay 1		5.33	4.93	4.88
King Bay 1		5.36		4.91
King Bay 1		5.17		
King Bay 1 mean		**5.16**	**4.90**	**4.81**
King Bay 1 st. dev.		**0.41**	**0.29**	**0.15**

27-Feb-04

King Bay 2		5.27	4.85	4.61
King Bay 2		5.24	4.89	4.75
King Bay 2		5.27	4.89	4.80
King Bay 2		5.41	4.74	4.95
King Bay 2		5.31	5.29	4.86
King Bay 2		4.59	4.77	5.30
King Bay 2		4.88	5.22	4.78
King Bay 2		3.82	5.41	4.76
King Bay 2		5.05	4.93	5.02
King Bay 2		4.91	5.17	3.54
King Bay 2		5.48		5.02
King Bay 2		5.44		4.78
King Bay 2 mean		**5.06**	**5.02**	**4.76**
King Bay 2 st. dev.		**0.5**	**0.2**	**0.42**

Withnell Bay		5.15	5.02
Withnell Bay		4.95	5.01

Withnell Bay		5.18	5.27
Withnell Bay		4.95	4.97
Withnell Bay		4.98	4.73
Withnell Bay		4.79	5.19
Withnell Bay		4.47	4.82
Withnell Bay		4.70	5.50
Withnell Bay		4.85	5.04
Withnell Bay		4.46	4.55
Withnell Bay		4.91	5.01
Withnell Bay mean		**4.85**	**5.01**
Withnell Bay st. dev.		**0.24**	**0.26**

Withnell Bay 2		4.92	5.76
Withnell Bay 2		4.73	5.28
Withnell Bay 2		4.26	5.52
Withnell Bay 2		4.45	5.52
Withnell Bay 2		4.89	5.24
Withnell Bay 2		4.97	5.26
Withnell Bay 2		4.78	5.44
Withnell Bay 2		4.83	5.26
Withnell Bay 2		4.93	5.50
Withnell Bay 2		4.66	5.68
Withnell Bay 2 mean		**4.74**	**5.45**
Withnell Bay 2 st. dev.		**0.23**	**0.18**

North Withnell Bay 1		4.48	4.66
North Withnell Bay 1		4.59	4.80
North Withnell Bay 1		4.17	4.85
North Withnell Bay 1		4.86	4.62
North Withnell Bay 1		4.37	4.66
North Withnell Bay 1		4.54	4.75
North Withnell Bay 1		4.29	4.76
North Withnell Bay 1		4.51	5.03
North Withnell Bay 1			5.16
North Withnell Bay 1			4.89
North Withnell Bay 1			
North Withnell Bay 1			
North Withnell Bay 1			
North Withnell Bay 1 mean		**4.48**	**4.82**
North Withnell Bay 1 st. dev.		**0.21**	**0.17**

North Withnell Bay 2		4.77	4.65
North Withnell Bay 2		4.74	3.45 soil area

North Withnell Bay 2		4.66	4.87
North Withnell Bay 2		4.31	4.79
North Withnell Bay 2		4.83	5.09
North Withnell Bay 2		4.65	4.76
North Withnell Bay 2		4.58	4.88
North Withnell Bay 2		4.50	5.13
North Withnell Bay 2		4.63	5.05
North Withnell Bay 2			4.73
North Withnell Bay 2			5.03
North Withnell Bay 2 mean, no soil		4.63	4.90
North Withnell Bay 2 st. dev. no soil		0.15	0.17
North Withnell Bay 2 mean			**4.9**
North Withnell Bay 2 st. dev.			**0.2**

Deep Gorge 1		4.91	4.71
Deep Gorge 1		4.54	5.06
Deep Gorge 1		4.87	4.74
Deep Gorge 1		4.72	4.87
Deep Gorge 1		4.89	4.90
Deep Gorge 1		4.10	5.14
Deep Gorge 1		4.32	4.98
Deep Gorge 1		4.06	4.80
Deep Gorge 1		5.19	4.80
Deep Gorge 1		4.17	5.07
Deep Gorge 1		4.14	
Deep Gorge 1 mean		**4.54**	**4.91**
Deep Gorge 1 st. dev.		**0.40**	**0.15**

Deep Gorge 2		4.59	4.69
Deep Gorge 2		4.93	4.97
Deep Gorge 2		4.46	5.45
Deep Gorge 2		4.63	5.31
Deep Gorge 2		4.57	5.20
Deep Gorge 2		4.79	5.04
Deep Gorge 2		4.71	5.16
Deep Gorge 2		4.36	5.12
Deep Gorge 2		4.70	5.31
Deep Gorge 2			3.85
Deep Gorge 2			
Deep Gorge 2 mean		**4.64**	**5.01**
Deep Gorge 2 st. dev.		**0.17**	**0.46**

Deep Gorge 3			5.19
Deep Gorge 3			4.91
Deep Gorge 3			5.06
Deep Gorge 3			4.73
Deep Gorge 3			4.78
Deep Gorge 3			4.91
Deep Gorge 3			5.39
Deep Gorge 3			5.27
Deep Gorge 3			5.23
Deep Gorge 3			5.10
Deep Gorge 3 mean			**5.06**
Deep Gorge 3 st. dev.			**0.22**

Climbing Man Gully 1		5.37	4.96
Climbing Man Gully 1		5.53	4.80
Climbing Man Gully 1		5.39	5.03
Climbing Man Gully 1		4.84	4.78
Climbing Man Gully 1		5.41	4.97
Climbing Man Gully 1		4.83	4.63
Climbing Man Gully 1		4.81	4.93
Climbing Man Gully 1		5.70	5.03
Climbing Man Gully 1		3.04	5.37
Climbing Man Gully 1		5.55	4.22
Climbing Man Gully 1		5.42	5.53
Climbing Man Gully 1		4.62	4.26
Climbing Man Gully 1			4.58
Climbing Man Gully 1 mean		**5.0**	**4.9**
Climbing Man Gully 1 st. dev.		**0.7**	**0.4**
Climbing Man Gully 1 mean (-acid spot)		5.22	
Climbing Man Gully 1 st. dev. (-acid spot)		0.37	

Climbing Man Gully 1-1		5.05	4.92
Climbing Man Gully 1-1		4.85	5.00
Climbing Man Gully 1-1		5.03	3.95
Climbing Man Gully 1-1		5.97	4.45
Climbing Man Gully 1-1		5.78	3.94
Climbing Man Gully 1-1		5.46	3.83
Climbing Man Gully 1-1		5.79	3.97
Climbing Man Gully 1-1		5.45	3.68
Climbing Man Gully 1-1		5.23	4.94
Climbing Man Gully 1-1		5.31	3.85
Climbing Man Gully 1-1 mean		**5.39**	**4.25**
Climbing Man Gully 1-1 st. dev.		**0.37**	**0.52**

June 03 Adjacent to Climbing Man	3.74		4.86

Feb 04 Climbing Man itself	4.31		4.85
Feb 04 Climbing Man itself	4.54		3.91
Feb 04 Climbing Man itself	4.19		3.61
Feb 04 Climbing Man itself	4.1		4.87
Feb 04 Climbing Man itself	4.27		3.75
Feb 04 Climbing Man itself	4.78		4.86
Feb 04 Climbing Man itself	4.55		4.82
Feb 04 Climbing Man itself	3.58		4.68
Feb 04 Climbing Man itself			5.13
Feb 04 Climbing Man itself			4.68
Feb 04 Climbing Man itself mean	**4.23**		**4.55**
Feb 04 Climbing Man itself st. dev.	**0.39**		**0.53**

Climbing Man gully 2B			5.19
Climbing Man gully 2B			5.04
Climbing Man gully 2B			5.23
Climbing Man gully 2B			5.28
Climbing Man gully 2B			5.21
Climbing Man gully 2B			5.06
Climbing Man gully 2B			5.35
Climbing Man gully 2B			5.43
Climbing Man gully 2B			5.29
Climbing Man gully 2B			5.53
Climbing Man gully 2B mean			**5.26**
Climbing Man gully 2B st. dev.			**0.15**

Compound, off site up hill		4.88	3.81
Compound, off site up hill		4.49	5.06
Compound, off site up hill		4.76	4.94
Compound, off site up hill		4.33	4.76
Compound, off site up hill		5.17	5.67
Compound, off site up hill		4.17	4.65
Compound, off site up hill		4.16	3.88
Compound, off site up hill		4.73	3.86
Compound, off site up hill		4.61	4.59
Compound, off site up hill		4.67	4.40
Compound, off site up hill		4.64	
Compound, off site, uphill, mean		**4.60**	**4.56**
Compound, off site, uphill st. dev.		**0.30**	**0.60**

Compound off site, 2			3.85
Compound off site, 2			4.62
Compound off site, 2			3.82
Compound off site, 2			4.66
Compound off site, 2			4.58
Compound off site, 2			4.91
Compound off site, 2			4.51
Compound off site, 2			4.52
Compound off site, 2			4.83
Compound off site, 2			3.94
Compound off site, 2 mean			**4.42**
Compound off site, 2 st. dev.			**0.40**

Rock 3	4.67		4.46
Rock 3	4.76		4.79
Rock 3			4.63
Rock 3			5.03
Rock 3			4.40
Rock 3			4.16
Rock 3			4.71
Rock 3			4.69
Rock 3			4.82
Rock 3			4.54
Rock 3 mean	**4.72**		**4.62**
Rock 3 st. dev.	**0.06**		**0.25**

Rock 86	4.56	4.71	4.98
Rock 86	4.67	4.72	4.95
Rock 86	4.46	4.62	5.09
Rock 86	4.63	5.04	5.08
Rock 86	5.57	4.89	4.86
Rock 86	5.3	4.96	5.10
Rock 86	5.12	5.22	4.90
Rock 86		4.99	4.92
Rock 86		4.96	4.64
Rock 86		5.05	5.21
Rock 86			5.05
Rock 86 mean	**4.90**	**4.92**	**4.98**
Rock 86 st. dev.	**0.43**	**0.18**	**0.15**

Rock 97	5.21		4.87
Rock 97	5.26		5.30
Rock 97	5.74		5.11
Rock 97			5.03
Rock 97			6.06
Rock 97			5.68
Rock 97			5.34
Rock 97			5.41
Rock 97			5.67
Rock 97			5.00
Rock 97 mean	**5.40**		**5.35**
Rock 97 st. dev.	**0.29**		**0.37**

Rock 162	4.92	4.72	4.88
Rock 162	5.87	4.63	4.82
Rock 162	5.29	4.86	4.81
Rock 162		4.73	4.88
Rock 162		4.68	5.21
Rock 162		4.50	5.41
Rock 162		4.54	5.12
Rock 162		4.68	5.14
Rock 162		4.71	5.21
Rock 162			5.06
Rock 162 mean	**5.36**	**4.67**	**5.05**
Rock 162 st. dev.	**0.48**	**0.11**	**0.20**

Rock 938		3.97	5.83
Rock 938		4.38	5.12
Rock 938		4.75	5.06
Rock 938		5.15	4.83
Rock 938		4.87	5.45
Rock 938		4.57	4.56
Rock 938		4.64	5.75
Rock 938		5.20	4.35
Rock 938		4.50	4.47
Rock 938		4.80	3.98
Rock 938		5.00	
Rock 938		4.85	
Rock 938		5.63	
Rock 938		**4.7**	
Rock 938		**5.4**	
Rock 938 mean		**4.82**	**4.94**
Rock 938 st. dev.		**0.41**	**0.61**

Rock 1681	5.63	4.57	4.14
Rock 1681	5.36	4.43	5.18
Rock 1681	5.53	4.38	4.93
Rock 1681	5.59	4.17	4.40
Rock 1681	5.28	4.29	4.88
Rock 1681	5.45	4.43	4.8
Rock 1681	5.40	4.21	4.93
Rock 1681	4.86	4.76	4.73
Rock 1681	5.34	4.32	4.85
Rock 1681	4.90	4.10	4.63
Rock 1681	5.64	4.15	
Rock 1681	5.67	3.92	
Rock 1681	4.74	3.86	
Rock 1681	5.81	3.85	
Rock 1681 mean	**5.37**	**4.25**	**4.75**
Rock 1681 st. dev.	**0.33**	**0.26**	**0.30**

Gidley Island 1			25-Feb-04
Gidley Island 1			10:00
Gidley Island 1			4.45
Gidley Island 1			4.81
Gidley Island 1			5.09
Gidley Island 1			4.96
Gidley Island 1			5.06
Gidley Island 1			4.93
Gidley Island 1			4.86
Gidley Island 1			5.08
Gidley Island 1			4.63
Gidley Island 1 mean			**4.17**
Gidley Island 1 st. dev.			**1.67**

Gidley Island 2			25-Feb-04
Gidley Island 2			10:30
Gidley Island 2			4.73
Gidley Island 2			4.52
Gidley Island 2			4.68
Gidley Island 2			4.67
Gidley Island 2			5.24
Gidley Island 2			4.94
Gidley Island 2			4.65
Gidley Island 2			4.78
Gidley Island 2			4.76
Gidley Island 2			5.00
Gidley Island 2			4.57
Gidley Island 2 mean			**4.78**
Gidley Island 2 st. dev.			**0.21**

Gidley Island 3			25-Feb-04
Gidley Island 3			11:00
Gidley Island 3			4.61
Gidley Island 3			5.54
Gidley Island 3			4.70
Gidley Island 3			5.10
Gidley Island 3			4.50
Gidley Island 3			4.92
Gidley Island 3			5.25
Gidley Island 3			5.26
Gidley Island 3			5.50
Gidley Island 3			4.21
Gidley Island 3 mean			**4.96**
Gidley Island 3 st. dev.			**0.45**

Dolphin Island 1			25-Feb-04
Dolphin Island 1			12:10
Dolphin Island 1			4.93
Dolphin Island 1			4.85
Dolphin Island 1			4.72
Dolphin Island 1			4.63
Dolphin Island 1			4.61
Dolphin Island 1			5.05
Dolphin Island 1			4.86
Dolphin Island 1			4.71
Dolphin Island 1			5.08
Dolphin Island 1			4.95
Dolphin Island 1			4.52
Dolphin Island 1 mean			**4.81**
Dolphin Island 1 st. dev.			**0.19**

Dolphin Island 2			25-Feb-04
Dolphin Island 2			12:35
Dolphin Island 2			5.14
Dolphin Island 2			4.91
Dolphin Island 2			4.89
Dolphin Island 2			3.68
Dolphin Island 2			3.74
Dolphin Island 2			5.04
Dolphin Island 2			4.85
Dolphin Island 2			5.07
Dolphin Island 2			4.79
Dolphin Island 2			5.04
Dolphin Island 2			4.72
Dolphin Island 2			0.54
Dolphin Island 2			
Dolphin Island 2 mean			**4.97**
Dolphin Island 2 st. dev.			**0.12**

Dolphin Island 3			25-Feb-04
Dolphin Island 3			12:55
Dolphin Island 3			5.22
Dolphin Island 3			5.32
Dolphin Island 3			5.15
Dolphin Island 3			5.66
Dolphin Island 3			5.07
Dolphin Island 3			4.65
Dolphin Island 3			3.87
Dolphin Island 3			4.81
Dolphin Island 3			5.25
Dolphin Island 3			5.07
Dolphin Island 3			5.22
Dolphin Island 3 mean			**5.03**
Dolphin Island 3 st. dev.			**0.46**